UNIVERSIDADE DE SÃO PAULO
INSTITUTO DE FÍSICA DE SÃO CARLOS

Guilherme de Araújo Nogueira

Higher-order QCD in Higgs to gluon gluon

São Carlos

2024

Guilherme de Araújo Nogueira

Higher-order QCD in Higgs to gluon gluon

Dissertation presented to the Graduate Program in Physics at the Instituto de Física de São Carlos da Universidade de São Paulo, to obtain the degree of Master of Science.

Concentration area: Theorical and Experimental Physics

Advisor: Prof. Dr. Diogo Rodrigues Boito

Corrected version
(Original version available on the Program Unit)

São Carlos
2024

Nogueira, Guilherme de Araújo
Higher-order QCD in Higgs to gluon gluon / Guilherme de Araújo Nogueira; advisor Diogo Rodrigues Boito - corrected version -- São Carlos 2024.
116 p.

Dissertation (Master's degree - Graduate Program in Theoretical and Experimental Physics) -- Instituto de Física de São Carlos, Universidade de São Paulo - Brasil , 2024.

1. QCD. 2. Gluons. 3. Higgs boson. I. Boito, Diogo Rodrigues, advisor. II. Title.

To my grandparents,
my greatest inspirations.

Agradecimentos

- Em primeiro lugar, agradeço aos meus avós, Luzia e Manoel, pelo apoio nesta jornada. Mesmo sem saber no que estavam apostando, acreditaram em mim, e tudo que eu fiz e ainda vou fazer é para honrar vocês. Agradeço também à minha irmãzinha Bia, que, apesar de já ser gente "grande", continua com cara de sagui.

- Agradeço à minha namorada, Anelise, por todo amor, ajuda e compreensão que demonstrou nos períodos mais críticos destes dois últimos anos.

- Ao meu orientador, Prof. Diogo Boito, por todos os ensinamentos e pelas oportunidades que possibilitaram a realização de muitos dos meus sonhos. Além de sempre me guiar durante o desenvolvimento do projeto, principalmente durante as fases que considerei mais desesperadoras. Agradeço também por todos os cafés e pizzas.

- Agradeço aos meus grandes amigos Nelto, Alan e Vini Alencar.

- Em seguida agradeço a todos amigos que fiz durante esse período de mestrado: João, Felipe, Guilherme, Gustavo, Giovani, Yara, Anderson e Cris. Juntos contruímos momentos incríveis. Principalmente ao João, por me levar café quando queria conversar.

- Por fim, agradeço a Fundação de Amparo à Pesquisa do Estado de São Paulo (FAPESP) pelo financiamento, processo n°2022/01861-9.

"Onde estiver, seja lá como for, tenha fé,
porque até no lixão nasce flor."
Racionais MC's

ABSTRACT

NOGUEIRA. G. A. **Higher-order QCD in Higgs to gluon gluon**. 2024. 116p. Dissertation (Master in Science) - Instituto de Física de São Carlos, Universidade de São Paulo, São Carlos, 2024.

One of the most prominent decay channels of the Higgs boson is the decay of the Higgs into two gluons. The decay width $\Gamma(h \to gg)$ starts at second order in the strong coupling α_s and is known up to $\mathcal{O}(\alpha_s^6)$ in perturbative QCD. However, the truncation error of this quantity needs to be investigated, considering that its precise theoretical knowledge is part of crucial tests of the Standard Model of particle physics. In order to achieve better control over this truncation error, it is necessary to know the coefficients at higher order. In this work, we produce accurate estimates for the first unknown coefficient of the Higgs decay into two gluons, at $\mathcal{O}(\alpha_s^7)$. We investigate the coefficients at high orders using rational approximants also known as Padé approximants, in combination with the Borel transform of the series, in addition to employing other methods such as the so-called Dlog Padés, renormalization scheme variation, and conformal mapping. We provide model-independent estimates for the first unknown coefficient, c_5, in the series for the Higgs decay into two gluons. We analyzed two prescriptions for the renormalization of the top-quark mass, considering the dependence on the number of flavors of light quarks, denoted as n_f. For the case of greatest interest, with $n_f = 5$, we obtained estimates of $c_5 = -304 \pm 106$ under the Scale Invariant prescription, and $c_5 = -293 \pm 78$ for the On-Shell top-quark mass. This allows us to assess the intrinsic truncation uncertainty of this quantity in light of our results.

Keywords: QCD. Gluons. Higgs boson.

RESUMO

NOGUEIRA. G. A. **QCD em altas ordens no decaimento do Higgs em dois glúons**. 2024. 116p. Dissertação (Mestrado em ciências) - Instituto de Física de São Carlos, Universidade de São Paulo, São Carlos, 2024.

Um dos canais de decaimento mais proeminentes do bóson de Higgs é o decaimento do Higgs em dois glúons. A largura de decaimento $\Gamma(h \to gg)$ começa em segunda ordem no acoplamento forte α_s e é conhecida até $\mathcal{O}(\alpha_s^6)$ na QCD perturbativa. No entanto, o erro de truncamento dessa quantidade precisa ser investigado, considerando que seu conhecimento teórico faz parte dos testes cruciais do Modelo Padrão da física de partículas. Para obter um controle mais preciso sobre esse erro de truncamento, é necessário conhecer os coeficientes de ordem superior. Neste trabalho, produzimos estimativas precisas para o primeiro coeficiente desconhecido do decaimento do Higgs em dois glúons, em $\mathcal{O}(\alpha_s^7)$. Investigamos os coeficientes em ordens elevadas usando aproximantes racionais, também conhecidos como aproximantes de Padé, em combinação com a transformada de Borel da série, além de empregar outros métodos, como os chamados Dlog Padés, variação de esquema de renormalização e mapeamento conforme. Fornecemos estimativas independentes de modelo para o primeiro coeficiente desconhecido, c_5, na série para o decaimento do Higgs em dois glúons. Analisamos duas prescrições para a renormalização da massa do quark top, considerando a dependência no número de sabores de quarks leves, denotado como n_f. Para o caso de maior interesse, com $n_f = 5$, obtivemos estimativas de $c_5 = -304 \pm 106$ sob a prescrição Invarante de Escala e $c_5 = -293 \pm 78$ para a massa do quark top On-Shell, permitindo-nos avaliar a incerteza intrínseca de truncamento dessa quantidade à luz de nossos resultados.

Palavras-chave: QCD. Glúons. Bóson de Higgs.

Contents

1 Introduction

The Standard Model of particle physics (SM) is the theory that incorporates the fundamental particles present in the universe and their interactions (except for gravity) (1). The history of the Standard Model is rooted in the development of gauge theories. Its origins trace back to the formulation of Quantum Electrodynamics (QED) in the 1940s by Dirac, Tomonaga, Schwinger, and Feynman (2–5), providing a precise description of electromagnetic interaction among charged particles. The introduction of non-abelian gauge theories, such as SU(2) and SU(3), was essential to describe strong forces among quarks, representing a significant contribution by Gell-Mann (6), Ne'eman (7), and others. Quantum Chromodynamics (QCD) has arisen as the fundamental gauge theory of the strong interactions, characterized by the $SU(3)_c$ group (8). The subscript c signifies that this group is associated with color symmetry. This theory governs strong interactions, elucidating the dynamics of the interactions between quarks and the eight gluons.

In the 1970s, a significant breakthrough occurred with the unification of electromagnetic and weak interactions in the electroweak theory by Glashow, Salam, and Weinberg (9–11). Despite the elegance of the eletroweak theory, a significant challenge was evident: particles did not exhibit mass. This gap was bridged with the discovery of the Higgs mechanism, proposed independently in the 1960s by François Englert, Robert Brout, Peter Higgs (12,13), representing a crucial advance in understanding particle physics. The central idea is the existence of a scalar field, called the Higgs field, permeating all space. Some of the elementary particles interact with this field and, in doing so, acquire mass.

The Standard Model incorporates the Higgs Mechanism to explain the origin of elementary particle masses. In the SM, the Higgs boson is the particle associated with the Higgs field. Its experimental discovery in 2012 at the Large Hadron Collider (LHC) (14) at CERN was a a significant achievement, validating the existence of this mechanism. Then, the SM interactions can be divided into sectors, reflecting the type of interaction. In the context of this work, the sectors of strong interaction and the Higgs boson sector stand out, as the primary focus is on the decay of the Higgs boson into two gluons.

In perturbative QCD, the width of the Higgs decay into two gluons $\Gamma(h \to gg)$ is currently known up to α_s^6 (15). Among the key decays of the Higgs boson is the decay $h \to gg$, representing the second principal decay channel of the Higgs boson. In the context of exploring Higgs physics, considering the absence of new physics observations at the LHC, an approach to search for physics beyond the Standard Model (BSM) is precision physics. An important quantity in this context is the signal strength μ, defined as the ratio of the experimental cross-section for Higgs production multiplied by Higgs decay in a specific channel, divided by the same quantity obtained through theoretical predictions in the Standard Model. This implies that if the Standard Model adequately

describes the analyzed processes, this quantity should be equal to one. The combination of ATLAS and CMS data (16) provides a averaged signal strength of $\mu = (1.09 \pm 0.11)$, this implies the necessity to attain higher levels of theoretical precision, to verify if the experiments and the theory are indeed fully consistent. To increase the accuracy of theory predictions, obtaining high-order cross-sections and decay widths in perturbation theory is necessary. It is essential to note that, although the Higgs decay into two gluons is not currently measured at the LHC, precise theoretical knowledge of this decay can enhance the theoretical accuracy of the process $gg \to h$, thus assisting in identifying any deviation in μ, if it exists.

Corrections at high orders for the decay of the Higgs into two gluons are calculated in an effective theory where the top quark mass is considered much larger than the typical energy scale of the process. The top quark mass is $m_t = 173$ GeV, while the Higgs mass is $m_h = 125$ GeV. In the calculation of the decay $h \to gg$, mass corrections are expressed in terms of a parameter $\tau = (m_h/m_t)^2 \approx 0.52$. Despite not being very close to zero, the coefficients multiplying the powers of τ further suppress these corrections, generating small mass corrections. Under these conditions for the calculation of loop diagrams it is reasonable to employ the limit where $m_t \to \infty$, resulting in an effective theory with five dynamical quark flavours. This limit is known as heavy-top limit (17).

The evaluation at high orders presents many theoretical and computational challenges (15), several years are required to perform a calculation at the next order in perturbation theory. Perhaps, the term at $\mathcal{O}(\alpha_s^7)$ will never be calculated. Given this state of affairs, we have performed the estimates for the coefficient of order $\mathcal{O}(\alpha_s^7)$ of the decay width of the Higgs boson into two gluons, using Padé Approximants (PAs), which is a model-independent method widely used in the literature for estimating unknown coefficients in perturbation theory, providing reliable estimates with realistic errors. This method involves employing a ratio of two polynomials to approximate a series. By matching the expansion of the rational approximant to the Taylor series of the function of interest, it is possible to determine all the free parameters of the Padé (provided sufficient information is available), and thereby one can reconstruct the function and obtain estimates of higher-order Taylor-series coefficients. Here, we use variants of the methods employed in Refs. (18–21).

Currently, in QCD processes, at most the first four or five coefficients in perturbation theory are known. In other words, only a small amount of information is available about the series. Therefore, to investigate the estimation methods employed in this work, we used the large-β_0 limit of QCD (22) for the gluon-gluon correlator D_{G^2}. A fundamental advantage of working in this limit is that the quantities analyzed in it can be evaluated to all orders in perturbation theory, serving as a kind of laboratory to test our estimates made by Padé Approximants. However, it is important to emphasize that the correlator D_{G^2} and the decay width $\Gamma(h \to gg)$ are different quantities, so that different methods

can be used to investigate them.

The large-β_0 limit is an extension of the large-n_f limit, where the number of flavors, n_f, tends to infinity ($n_f \to \infty$), while the product $\alpha_s n_f$ remains of order $\mathcal{O}(1)$. Consequently, α_s scales as $1/n_f$. In this limit, the analysis focuses on evaluating an infinite number of $q\bar{q}$ bubble corrections to the gluon propagators, where each of these bubbles contributes at $\mathcal{O}(1)$. These bubbles are proportional to the ferminonic contribution to leading order coefficient of the QCD beta function $\beta_{0f} = -n_f/6\pi$. Then, the large-β_0 limit is reached by replacing the fermionic contribution with the complete β_0 term: $\beta_{0f} \to \beta_{0f} + \beta_{0A}$. Here, the non-abelian term β_{0A} is taken into account, ensuring that β_0 has the correct sign, recovering the asymptotic freedom characteristics of QCD coupling. This procedure is called *naive non-Abelianization* (22).

In the large-β_0 limit, it is possible to investigate the behavior of series at high orders. The series in QCD are expected to be divergent, and it is conjectured that these series are asymptotic. In this context, it is known that this divergence is related to the factorial growth of the coefficients. At a certain order N, the contribution $N!$ of this coefficient is no longer suppressed by the small value of α_s^N, and the series diverges. The divergences of these series can be better investigated through the so-called Borel transform —in terms of a new variable u — that suppresses the factorial growth of the coefficients by dividing them by $N!$. The singularities of the Borel transform present on the real axis of this transformation, with integer values of u, are called renormalons and govern the behaviour of the series for high orders.

In addition, we employed several types of Padé Approximants evaluated in conjunction with methods of varying the renormalization scheme (23) and conformal mapping (24), analyzed in the gluon-gluon correlator in the large-β_0 limit. Variation in the renormalization scheme can be used to change the relative weight of each renormalon, while the conformal mapping of the Borel plane was employed to examine the behavior of the correlator after modifying the relative weight of the different renormalon singularities.

This dissertation is structured as follows. In Chapter 2, an overview of the Standard Model, with a focus on Higgs boson physics and Quantum Chromodynamics, is presented. Chapter 3 explores the details of the Higgs boson decay into two gluons at LO, providing insights into the current status of this decay in perturbation theory. Chapter 4 introduces the methods utilized for estimation and details the calculation of the gluon-gluon correlator in the large-β_0 limit. Moving on to Chapter 5, it reveals the results obtained in large-β_0, discussing the convergence properties of the analyzed perturbative series. This discussion encompasses the use of Padé approximants, variation of the renormalization scheme, and conformal mapping. Finally, Chapter 6 presents the ultimate results of the decay $h \to gg$ estimation at higher orders, accompanied by a discussion on the intrinsic uncertainty associated with truncation and an analysis of variations in the renormalization scale.

2 The Standard Model of Particle Physics

The Standard Model (SM) of particle physics is characterized by the combination of the symmetry groups of the electroweak interaction, $\mathrm{SU}(2)_L \otimes \mathrm{U}(1)_Y$, composed of the weak isospin interaction of left-handed particles and hypercharge, along with the strong sector represented by the $\mathrm{SU}(3)_C$ symmetry group, which describes quantum chromodynamics (QCD), the interaction of quarks and gluons that carry color charge. In addition to these interactions, the SM also includes the Higgs boson and its interactions. The SM characterizes a universe evolving in a manner that leads to spontaneous symmetry breaking, causing dissociations among the fundamental interactions of nature. The electroweak symmetry breaking, which accounts for the electromagnetic and weak interactions between quarks and leptons, contains rich information regarding the role of the Higgs boson and its interactions, responsible for giving mass to the fundamental particles in the SM.

For sake of simplicity we can start by investigating how Dirac's Lagrangian,

$$\mathscr{L}_D^0 = i\bar{\psi}\gamma^\mu\partial_\mu\psi, \tag{2.1}$$

without the mass term gives rise to QED due to the *gauge principle*, i.e., the requirement that the Lagrangian must be invariant under local gauge transformations. In Eq. (2.1), ψ represents the fermionic field, and $\bar{\psi}$ is the adjoint of ψ, which is $\bar{\psi} = \psi^\dagger\gamma^0$.

The Eq. (2.1) is clearly invariant under a global transformation, where the phase parameter α does not depend on space-time coordinates in the transformation $\psi \to \psi' = e^{i\alpha}\psi$. The dynamics of quantum field theories are constructed to be invariant under local phase transformations, i.e., when the fields transform with $\alpha \equiv \alpha(x)$. Hence, for a local transformation, the massless Dirac Lagrangian changes to

$$\mathscr{L}_D^0 \to \mathscr{L}_D^{0'} = \bar{\psi}i\gamma^\mu\partial_\mu\psi + \bar{\psi}\gamma^\mu\psi\partial_\mu\alpha(x). \tag{2.2}$$

Then, the second term of Eq. (2.2) tells us that this Lagrangian is not invariant under local phase transformation due to the appearance of a term coupling the fermionic current $j^\mu = \bar{\psi}\gamma^\mu\psi$ and the term $\partial_\mu\alpha(x)$. Consequently, for the Dirac Lagrangian to be invariant under local phase transformation, we need to couple j^μ with a new vector field, the gauge field A_μ — such that $\mathscr{L}_D^0$ becomes a new Lagrangian $\mathscr{L}_D^0(\psi, A_\mu)$ —, and after the phase transformation in the fermionic field, a specific transformation in photon field, A_μ, will be necessary for maintaining the Lagrangian invariant under this gauge transformation. To verify this, it is necessary to analyze how the modified Lagrangian transforms

$$\mathscr{L}_D^0(\psi, A_\mu) \to \mathscr{L}_D^{0'}(\psi, A_\mu) = \bar{\psi}i\gamma^\mu\partial_\mu\psi + ej^\mu\left(A_\mu + \frac{1}{e}\partial_\mu\alpha(x)\right). \tag{2.3}$$

So, to keep (2.3) invariant, we must perform the transformation, called *gauge transformation*

$$A_\mu \to A'_\mu = A_\mu - \frac{1}{e}\partial_\mu\alpha(x), \tag{2.4}$$

such that

$$\mathscr{L}_D^0(\psi', A'_\mu) = \mathscr{L}_D^0 + \mathscr{L}_{int}. \tag{2.5}$$

Where $\mathscr{L}_{int} = ej^\mu A_\mu$ represents the interaction term of the Lagrangian. However, in addition to the interaction term, A_μ must contribute a kinetic term $\mathscr{L}_k$, as it must also have its own kinematic Lagrangian. This term is

$$\mathscr{L}_k = -\frac{1}{4}F_{\mu\nu}F^{\mu\nu}. \tag{2.6}$$

Here, $F_{\mu\nu} = \partial_\mu A_\nu - \partial_\nu A_\mu$ represents the electromagnetic field tensor, and A_μ represents the particle associated with this field, which is the photon. In light of this, we can indeed write the total Lagrangian as

$$\mathscr{L}(\psi,A_\mu) = i\bar{\psi}\gamma^\mu(\partial_\mu - ieA_\mu)\psi + \mathscr{L}_k = i\bar{\psi}\gamma^\mu D_\mu\psi + \mathscr{L}_k. \tag{2.7}$$

Here, due to the gauge transformation, there is a transition from ∂_μ to another derivative called the covariant derivative

$$D_\mu = \partial_\mu - ieA_\mu. \tag{2.8}$$

Concluding that, to build a theory invariant under local field transformations, it is necessary to modify the derivative in order to preserve local gauge invariance. This is the principle that is generalized in other sectors of the SM, as we discuss briefly in the next sections.

2.1 Strong Interaction Sector

The next step in building the standard model of particle physics is the description of strong interactions, which are described by quantum chromodynamics and aim at explaining the interaction between the constituents of hadrons, i.e., quarks and gluons (25). The existence of a vast number of baryons and mesons isolated is an indication that there is still a more fundamental level in this picture. Baryons (B) are composed of three quarks, and mesons (M) consist of a quark-antiquark pair

$$B = \frac{1}{\sqrt{6}}\varepsilon^{\alpha\beta\gamma}|q_\alpha q_\beta q_\gamma\rangle, \qquad M = \frac{1}{\sqrt{3}}\delta^{\alpha\beta}|q_\alpha \bar{q}_\beta\rangle, \tag{2.9}$$

where $\varepsilon^{\alpha\beta\gamma}$ is the Levi-Cevita tensor, $\delta^{\alpha\beta}$ is the Kronecker delta and each quark q carries a corresponding new quantum number, represented by the index α, with α = 1,2,3, or commonly identified by colors: red, green, and blue.

The necessity of incorporating this new quantum number arises in order for hadrons to obey Fermi-Dirac statistics. In the case of the Δ^{++} hadron — without the inclusion of the color number —, which is composed of three quarks $u^\uparrow u^\uparrow u^\uparrow$ with spins in the same direction and consequently with zero relative angular momentum the wave function is symmetric and therefore does not respect the correct statistics. It is necessary that, in order for Fermi-Dirac statistics to be respected, a new quantum number be introduced. In

this case, the required quantum number is the color charge, which needs at least 3 colors to produce an antisymmetric state as

$$\Delta^{++} = \frac{1}{\sqrt{6}}\varepsilon^{\alpha\beta\gamma}|u^{\uparrow}_{\alpha}u^{\uparrow}_{\beta}u^{\uparrow}_{\gamma}\rangle. \tag{2.10}$$

The construction of QCD is based on the color symmetry group of this interaction, the $SU(3)_C$ group. The choice of this symmetry group arises from a series of tests based on certain conditions (25)

- The quarks must belong to the triplet representation of the group, because $N_c = 3$;
- The triplet representation of this group must be complex, as quarks and anti-quarks are distinct states.

This uniquely restricts the $SU(3)_C$ group as the representative of this symmetry since, among compact Lie groups, there are only four with three-dimensional representations: $SO(3) \simeq SU(2) \simeq Sp(3)$ and $SU(3)$. However, three of them are isomorphic to each other, which directly leads us to the $SU(3)$ group as the only one that satisfies the listed conditions, as the triplet representation of the $SO(3)$ group is real.

A Lie group emerges from the elements of a Lie algebra through the process of exponential mapping (26). Lie algebras, when adhering to specific conditions, can exhibit diverse structures, giving rise to a variety of algebras. Within this framework, the concepts of roots and weights are crucial in shaping the algebra's structure.

The roots, generally denoted as α, are indispensable for understanding the internal mechanisms of a Lie algebra. They originate from the eigenvalues of the adjoint representation, providing crucial insights into how the algebra can be decomposed into simpler components. The unique combinations and properties of roots lead to the emergence of different algebras, each with its own distinct characteristics.

On the other hand, weights, represented as λ, are associated with elements within a Cartan subalgebra of the Lie algebra (26, 27). They clarify how algebraic elements behave under specific transformations. When combined with the information derived from roots, weights offer a comprehensive perspective on the algebra's representation theory. Fundamental weights, in particular, constitute a fundamental set, enabling the characterization of irreducible representations and enhancing our understanding of the underlying algebraic structures.

After selecting the symmetry group of the interaction, it is important to mention the postulate that quarks must be confined and cannot be found isolated in nature. Therefore, the hadrons are represented by the product of the representations of each quark (or anti-quark) that constitutes it. The decomposition of products of this reducible representations into irreducible representations must contain at least one singlet state, as hadrons are color singlets. A concrete example of this decomposition can be found in Appendix A.

2.2 QCD Lagrangian

Non-Abelian gauge theories, also known as Yang-Mills theories, exhibit greater complexities compared to theories like QED, mainly because in this case, there is interaction among the gauge bosons of the theory. In the scattering process $gg \to ggg$, for example, there are around 10000 terms present in tree-level calculations (1). The starting point for performing perturbative calculations in QCD is to work with Feynman rules, which can be extracted from the Lagrangian of this theory. To describe the dynamics of strong interactions, we must have a Lagrangian invariant under local transformations of the $SU(3)_C$ group. A first starting point to achieve the QCD Lagrangian is Dirac's Lagrangian, $\mathscr{L}_D$, for the quark fields q_α^f, as follows

$$\mathscr{L}_D = \sum_f \bar{q}_\alpha^f (i\gamma^\mu \partial_\mu - m_f) q_\alpha^f, \tag{2.11}$$

where the index f refers to the quark flavor and m_f is the quark mass. Calling the generators of the fundamental representation of the algebra as λ^a, with a = 1,2...,8, the field transforms as

$$q_f^\alpha \longrightarrow (q_\alpha^f)' = G_{\alpha\beta}\, q_f^\alpha \equiv \left[\exp\left(-ig_s \frac{\lambda^a}{2}\theta_a\right)\right]_{\alpha\beta} q_\alpha^f, \tag{2.12}$$

where g_s represents the coupling of strong interaction and θ_a denotes a phase parameter, which remains constant under global transformations, while in local transformations, $\theta \equiv \theta(x)$ depends on the spacetime coordinates. The Lagrangian in Eq. (2.11) preserves its invariance under global transformations, but under local transformations, it transforms as follows

$$\begin{aligned}\mathscr{L}_D \to \mathscr{L}'_D =& \mathscr{L}_D + \frac{i}{2}\bar{q}^f{}_\alpha(x)\gamma_\mu[G^\dagger(x)\partial^\mu G(x)]_{\alpha\beta} q_\beta^f(x) \\ &- \frac{i}{2}\bar{q}_\alpha^f(x)\gamma_\mu[(\partial^\mu G^\dagger)G(x)]_{\alpha\beta} q_\beta^f(x),\end{aligned} \tag{2.13}$$

which is clearly not invariant under the transformation. The prescription used to obtain an invariant Lagrangian is, again, the modification in the derivative $\delta_{\alpha\beta}\partial^\mu$ by the covariant derivative:

$$D_{\alpha\beta}^\mu \equiv \delta_{\alpha\beta}\partial^\mu - ig_s \frac{\lambda^a}{2} A_a^\mu(x), \tag{2.14}$$

wich act in a quarks field as

$$D'^\mu_{\alpha\beta}(x) q_\beta^f(x) = G(x)_{\alpha\gamma} D^\mu_{\gamma\delta} q_\delta^f(x). \tag{2.15}$$

Here, A_a^μ denotes the gluon field and $T^a = \lambda^a/2$ are the generators of su(3) algebra, up to a constant. Additionally, it is already possible to write a gauge-invariant Lagrangian. However, this Lagrangian does not describe the equation of motion for the gluon field. To accomplish this, we can add terms to ensure the completeness of the dynamics of this

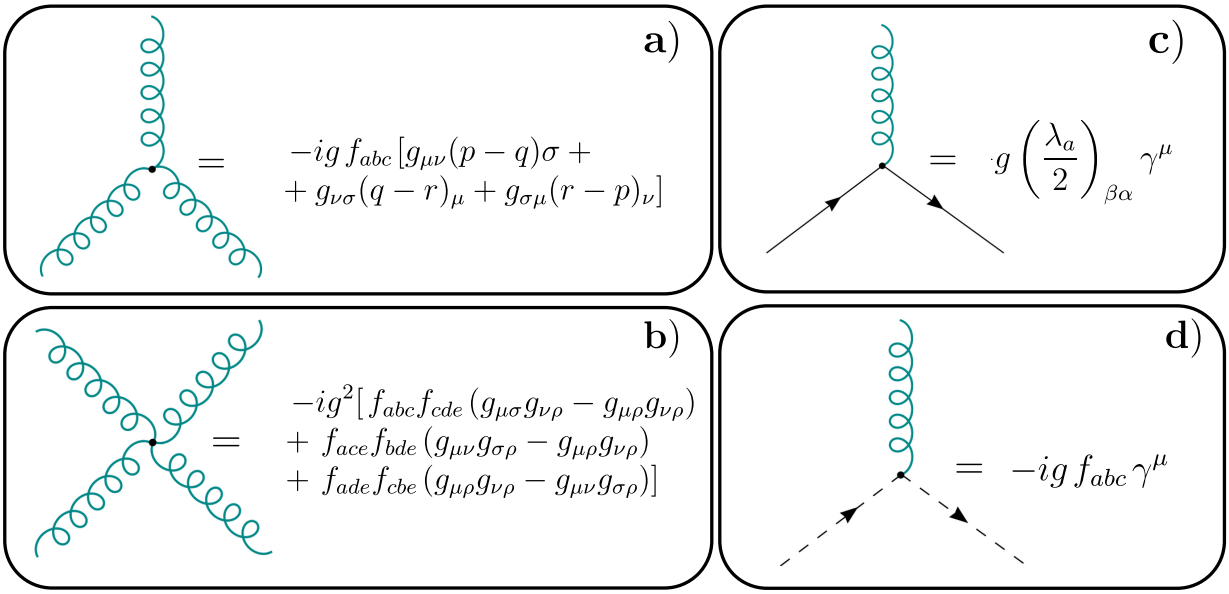

Figure 2.1 – QCD Feynman Diagrams: In parts **a)** and **b)**, the self-interaction terms of 3 and 4 legs among the gluons are depicted. In figure **c)**, the explicit interaction vertices between quarks and gluons are shown, while in part **d)**, it illustrates the interaction between gluons and the theory's ghosts. In these parts, we are considering $g \equiv g_s$.

Source: By the author.

field, as long as the invariance is maintained, which are the field tensors of QCD, obtained directly from the commutation relation

$$G^{\mu\nu}(x) \equiv \frac{i}{g_s}[D^\mu, D^\nu] = \partial^\mu A_a^\nu - \partial^\nu A_a^\mu - ig_s[A_a^\mu, A_a^\nu] \equiv \frac{\lambda^a}{2}G_a^{\mu\nu}. \tag{2.16}$$

Here, it is possible to express the tensor as

$$G_a^{\mu\nu}(x) = \partial^\mu A_a^\nu - \partial^\nu A_a^\mu + g_s f^{abc} A_b^\mu A_c^\nu, \tag{2.17}$$

playing a crucial role in the computation of the gluon-gluon correlator discussed in Chapter 4. This quantity holds significant importance in the scope of this work. Keeping this in mind, the Lagrangian of QCD can be written as

$$\mathscr{L}_{\text{QCD}}^{(0)} \equiv -\frac{1}{4}G_a^{\mu\nu}G_{\mu\nu}^a + \sum_f \bar{q}_\alpha^f(i\gamma^\mu D_\mu - m_f)q_\alpha^f. \tag{2.18}$$

In this compact form, the types of interactions contained in this theory are not evident, but if we expand the terms of Eq. (2.18), we arrive at

$$\begin{aligned}\mathscr{L}^{(0)}_{\text{QCD}} &= -\frac{1}{4}(\partial^\mu A^\nu_a - \partial^\nu A^\mu_a)(\partial_\mu A^a_\nu - \partial_\nu A^a_\mu) + \sum_f \bar{q}^f_\alpha (i\gamma^\mu \partial_\mu - m_f) q^f_\alpha \\ &- \frac{g_s}{2} f^{abc}(\partial^\mu A^\mu_a - \partial^\nu A^\mu_a) A^b_\mu A^c_\nu - \frac{g_s^2}{2} f^{abc} f_{ade} A^\mu_b A^\nu_c A^d_\mu A^e_\nu \\ &+ g_s A^\mu_a \sum_f \bar{q}^f_\alpha \gamma_\mu \left(\frac{\lambda^a}{2}\right)_{\alpha\beta} q^f_\beta.\end{aligned} \tag{2.19}$$

In the first line, one can observe the presence of terms that give rise to the propagators of gluons and quarks, whereas in the second line, terms stemming from the non-abelian character of this theory, which underlie the three- and four-legged interactions among gluons, are evident. Lastly, in the third line, the color interaction term between quarks and gluons is depicted.

These interactions can be encoded in the Feynman rules of this theory, as illustrated in Figure 2.1, with the exception of interaction 2.1 **d)**. This is because, in the case of QCD, there is an additional complication related to a non-physical contribution that arises in perturbative calculations due to complexities in the quantization of the theory, stemming from the A^μ_a field having four Lorentz degrees of freedom, while the massless spin-1 gluon possesses only two of them. The problem mainly appears in the component A^0_a, which does not satisfy the standard second quantization. One possible solution is to adopt a non-covariant quantization, similar to the Gupta-Bleuler QED quantization (28), but this trick increases the complexity of computations. The better way to solve this problem is by introducing unphysical particles that cancel the unphysical spin contributions; these particles are referred to as ghosts. These ghosts are spin-zero particles obeying Dirac statistics and must be considered in the Lagrangian of the theory.

The first modification is to maintain covariant quantization, which can be preserved by adding a gauge-fixing term $\mathscr{L}_{GF} = -(\partial^\mu A^\mu_0)(\partial_\nu A^\nu_0)/\xi$. The second one involves introducing ghost dynamics to the gluon field through its kinematical term and coupling it with the gluon field by employing modifications to the covariant derivative (25)

$$\mathscr{L}_{\text{QCD}} = \mathscr{L}^{(0)}_{\text{QCD}} - \frac{1}{\xi}(\partial^\mu A^\mu_0)(\partial_\nu A^\nu_0) + (\partial_\mu \bar{c}^a)(\delta^{ac}\partial_\mu + g f^{abc} A^b_\mu) c^c.$$

Here, we denote the ghost field as c^i, where i represents the color index.

2.3 Standard Model Lagrangian

The Lagrangian of the Standard Model, introduced in the 1970s (9, 11, 29), provides a comprehensive formulation that explains the interactions among elementary particles and the fundamental forces in particle physics. This theoretical framework has gained universal acceptance due to its success in describing the behavior of subatomic particles observed in experiments.

Table 2.1 – Hypercharge of fermion families of equation 2.20

	L_i	e_{R_i}	Q_i	u_{R_i}	d_{R_i}
Y_f	-1	-2	$1/3$	$4/3$	$-2/3$

Source: By the author.

One interesting aspect within the Standard Model that is relevant for the present work is understanding why the Higgs boson does not directly interact with massless particles like gluons. To investigate the decay of the Higgs boson into two gluons, it is essential to study the matter fields within the Standard Model. These fields consist of three generations of left-handed chiral leptons and quarks, known as weak isodublets. Additionally, there are right-handed fermions, which are isospin singlets under weak interaction (30)

$$\begin{aligned}
L_1 &= \begin{pmatrix}\nu_e\\ e^-\end{pmatrix}_L, \; e_{R_1} = e^-_R, \qquad Q_1 = \begin{pmatrix}u\\ d\end{pmatrix}_L, \; u_{R_1} = u_R, d_{R_1} = d_R;\\
L_2 &= \begin{pmatrix}\nu_\mu\\ \mu^-\end{pmatrix}_L, \; e_{R_2} = \mu^-_R, \qquad Q_2 = \begin{pmatrix}c\\ s\end{pmatrix}_L, \; u_{R_2} = c_R, d_{R_2} = s_R;\\
L_3 &= \begin{pmatrix}\nu_\tau\\ \tau^-\end{pmatrix}_L, \; e_{R_3} = \tau^-_R, \qquad Q_3 = \begin{pmatrix}t\\ b\end{pmatrix}_L, \; u_{R_3} = t_R, d_{R_3} = b_R.
\end{aligned} \tag{2.20}$$

In the provided context, left-handed or right-handed fermions $f_{L/R}$ are particles that satisfy the following relation

$$f_{L,R} = \frac{1}{2}(1 \pm \gamma_5) f. \tag{2.21}$$

The equation 2.21 involves the use of projection operators. The right-handed P_R and left-handed P_L projection operators, denoted by $P_R = (1 + \gamma_5)/2$ and $P_L = (1 - \gamma_5)/2$ respectively, are applied to the fermion f to obtain the corresponding right-handed and left-handed components. Here, $\gamma_5 \equiv i\gamma^0\gamma^1\gamma^2\gamma^3$, and f represents the fermion field.

The electroweak interaction, defined in terms of on left-handed fermions, involves the hypercharge number Y_f of the fermion. The hypercharge is defined in terms of the third component of weak isospin I^3_f and electric charge Q_f as follows

$$Y_f = 2(Q_f - I^3_f), \tag{2.22}$$

where the third component of weak isospin is the projection of weak isospin in the z-direction. Additionally, the theory necessitates the condition that the sum over fermion families, with each sum component explicitly stated in the second row of table 2.1, must be zero

$$\sum_f Y_f = \sum_f \left(2Q_f - 2I^3_f\right) = 0, \tag{2.23}$$

to cancel the chiral anomalies (31, 32) of the theory.

In the electroweak sector the gauge fields are B_μ and W^i_μ, with i = 1,2,3. The next topic to be mentioned is about the self-interaction between the gauge bosons, originating from non-Abelian theories. If we denote the previously mentioned gauge fields as V_μ (both W_μ and A_μ), with coupling g_i, the non-Abelian nature of the algebra corresponding to the symmetry groups of this interaction leads to self-interaction terms in these fields via coupling with three and four gauge bosons.

As already demonstrated in QED and QCD, the conventional approach used for employing the gauge principle is through the covariant derivative, resulting in a single type of coupling between fermions and gauge fields of the form $-g_i\bar{\psi}V_\mu\gamma^\mu\psi$, which couples these two types of fields minimally. For instance, within the derivative

$$D_\mu\psi = \left(\partial_\mu - ig_sT_aA^a_\mu - \frac{i}{2}gW^a_\mu\sigma^a - \frac{i}{2}g'B_\mu\right)\psi, \tag{2.24}$$

where g_s, g, and g' represent, respectively, the strong coupling and the W^a_μ and B_μ couplings. Here, σ^a are the Pauli matrices. With this in mind, it is possible to write the Lagrangian of SM without the mass terms for the bosons and fermions as follows

$$\begin{aligned}\mathscr{L}^{(0)}_{SM} = &-\frac{1}{4}G^a_{\mu\nu}G^{\mu\nu}_a - \frac{1}{4}W^a_{\mu\nu}W^{\mu\nu}_a - \frac{1}{4}B_{\mu\nu}B^{\mu\nu} + i\bar{L}_iD_\mu\gamma^\mu L_i + i\bar{e}_{R_i}D_\mu\gamma^\mu e_{R_i} + \\ &+ i\bar{Q}_iD_\mu\gamma^\mu Q_i + i\bar{u}_{R_i}D_\mu\gamma^\mu u_{R_i} + i\bar{d}_{R_i}D_\mu\gamma^\mu d_{R_i}.\end{aligned} \tag{2.25}$$

A crucial principle that must be addressed at this point is the gauge invariance of the theory. The SM is constructed to be invariant under transformations of the product of symmetry groups for each interaction group: $\mathrm{SU}(3)_C \otimes \mathrm{SU}(2)_L \otimes \mathrm{U}(1)_Y$.

Similarly to what was previously developed for QED, ignoring the fermion mass, we can also do it for the SM lagrangian indicated by Eq. (2.41). Restricting only to the electroweak sector of the standard model, the left-handed fermionic fields $L(x)$ and the right-handed ones $R(x)$ transform as follows

$$\begin{aligned}L(x) \to L'(x) &= e^{i\xi_a(x)\sigma^a/2 \, + \, i\beta(x)Y}L(x), \\ R(x) \to R'(x) &= e^{i\beta(x)Y}R(x).\end{aligned}$$

In this expression, $\xi_a(x)$ is a phase parameter of the SU(2) group and carries the dependence on spacetime coordinates, while $\beta(x)$ parametrizes the transformations of the U(1) group. These changes in the fields give rise to a gauge transformation similar to the minimal coupling observed in QED, as illustrated in Eq. (2.4)

$$W(x) \to W_\mu - \frac{1}{g}\partial_\mu\xi(x) - \xi(x)W_\mu, \tag{2.26}$$

$$B_\mu(x) \to B_\mu(x) - \frac{1}{g'}\partial_\mu\beta(x). \tag{2.27}$$

Eq. (2.27) shares the same structure with (2.4), with a slight distinction as compared to Eq. (2.26). An important fact to consider at this point in the development is that the

unification of the electromagnetic interaction with the weak force has not been discussed yet. This relationship is achieved through the Weinberg-Salam ([10,11]) mixing

$$A_\mu = \sin\theta_w W_\mu^3 + \cos\theta_w B_\mu, \tag{2.28}$$

$$Z_\mu = \cos\theta_w W_\mu^3 - \sin\theta_w B_\mu. \tag{2.29}$$

These equations allow the bosons Z_μ and A_μ to be obtained through the fields of the electroweak interaction and the mixing angle θ_w.

At this point, an interesting question arises. The invariance of the Lagrangian under the mentioned transformations no longer holds true when adding mass terms to the weak sector. In purely SU(3) QCD, gauge bosons are massless, while quark masses can be introduced with a term of the form $-m_q\bar{\psi}\psi$ that respect the gauge invariance but breaks the isospin symmetry. Other example can be visualized when we introduce terms like $\frac{1}{2}M_V^2 W_\mu W^\mu$, knowing that the mass of this boson is experimentally observed, gauge symmetry is broken. Taking QED as an example, a question in this context would be: why do photons not possess a mass? Essentially, the reason is that Gauge symmetry is explicitly broken by a photon mass term

$$\frac{1}{2}m_\gamma^2 A_\mu A^\mu \rightarrow \frac{1}{2}m_\gamma^2(A_\mu - \frac{1}{e}\partial_\mu\alpha)(A^\mu - \frac{1}{e}\partial^\mu\alpha), \tag{2.30}$$

which is clearly not gauge invariant and would, therefore, break the electroweak symmetry of the Lagrangian of the Standard Model. Similarly, when adding mass terms for fermions, the isospin symmetry is broken.

So, despite Yang-Mills Theory elegantly describing the interactions of the Standard Model, there remained the problem of finding a mechanism capable of assigning mass to particles while preserving gauge symmetry. This mechanism is known as the Higgs mechanism.

2.4 Higgs Mechanism

The mechanism that acts as the generator of mass for elementary particles is based on spontaneous symmetry breaking. To better understand how this situation develops, it is possible to analyze the Lagrangian of the purely electroweak sector along with the Higgs Lagrangian

$$\mathscr{L}_{\text{EW}} = -\frac{1}{4}\left(W_{\mu\nu}^a\right)^2 - \frac{1}{4}B_{\mu\nu}^2 + \mathscr{L}_H(\Phi), \tag{2.31}$$

$$W_{\mu\nu}^a = \partial_\mu W_\nu^a - \partial_\nu W_\mu^a + g\varepsilon^{amn}W_\mu^m W_\nu^n, \qquad B_{\mu\nu} = \partial_\mu B_\nu - \partial_\nu B_\mu. \tag{2.32}$$

Here, the Higgs sector is represented by $\mathscr{L}_H(\Phi)$ and is essentially constituted by the covariant derivative defined in (2.24) and the Higgs potential represented by the quadratic and quartic terms in the Higgs field according to

$$\mathscr{L}_H = (D_\mu\Phi)^\dagger(D_\mu\Phi) + m^2|\Phi|^2 - \lambda|\Phi|^4, \tag{2.33}$$

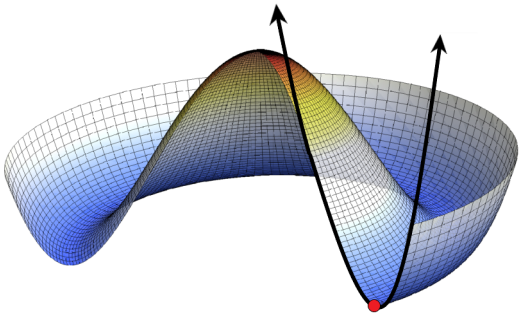

Figure 2.2 – Higgs potential with qualitative color distribution.

Source: By the author.

where the m^2 is the mass parameter and λ is coupling. The Higgs field, denoted as Φ, is a complex doublet with a hypercharge of 1, also known as the Higgs multiplet. This field is responsible for generating masses for the gauge bosons of this interaction through spontaneous symmetry breaking (SSB), which leads to a non-zero vacuum expectation value. The field Φ is defined in terms of four other scalar fields

$$\Phi = \begin{pmatrix} \phi^+ \\ \phi^0 \end{pmatrix}, \tag{2.34}$$

two for the charged part ϕ^+ and two for the neutral part ϕ^0. The neutral component, after symmetry breaking, introduces a perturbation in the form of a real field $h(x)$ around the vacuum expectation value v. This choice not only simplifies the representation of the Higgs field but also aligns with the concept of unitary gauge, which basically chooses the $\mathrm{SU}(2)_L$ phase transformation ξ^a equal to zero

$$\Phi = \exp\left\{ i\frac{\sigma_a}{2}\xi^a(x) \right\} \begin{pmatrix} 0 \\ v + h(x) \end{pmatrix} \xrightarrow{\xi^a = 0} \frac{1}{\sqrt{2}} \begin{pmatrix} 0 \\ v + h(x) \end{pmatrix}, \tag{2.35}$$

enabling an analysis of quantized excitations above the true vacuum state along the radial direction.

Within the Higgs sector, a kinematical component involves the covariant derivative, and an interaction component is described by the Higgs potential, as can be visualized in Figure (2.2). The potential is depicted in terms of the real and imaginary components of the Higgs field. The red point on the figure indicates the chosen minimum of the potential, a condition met when $m^2 < 0$, leading to spontaneous symmetry breaking. Therefore, adopting a unitary gauge permits the analysis of quantized excitations solely above the real vacuum state in the radial direction, denoted by the black arrows. This limitation arises due to the presence of infinitely degenerate vacua connected by rotational symmetry within the potential.

In light of SSB, the Higgs sector Lagrangian can be reformulated as follows

$$\mathscr{L}_H = \frac{1}{2}(\partial_\mu h)^2 + \frac{g}{8}(W_\mu^1 + iW_\mu^2)(W_\mu^1 - iW_\mu^2)(v+h)^2 + \frac{1}{8}(gW_\mu^3 - g'B_\mu)^2(v+h)^2 - V(\Phi),$$

where the second term in the previous equation allows for the identification of bosons that possess charge

$$W_\mu^\pm = \frac{1}{\sqrt{2}}(W_\mu^1 \mp iW_\mu^2), \tag{2.36}$$

where $\tan\theta_w = g'/g$. In order to rewrite the Higgs Lagrangian by expanding the quadratic terms and already considering equations (2.36) and (2.29), resulting in (33)

$$\begin{aligned}\mathscr{L}_H = {} & \frac{1}{2}(\partial_\mu h)^2 - \lambda v^2 h^2 - \lambda v h^3 - \frac{1}{4}\lambda h^4 + \frac{1}{4}g^2 v^2 W_\mu^- W^{\mu+} + \frac{g^2 v^2}{8cos^2\theta_w} Z_\mu Z^\mu \\ & + \frac{1}{2}g^2 v W_\mu^- W^{\mu+} h + \frac{g^2}{4cos^2\theta_w} Z_\mu Z^\mu v h + \frac{g^2}{8cos^2\theta_w} Z_\mu Z^\mu h^2 + \frac{1}{4}g^2 W_\mu^- W^{\mu+} h^2. \end{aligned} \tag{2.37}$$

Therefore, the Lagrangian provides the way in which gauge bosons interact with the Higgs boson, shown in the second line of Eq. (2.37), in addition to the mass terms of the gauge bosons that arise after spontaneous symmetry breaking, which in this context is known as the Higgs mechanism. An interesting point to note in this Lagrangian is the presence of 3- and 4-legged self-interaction terms for the physical Higgs field. These terms contribute to the self-energies of this field and are responsible for assigning mass to the Higgs boson (34).

2.5 Yukawa Coupling

The Yukawa coupling (35) describes the strength of the interaction between a scalar or pseudoscalar field with a fermionic field. In the context of the SM of particle physics, Yukawa couplings play a crucial role in explaining the masses of elementary particles through the coupling of the Higgs field Φ and the fermionic fields. These couplings are governed by the usual constraints, such as the requirement of gauge invariance and renormalizability (36, 37).

The Yukawa Lagrangian density is given by (32)

$$\mathscr{L}_{\text{Yukawa}} = -\lambda_e \bar{L}\Phi e_R - \lambda_d \bar{Q}\Phi d_R - \lambda_u \bar{Q}\tilde{\Phi} u_R + \text{h.c.} \tag{2.38}$$

where λ_i is the Yukawa coupling constant, and $\tilde{\Phi} = i\sigma_2\Phi^\dagger$ has hypercharge $Y = -1$.

To elucidate the origin of mass, consider the vacuum expectation value of the scalar field Φ, denoted as v, which is non-zero due to the breaking of electroweak symmetry according to the Eq. (2.35). By substituting Φ with $v + h$, where h is the Higgs boson, the Yukawa Lagrangian density can be expanded as follows

$$\begin{aligned}\mathscr{L}_{\text{Yukawa}} &= -\frac{1}{\sqrt{2}}\lambda_e(\bar{\nu}_e, \bar{e}_L)\begin{pmatrix} 0 \\ v+h \end{pmatrix} e_R + \cdots \\ &= -\left(1 + \frac{h}{v}\right)\frac{\lambda_e v}{\sqrt{2}}\bar{e}_L e_R + \text{ h.c } + \cdots. \end{aligned} \tag{2.39}$$

In this expanded form (2.39), it is evident, following the same development for all terms of Eq. (2.38), that the mass terms are

$$m_e = \frac{\lambda_e v}{\sqrt{2}},\ m_u = \frac{\lambda_u v}{\sqrt{2}},\ m_d = \frac{\lambda_d v}{\sqrt{2}}. \tag{2.40}$$

Therefore, at this point, we have a mechanism for generating mass for gauge bosons of weak interaction and also for fermions, in order to preserve the gauge symmetry of the theory. This occurs through the spontaneous breaking of the SU(2) × U(1) symmetry. With the elements discussed so far, it is possible to rewrite the Lagrangian of the Standard Model

$$\begin{aligned}\mathscr{L}_{SM} = &-\frac{1}{4}G^a_{\mu\nu}G^{\mu\nu}_a - \frac{1}{4}W^a_{\mu\nu}W^{\mu\nu}_a - \frac{1}{4}B_{\mu\nu}B^{\mu\nu} + i\bar{L}_i D_\mu \gamma^\mu L_i + i\bar{e}_{R_i} D_\mu \gamma^\mu e_{R_i} + \\ &+ i\bar{Q}_i D_\mu \gamma^\mu Q_i + i\bar{u}_{R_i} D_\mu \gamma^\mu u_{R_i} + i\bar{d}_{R_i} D_\mu \gamma^\mu d_{R_i} \\ &- \lambda_e \bar{L}\Phi e_R - \lambda_d \bar{Q}\Phi d_R - \lambda_u \bar{Q}\tilde{\Phi} u_R + \text{h.c.} \\ &+ (D_\mu \Phi)^\dagger (D_\mu \Phi) + m^2|\Phi|^2 - \lambda|\Phi|^4.\end{aligned} \tag{2.41}$$

With the interactions of the Higgs boson discussed in relation to other particles in the standard model, we can understand why this boson does not directly interact with gluons or photons. The Higgs boson, denoted as h, does not couple to massless particles. However, one of the primary methods of detecting the Higgs is through the decay process $h \to \gamma\gamma$, or via one of the most prominent decay channels of the Higgs boson, which is the decay $h \to gg$. These two processes occur through a loop involving other particles that interact with the Higgs boson, particularly, weak interaction bosons and quarks. This specific class of interaction shall be elucidated in Chapter 3.

2.6 Aspects of QCD Renormalization

The observable quantities in Quantum Field Theory (QFT) are mainly cross sections and decays rates, which depend on the square of transition amplitudes. Their computation can be expressed in terms of vacuum expectation values of the time-ordered product of n-point function which go under the name of Green functions (38)

$$G(x_1, x_2, ..., x_n) \equiv \langle\Omega|T\{\phi(x_1), \phi(x_2), ..., \phi(x_n)\}|\Omega\rangle, \tag{2.42}$$

where $|\Omega\rangle$ stands for the non-perturbative vacuum, i.e., the ground state of a full Hamiltonian of the theory in Heisenberg representation, such as $H|\Omega\rangle = 0$. The field $\phi(x_n)$ is a generic field. This Green function contains, in perturbation theory, all diagrams, connected and disconnected. To eliminate the disconnected vacuum diagrams which do not contribute to S-matrix elements, it is necessary to use the Gell-Mann-Low theorem (6)

$$G_c(x_1, x_2, ..., x_n) = \frac{\langle 0|T\{\phi^{(0)}(x_1), \phi^{(0)}(x_2), ..., \phi^{(0)}(x_n) \exp\left[i\int \mathrm{d}^4x\, \mathscr{L}^{(0)}_{int}(x)\right]\}|0\rangle}{\langle 0|T\{\exp\left[i\int \mathrm{d}^4x\, \mathscr{L}^{(0)}_{int}(x)\right]\}|0\rangle}. \tag{2.43}$$

Where the subscript c indicates connected diagrams, and $\mathscr{L}_{\text{int}}$ represents the interaction part of the Lagrangian density. Furthermore, the denominator eliminates all disconnected diagrams from the numerator. In this context, "connected" implies that every segment of the diagram is linked to at least one of the external legs. The function $G_c(x_1, x_2, ..., x_n)$ can be affected by divergences that can be initially analyzed through the superficial degree of divergence.

For exploring the emergence of infinities, we can start by considering a Lagrangian (38)

$$\mathscr{L} = \mathscr{L}_0 + \sum_i g_i \mathscr{L}_i, \tag{2.44}$$

with a free part $\mathscr{L}_0$, which is the sum of kinematic terms, and an interaction part $\mathscr{L}_i$ and coupling given by g_i. We will make the assumption here that $\mathscr{L}_i(x)$ has f_i fermionic fields, b_i bosonic fields, and ∂_i partial derivatives, which have, respectively, dimensions of $M^{3/2}$, M, and M. In this context, it is useful to employ dimensional analysis to $\mathscr{L}$, which must have dimension $[\mathscr{L}(x)] = M^4$, and as a direct consequence, the dimension of the coupling is

$$[g_i] = M^{4-d_i}, \tag{2.45}$$

with

$$d_i \equiv \frac{3}{2} f_i + b_i + \partial_i; \tag{2.46}$$

which has a huge importance in the analysis of the superficial degree of divergence ($\mathscr{D}$). This quantity $\mathscr{D}$ is defined as the power of momentum k in the numerator (that comes from vertices) minus the power of k in the denominator (due to the propagator).

After the derivation of Feynman rules according section 2.3, the amplitudes of these diagrams can be built, and these amplitudes are, in most cases, divergent. One tool to analyze this behavior is computing $\mathscr{D}$ by employing the external (internal) bosons ϕ_e (ϕ_i) and external (internal) fermions ψ_e (ψ_i), along with the total vertex number. According to (38)

$$\mathscr{D} = -\sum_i n_i(4 - d_i) - \left(\frac{3}{2}\psi_e + \phi_e - 4\right), \tag{2.47}$$

where the value of $\mathscr{D}$ defines the type of contribution, whether finite or not, to the given process. If $\mathscr{D} = 0, 1, 2, 3, \ldots$, the contribution is logarithmically, linearly, quadratically, or cubically divergent, respectively. It is also possible to have a negative value of $\mathscr{D}$. In these cases, we say that the contribution is superficially convergent, implying that the momentum integral can be either finite or not. In fact, there are proofs that a Feynman diagram provides a finite contribution to the S-matrix if this and all sub-diagrams (higher orders) are superficially convergent.

In the Eq. (2.47), it is evident that couplings satisfying $4 - d_i \geq 0$ are necessary to observe a finite number of superficially divergent diagrams. Fortunately, QCD is renormalizable — essentially implying that the infinite quantities can be absorbed by

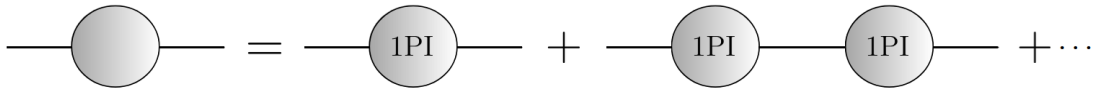

Figure 2.3 – Contributions of self-interaction of the quarks present in the Dyson series. The rightmost loops represent the 1-particle irreducible (1PI) contributions of the propagator.

Source: By the author.

redefining a finite number of coupling constants and masses. Moreover, its superficial degree of divergence is

$$\mathscr{D}_{\text{QCD}} = 4 - \frac{3}{2}\psi_e - \phi_e. \tag{2.48}$$

The main point in this section is how to treat the divergences from quark and gluon self-energies. By employing the superficial degree of divergence in these cases, we obtain

$$\psi_e = 2, \phi_e = 0 \Rightarrow \mathscr{D} = 1,\ \mathscr{D}_{\text{eff}} = 0, \tag{2.49}$$

for the quark self-energy and

$$\psi_e = 0, \phi_e = 2 \Rightarrow \mathscr{D} = 2,\ \mathscr{D}_{\text{eff}} = 0, \tag{2.50}$$

for the gluon self-energy. Here, $\mathscr{D}_{\text{eff}}$ represents the effective degree of divergence that remains after the computation. Generally, certain Green functions are necessarily proportional to powers of external momenta or masses, which decrease the degree of divergence. For example, in the quark self-energy, terms such as p and m are present. On the other hand, the gluon self-energy contains the term $(k^\mu k^\nu - k^2 g^{\mu\nu})$, which ultimately leads to a divergence degree of zero in the final result.

2.6.1 Quark Self-Energy

Before probing into the modifications of the gluon propagator due to self-energy corrections, it is essential to examine a renormalization case in QCD where it will be necessary to introduce specific renormalization constants Z_m and Z_g for the quark mass m and the coupling g, respectively. In this context, the relevant Green function is expressed in momentum space as follows (39)

$$S_{\alpha\beta}(p) = -i \int d^4x\, \mathrm{e}^{ip\cdot x} \langle 0|T q_\alpha(x)\bar{q}_\beta(0)\mathrm{e}^{i\int d^4z \mathscr{L}_{int}(z)}|0\rangle, \tag{2.51}$$

where α and β are the color indices, and $\mathscr{L}_{\text{int}}$ is the interaction part of the Lagrangian. The most general form of the quark propagator, considering irreducible bubble diagrams as shown on the right-hand side of Figure 2.3, can be expressed as a Dyson series

$$S_{\alpha\beta}(q^2) = \delta_{\alpha\beta} S^{(0)}(q^2) - \delta_{\alpha\beta} S^{(0)}(q^2)\Sigma(q^2)S^{(0)}(q^2) + \cdots. \tag{2.52}$$

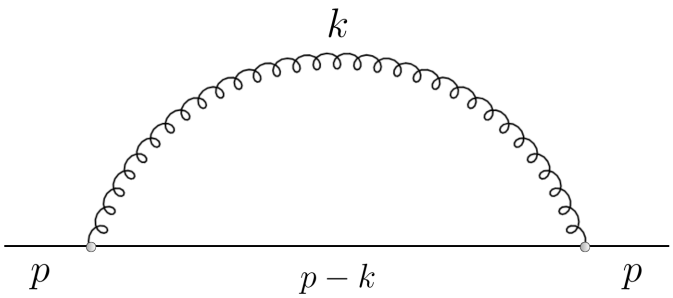

Figure 2.4 – Feynman diagram showing the first-order quark propagator correction.

Source: By the author.

This series considers the one-particle irreducible diagram (1P1), which cannot be split into two different diagrams by removing one line. In Eq. (2.52), $S^{(0)}(q^2)$ represents the bare quark propagator (39)

$$S^{(0)}_{\alpha\beta}(q^2) = \frac{q+m}{q^2-m^2+i\varepsilon}. \tag{2.53}$$

Summing the terms in Eq. (2.52), it simplifies to

$$iS(p) = i\frac{1}{p-m-\Sigma(p)+i\varepsilon}. \tag{2.54}$$

The modification in the quark's self-energy up to order α_s is indicated in Figure 2.4 and is given by (39)

$$\Sigma^{(1)}(p) = ig_s^2 C_F \int \frac{d^D k}{(2\pi)^D} \frac{[\gamma^\mu(p-k+m)\gamma^\nu]}{k^2[(p-k)^2-m^2]} \left[g_{\mu\nu} - (1-\xi)\frac{k_{\mu\nu}}{k^2}\right]. \tag{2.55}$$

Here g_s represents the QCD coupling. In order for the coupling of the theory to be dimensionless, a scale parameter $\mu^{-2\varepsilon}$ is introduced, and the integrals are solved using methods outlined in chapter 3. It is necessary to separate $\Sigma(p)$ into two parts

$$\Sigma(p) = p\Sigma_p + m\Sigma_m(p), \tag{2.56}$$

where each component requires solving different loop computations (38), yielding the results (39)

$$\Sigma^{(1)}_p(p) = \xi\frac{C_F}{4}\frac{\alpha_s}{\pi}\left[-\frac{1}{\varepsilon} + \ln\frac{m^2}{\mu^2} - 1 - \frac{m^2}{p^2} + \left(1-\frac{m^4}{p^4}\right)\ln\left(1-\frac{p^2}{m^2}\right)\right], \tag{2.57}$$

$$\Sigma^{(1)}_m(p) = \frac{C_F}{4}\frac{\alpha_s}{\pi}\left[(3-\xi)\left(\frac{1}{\varepsilon} - \ln\frac{m^2}{\mu^2}\right) - 4 + 2\xi - (3+\xi)\left(1-\frac{m^2}{p^2}\right)\ln\left(1-\frac{p^2}{m^2}\right)\right]. \tag{2.58}$$

In these equations, $\alpha_s \equiv g_s^2\mu^{-2\varepsilon}/4\pi$. Note that these equations exhibit the expected behavior for Green functions as they are analytical functions of p^2 for $p^2 < m^2$. However, as $\varepsilon \to 0$, the quantities become infinite, requiring renormalization.

As QCD is a renormalizable theory, all Green functions in this theory must remain finite after redefining the parameters in the Lagrangian. These redefinitions should cancel the divergences arising from loop corrections to these Green functions. In the framework of Quantum Field Theory, physical quantities in nature do not depend on the renormalization scheme; this independence must be analyzed through the renormalization group. To discuss the renormalization group equation, it is necessary to define how the renormalized quantities are related to the bare quantities

$$q_\alpha(x) = Z_{2F}^{1/2} q_\alpha^R(x) \qquad \text{and also} \qquad m = Z_m m^R. \tag{2.59}$$

Here, the quantities on the right-hand side are the renormalized quantities, while those on the left-hand side are referred to as bare quantities.The factor $1/2$ appears in Z_{2F} because of the bilinear form $\bar{\psi}\Gamma\psi$ in the terms of the Lagrangian, where Γ is a 4×4 matrix. The difference between these quantities lies in the renormalization constants, which are quantities representable in perturbation theory, canceling the divergences order by order ([39])

$$Z_{2F} = 1 + \frac{\alpha_s}{\pi} Z_{2F}^{(1)} + \mathcal{O}(\alpha_s^2), \qquad Z_m = 1 + \frac{\alpha_s}{\pi} Z_m^{(1)} + \mathcal{O}(\alpha_s^2). \tag{2.60}$$

By considering the inverse of the quark propagator, the renormalization constants give rise to additional terms originating from both the kinetic and mass components of the QCD Lagrangian

$$S^{-1}(p) = p + pZ_{2F}^{(1)} \frac{\alpha_s}{\pi} - m^R - m^R (Z_m^{(1)} + Z_{2F}^{(1)}) \frac{\alpha_s}{\pi} - p\Sigma_p^{(1)}(p) - m^R \Sigma_m^{(1)}(p). \tag{2.61}$$

Requiring this expression to be finite, in conjunction with the outcomes from Eq. (2.57), results in

$$Z_m^{(1)} = -\frac{3}{4} C_F \frac{1}{\hat{\varepsilon}}, \qquad \text{and} \qquad Z_{2F}^{(1)} = -\xi \frac{C_F}{4} \frac{1}{\hat{\varepsilon}}. \tag{2.62}$$

This holds true for the $\overline{\text{MS}}$ scheme, commonly known as the modified minimal subtraction scheme. Minimal subtraction schemes involve removing the $1/\varepsilon$ term that appears in the final result of loop integrals. The main difference between $\overline{\text{MS}}$ and MS is that in the latter, only the singular term as $\varepsilon \to 0$ is removed, whereas in the modified scheme, certain constants such as $\ln(4\pi)$ and the Euler-Mascheroni constant γ are also subtracted along with the divergent part.

2.6.2 Resummed Gluon Propagator

The most general form of the gluon propagator is similar to Eq. (2.52). Despite the difference in the nature of the particles, the Dyson series has the same structure. The

free gluon propagator will be denoted by $D^{(0)\mu\nu}$, and the gluon self-energy as $\Pi_{\lambda\rho}(k)$. Furthermore, in this case, we will multiply the Dyson series by a four-momentum k_μ, since this can produce a huge simplification in computations

$$ik_\mu D^{\mu\nu}(k) = ik_\mu D^{\mu\nu}(k) + ik_\mu D^{\mu\lambda}(k)\Pi_{\lambda\rho}(k)iD^{\rho\nu}(k) + \cdots \tag{2.63}$$

To develop the Eq. (2.63), we can employ the Slanov-Taylor identity (38)

$$k_\mu k_\nu D^{\mu\nu}_{ab} = k_\mu k_\nu D^{(0)\mu\nu}_{ab}(k), \tag{2.64}$$

which basically state that in perturbation theory, the non-transverse part of the gluon propagator is equal to the non-transverse part the free propagator. Taking into account the condition (2.64), Eq. (2.63) can be reformulated as

$$ik_\mu D^{(0)\mu\lambda}[i\Pi_{\lambda\rho}(k)]\left\{iD^{(0)\rho\nu}(k) + iD^{(0)\rho\tau}(k)\,[i\Pi_{\lambda\rho}(k)]\,iD^{(0)\sigma\nu} + \cdots\right\}, \tag{2.65}$$

and as a direct consequence, it is possible to write

$$-\xi\frac{1}{k^2+i\eta}k^\lambda i\Pi_{\lambda\rho}(k)iD^{\rho\nu} = 0, \tag{2.66}$$

which leads to the following relation

$$k_\mu\Pi^{\mu\nu} = k_\nu\Pi^{\mu\nu} = 0. \tag{2.67}$$

Furthermore, the correlation function can be written in the Lorentz invariant form, which will be useful for scrutinizing the $h \to gg$ process using the low-energy theorem, as demonstrated in Chapter 3, where the correlator is written with the following Lorentz-invariant structure

$$\Pi^{\mu\nu} = [k^\mu k^\nu - k^2 g^{\mu\nu}]\Pi(k^2), \tag{2.68}$$

which is justified by effective superficial degree of divergence beeing zero. Taking these things into consideration, we were able to write the propagator equation in a more simplified way than before

$$iD^{\mu\nu} = iD^{(0)\mu\nu}(k) + iD^{(0)\mu\lambda}[i\Pi_{\lambda\rho}(k)]iD^{\rho\nu}(k). \tag{2.69}$$

In this context, it is necessary to use the equation for the free gluon propagator

$$iD^{(0)\mu\nu}_{ab} = \delta_{ab}i\left[-g_{\mu\nu} + (1-\xi)\frac{k_\mu k_\nu}{k^2+i\eta}\right], \tag{2.70}$$

in addition to the condition (2.67) in Eq. (2.69), to arrive at

$$D_{\mu\nu}(k^2) = \left[\left(-g_{\mu\nu} + \frac{k_\mu k_\nu}{k^2}\right)\frac{1}{1+\Pi(k^2)} - \xi\frac{k_\mu k_\nu}{k^2}\right]\frac{1}{k^2}, \tag{2.71}$$

which is a fundamental component for exploring the two-gluon correlator, as will be shown later.

2.7 The Renormalization Group: Coupling and Mass Evolution

The exploration of the differential form of renormalization invariance began with Stueckelberg and Perterman (40), as well as Gell-Mann and Low (6). Then, the investigation into scaling in quantum field theory, driven by experimental observations of Bjorken scaling in deep inelastic scattering during electron-proton collisions, led to the development of the Callan-Symanzik equations (41, 42). These equations serve as potent tools for examining the constraints imposed by renormalization invariance on the behavior of Green's functions at small distances.

The physical quantities in nature do not depend on the renormalization scheme, in other words, there exists a unique value for these quantities. However, from the perspective of QFT the Green functions will be denoted as $\Gamma \equiv \Gamma(q, \alpha_s, m)$, where q represents the external momentum, are constructed in a way that ensures this independence through the Renormalization Group Equation, which exhibits invariance under the renormalization group.

Let us choose two renormalization schemes R and R'. The renormalized Green functions Γ_R and $\Gamma_{R'}$ are

$$\begin{aligned} \Gamma_R &= Z(R)\Gamma, \\ \Gamma_{R'} &= Z(R')\Gamma, \end{aligned} \tag{2.72}$$

where the two schemes can be related through the parameter $Z(R',R)$ as

$$\Gamma_{R'} = Z(R',R)\Gamma_R, \tag{2.73}$$

where

$$Z(R',R) = Z(R')/Z(R). \tag{2.74}$$

At this point, we will consider arbitrary schemes R and R'. Additionally, we will introduce a third scheme, denoted as R'', such as to satisfy the composition structure

$$Z(R'',R) = Z(R'',R')Z(R',R). \tag{2.75}$$

To each element $Z(R',R)$, we can associate an inverse and a unite element, respectively (38, 39)

$$Z^{-1}(R',R) = Z(R,R'), \qquad Z(R,R) = 1.$$

Here, we can clearly see that the group has forbidden some schemes by the composition rule since $Z(R_i,R_j)Z(R_k,R_e)$ is not an element of the group unless the product rule is respected, i.e., in the case where $R_j = R_k$. Therefore, not any renormalization scheme will be possible for a quantity in QFT, only those that satisfy the groupoid structure presented here are allowed.

Besides the renormalization scheme, it is important to investigate the variation of quantities as the renormalization scale μ changes. A physical observable must be invariant under this quantity since it is arbitrarily introduced in the regularization process, and this invariance is encoded in the equation

$$\mu\frac{d}{d\mu}\Gamma(q,a_s,m)=\left\{\mu\frac{\partial}{\partial\mu}+\mu\frac{da_s}{d\mu}\frac{\partial}{\partial a_s}+\mu\frac{dm}{d\mu}\frac{\partial}{\partial m}\right\}\Gamma(q,\alpha_s,m)=0, \tag{2.76}$$

So that, from the Eq. (2.76), it is possible to define the functions

$$\gamma(a_s)\equiv-\frac{\mu}{m}\frac{dm}{d\mu}=\sum_{n=1}^{\infty}\gamma_n a_s^n, \tag{2.77}$$

which is known as the anomalous dimension, and

$$\beta(a_s)\equiv-\mu\frac{da_s}{d\mu}=\sum_{n=1}^{\infty}\beta_n a_s^{n+1}, \tag{2.78}$$

is called the Beta function. Both functions take into account the dependence of quantities on the renormalization parameter. Then, replacing these functions in Eq. (2.76) makes it possible to write the full renormalization equation, known as the Callan–Symanzik equation

$$\left[\mu\frac{\partial}{\partial\mu}-\beta(a_s)\frac{\partial}{\partial a_s}-\gamma(a_s)m\frac{\partial}{\partial m}\right]\Gamma(q,\alpha_s,m)=0. \tag{2.79}$$

Currently, the β and γ functions are known up to $\mathcal{O}(a_s^5)$ (43).

In order to show how these functions work, starting with the quark mass, it can be integrated employing separation of variables

$$\int_{m(\mu_1)}^{m(\mu_2)}\frac{dm}{m}=\ln\frac{m(\mu_2)}{m(\mu_1)}=-\int_{\mu_1}^{\mu_2}\frac{d\mu}{\mu}\gamma(a_s)=\int_{a_s(\mu_1)}^{a_s(\mu_2)}da_s\frac{\gamma(a_s)}{\beta(a_s)}, \tag{2.80}$$

wich can be written as

$$m(\mu_2)=m(\mu_1)\exp\left[\int_{a_s(\mu_1)}^{a_s(\mu_2)}\mathrm{d}a_s\frac{\gamma_m(a_s)}{\beta(a_s)}\right]. \tag{2.81}$$

The β and γ_m functions are invariant with respect to the quark mass. In fact, due to these properties, the ratio of the masses $m(\mu_1)/m(\mu_2)$ is invariant. On the other hand, the effect on the evolution of the top-quark mass does not have a significant impact on the decay of the Higgs boson into two gluons (15) and can be neglected.

Furthermore, the function $\beta(a_s)$ can also be obtained by solving the differential equation

$$\int_{a_s(\mu_1)}^{a_s(\mu_s)}\frac{\mathrm{d}a}{\beta(a_s)}=-\int_{\mu_1}^{\mu_s}\frac{\mathrm{d}\mu}{\mu}=\ln\frac{\mu_1}{\mu_2},$$

which for one loop can be solved analytically

$$\int_{a_s(\mu_1)}^{a_s(\mu_2)}\frac{\mathrm{d}a_s}{\beta_1 a_s^2}=\frac{1}{\beta_1}\left[\frac{1}{a_s(\mu_1)}-\frac{1}{a_s(\mu_2)}\right]=\ln\frac{\mu_1}{\mu_2}, \tag{2.82}$$

where the coupling can be rewritten as

$$a_s(\mu_2) = \frac{a_s(\mu_1)}{1 - a_s(\mu_1)\beta_1 \ln(\mu_1/\mu_2)}. \tag{2.83}$$

From this equation, it becomes evident that at high energies, quarks exhibit the phenomenon of asymptotic freedom (44, 45), behaving as if they are freely moving particles. However, in the low-energy regime, the coupling becomes significantly large, approaching infinity at the Landau pole. The evolution profile of $\alpha_s(Q)$ is depicted in Figure 2.5, displaying the global average of the coupling at the mass of the Z^0 boson along with its corresponding error. At low values of Q, only a few determinations are available, whereas in the regime where $Q \gg \Lambda_{\mathrm{QCD}}$, numerous extractions are provided.

The $\beta(a_s)$ function is currently known up to five loops, thanks to the work by Baikov et al.(43), which employs a different convention for the derivative. In our convention, according to Eq. (2.78), the coefficients in terms of n_f are

$$\beta_1 = \frac{11}{2} - \frac{n_f}{3}, \quad \beta_2 = \frac{51}{4} - \frac{19}{12}n_f, \quad \beta_3 = \frac{2857}{64} - \frac{5033}{576}n_f + \frac{325}{1728}n_f^2,$$

$$\beta_4 = \frac{149753}{768} - \frac{891}{32}\zeta_3 - \left(\frac{1078361}{20736} + \frac{1627}{864}\zeta_3\right) n_f + \left(\frac{50065}{20736} + \frac{809}{1296}\zeta_3\right) n_f^2 + \frac{1093}{93312}n_f^3,$$

$$\begin{aligned}\beta_5 =& \frac{8157455}{8192} + \frac{621885}{1024}\zeta_3 - \frac{88209}{1024}\zeta_4 - \frac{144045}{256}\zeta_5 \\ &- \left(\frac{336460813}{995328} + \frac{1202791}{10368}\zeta_3 - \frac{33935}{3072}\zeta_4 - \frac{1358995}{13824}\zeta_5\right) n_f \\ &+ \left(\frac{25960913}{995328} + \frac{698531}{41472}\zeta_3 - \frac{5263}{2304}\zeta_4 - \frac{5965}{648}\zeta_5\right) n_f^2 \\ &- \left(\frac{630559}{2985984}\frac{24361}{62208}\zeta_3 - \frac{809}{6912}\zeta_4 - \frac{115}{1152}\zeta_5\right) n_f^3 + \left(\frac{1205}{1492992} - \frac{19}{5184}\zeta_3\right) n_f^4.\end{aligned} \tag{2.84}$$

Through the result obtained from Eq. (2.83), it is possible to determine the QCD scale parameter

$$\Lambda_{\mathrm{QCD}}^{\text{1-loop}} = \mu \mathrm{e}^{-\frac{1}{\beta_1 a_s(\mu)}}.$$

In the first instance, it is important to note that $\frac{\mathrm{d}\Lambda}{\mathrm{d}\mu} = 0$, and therefore, the QCD scale parameter is scale-invariant; however, it is not invariant under the renormalization scheme, since it explicitly shows the dependence on α_s. The same applies to the generalization of Λ to more loops (47), which employs the definition

$$\frac{1}{\tilde{\beta}(a_s)} = \frac{1}{\beta(a_s)} - \frac{1}{\beta_1 a_s^2} + \frac{\beta_2}{\beta_1^2 a_s}, \tag{2.85}$$

this variable change ensures that this alteration (2.85) remains nonsingular as a_s approaches zero for generalization

$$\Lambda = \mu \mathrm{e}^{-\frac{1}{\beta_1 a_s}} \left[a_s(\mu)\right]^{-\frac{\beta_2}{\beta_1^2}} \exp\left(\int_0^{a_s(\mu)} \mathrm{d}a \frac{1}{\tilde{\beta}(a)}\right), \tag{2.86}$$

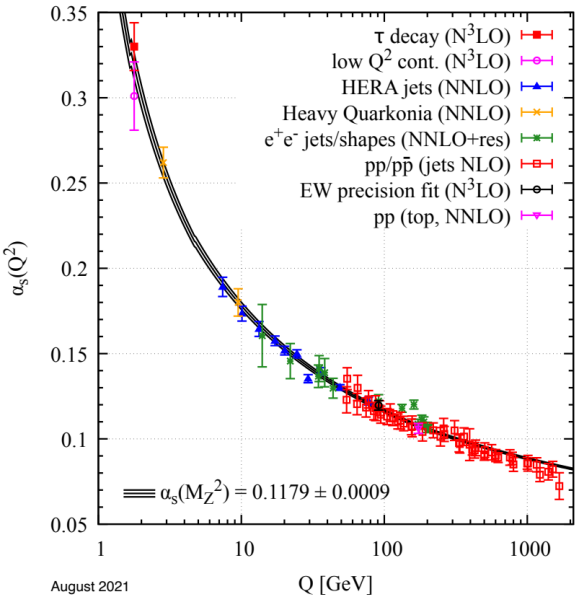

Figure 2.5 – The $\overline{\text{MS}}$ scheme determinations of $\alpha_s(Q)$, as cataloged by the Particle Data Group, are illustrated. The solid lines signify the outcomes derived from solving the renormalization group equation with the five-loop β function, employing the global average of $\alpha_s(m_Z)$ the initial condition.

Source: Adapted from ZYLA *et al.* (46).

which is still valid for more than two loops. Furthermore, note that this equation is still scale-invariant but not renormalization scheme invariant.

In this work, we will employ variations of the renormalization scheme. To understand this idea, we can start with a general case that could represent, e.g., a change from $\overline{\text{MS}}$ to MS. In one of them, we define the reference coupling a_s, and in the other, the modified coupling $\hat{a}_s$. The transition between these two schemes is given in perturbation theory as follows

$$\hat{a}_s = a_s + c_1 a_s^2 + c_2 a_s^3 + c_3 a_s^4 + \cdots \tag{2.87}$$

A well-known result, attributed to Celmaster and Gonsalves (48), guarantees that the relation between Λ and $\hat{\Lambda}$ in the two different schemes is quite straightforward, relying solely on the first non-trivial coefficient, c_1 and the first coefficient of the β function

$$\hat{\Lambda} = \Lambda e^{c_1/\beta_1}, \tag{2.88}$$

where we introduce a new scheme parameter $C = -2c_1/\beta_1$. This allows us to write

$$\hat{\Lambda} = \Lambda e^{-C/2}. \tag{2.89}$$

This parameter C is of fundamental importance in this work, as it parameterizes the relationship between different couplings $a_s(\mu)$ and $\hat{a}_s(\mu)$. In order to obtain the relation between these couplings for any n_f value, we will investigate the relation for a general β

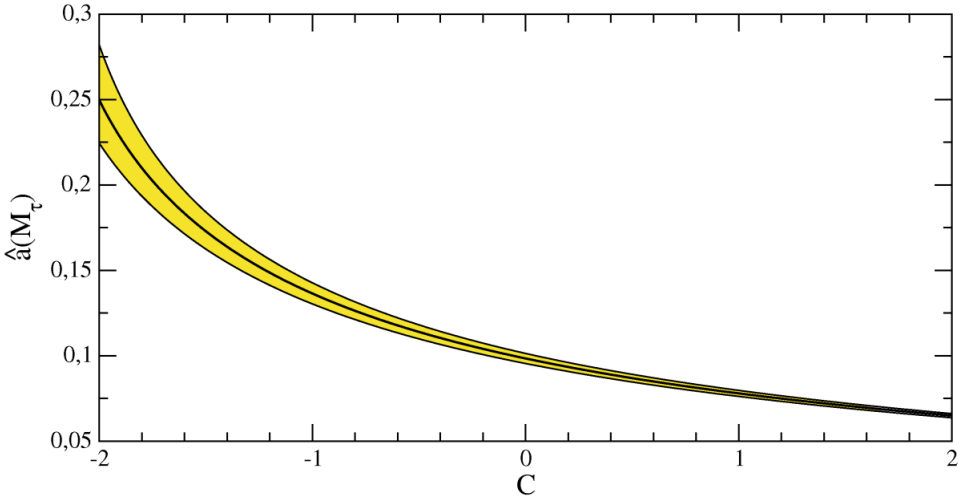

Figure 2.6 – Graphics of strong coupling evaluated at the τ lepton mass $\hat{a}(m_\tau)$ as a function of parameter C. Here, the yellow band represents the α_s uncertainty.

Source: Adapted from BOITO *et al.*([23]).

function, i.e., independent of conventions. We can start with the following relation ([23])

$$\frac{1}{\hat{a}_s} + \frac{\beta_2}{\beta_1}\ln\hat{a}_s - \frac{\beta_1}{2}C = \frac{1}{a_s} + \frac{\beta_2}{\beta_1}\ln a_s - \beta_1\int_0^{a_s}\frac{\mathrm{d}a}{\tilde{\beta}(a)}. \tag{2.90}$$

The equation 2.90 must be solved iteratively in perturbation theory, and the left-side logarithmic term was included to match the right-side logarithmic term, ensuring that no undesirable logarithmic terms are present in the perturbation series. Additionally, the relation between the coupling in a general scheme, a_Q, and the coupling in the $\overline{\text{MS}}$ scheme, given by $\hat{a} \equiv \hat{a}^{C=0}$, is as follows ([23])

$$\frac{1}{a_s} = \frac{1}{\hat{a}_s} + \frac{\beta_2}{\beta_1}\ln\frac{\hat{a}_s}{a_s} + \beta_1\int_0^{a_s}\frac{\mathrm{d}a}{\tilde{\beta}(a)}. \tag{2.91}$$

In the iterative sense its possible, at the first level, to take $a_s \approx \hat{a}_s$ in Eq. (2.91). Furthermore, this involves considering all the terms of the function $\beta(a)$ that are currently known, as specified by Eq. (2.84). Then, in this first approximation

$$\frac{1}{a_s} = \frac{1}{\hat{a}_s} + \beta_1\int_0^{\hat{a}_s}\frac{\mathrm{d}a}{\tilde{\beta}(a)}, \tag{2.92}$$

where it still needs to be expanded in a Taylor series to obtain a series for a_s in terms of $\hat{a}_s$. The exact solution takes the form

$$\begin{aligned}\frac{1}{a_s} = \frac{1}{\hat{a}_s} + \beta_1\Bigg[&\hat{a}_s\left(\frac{\beta_2^2}{\beta_1^3} - \frac{\beta_3}{\beta_1^2}\right) + \hat{a}_s(\mu)^2\left(-\frac{\beta_2^3}{2\beta_1^4} + \frac{\beta_2\beta_3}{\beta_1^3} - \frac{\beta_4}{2\beta_1^2}\right) + \\ &+ \hat{a}_s(\mu)^3\left(-\frac{\beta_2^2\beta_3}{\beta_1^4} + \frac{\beta_2^4}{3\beta_1^5} + \frac{2\beta_2\beta_4}{3\beta_1^3} + \frac{\beta_3^2}{3\beta_1^3} - \frac{\beta_5}{3\beta_1^2}\right) \\ &+ \hat{a}_s(\mu)^4\left(\frac{\beta_2^3\beta_3}{\beta_1^5} - \frac{3\beta_2^2\beta_4}{4\beta_1^4} - \frac{\beta_2^5}{4\beta_1^6} - \frac{3\beta_2\beta_3^2}{4\beta_1^4} + \frac{\beta_2\beta_5}{2\beta_1^3} + \frac{\beta_3\beta_4}{2\beta_1^3}\right) + \mathcal{O}(\hat{a}_s^5)\Bigg].\end{aligned} \tag{2.93}$$

Therefore, when we expand the Eq. (2.93) we obtain the following relation

$$a_s(\mu) = \hat{a}_s(\mu) + \hat{a}_s(\mu)^3\left(\frac{\beta_3}{\beta_1} - \frac{\beta_2^2}{\beta_1^2}\right) + \cdots.$$

The idea is to substitute this result into Eq. (2.91) iteratively until reaching the outcome

$$\begin{aligned} a_s = \hat{a}_s + \hat{a}_s^3\left(\frac{\beta_3}{\beta_1} - \frac{\beta_2^2}{\beta_1^2}\right) + \hat{a}_s^4\left(\frac{\beta_4}{2\beta_1} - \frac{\beta_2^3}{2\beta_1^3}\right) + \\ + \hat{a}_s^5\left(-\frac{3\beta_2^2\beta_3}{\beta_1^3} + \frac{7\beta_2^4}{6\beta_1^4} - \frac{\beta_2\beta_4}{6\beta_1^2} + \frac{5\beta_3^2}{3\beta_1^2} + \frac{\beta_5}{3\beta_1}\right) + \mathcal{O}(\hat{a}_s^6). \end{aligned} \tag{2.94}$$

Using the last equation, we can derive the successive relation between the coupling $\hat{a}_s$ at arbitrary C and a_s

$$\begin{aligned} \hat{a}_s = a_s - \frac{23}{12}Ca_s^2 + \left(\frac{17521}{152352} - \frac{29}{12}C + \frac{529}{144}C^2\right)a_s^3 + \left(\frac{1075144295}{756884736} - \frac{138625}{39744}C + \frac{3335}{288}C^2\right. \\ \left. - \frac{12167}{1728}C^3 - \frac{11027}{2484}\zeta_3\right)a_s^4 + \left[\frac{1743062365679}{278533582848} - \left(\frac{1998367067}{197448192} - \frac{11027}{648}\zeta_3\right)C + \frac{380833}{13824}C^2\right. \\ \left. \frac{199433}{5184}C^3 + \frac{279841}{20736}C^4 + \frac{2149885883}{65816064}\zeta_3 + \frac{11027}{1728}\zeta_4 + \frac{11976865}{476928}\zeta_5\right]a_s^5 + \cdots. \end{aligned} \tag{2.95}$$

Where $\zeta_n = \sum_{k=1}^{\infty} k^{-s}$ is the Riemann zeta function. Futhermore, is possible to get the reverse transformation

$$\begin{aligned} a_s = \hat{a}_s - \frac{23}{12}C\hat{a}_s^2 - \left(\frac{17521}{152352} - \frac{29}{12}C - \frac{529}{144}C^2\right)\hat{a}_s^3 - \left(\frac{1075144295}{756884736} - \frac{63215}{26496}C - \frac{3335}{288}C^2\right. \\ \left. - \frac{12167}{1728}C^3 - \frac{11027}{2484}\zeta_3\right)\hat{a}_s^4 - \left[\frac{1743062365679}{278533582848} + \left(\frac{778160225}{98724096} - \frac{11027}{324}\zeta_3\right)C - \frac{164135}{6912}C^2\right. \\ \left. - \frac{199433}{5184}C^3 - \frac{279841}{20736}C^4 - \frac{2149885883}{65816064}\zeta_3 + \frac{11027}{1728}\zeta_4 + \frac{11976865}{476928}\zeta_5\right]\hat{a}_s^5 + \cdots. \end{aligned} \tag{2.96}$$

It is possible to variably adjust the renormalization scheme to transform the series to be more perturbative or less perturbative, according to the Figure 2.6, which shows in practice the change of the coupling $\hat{a}_s(m_\tau)$ in terms of the C parameter. Here, it will be employed to investigate how the two-gluon correlator (39) changes in relation to the variation of the parameter C. Since, in the large-β_0 limit, as will be discussed later, only the first coefficient of the function $\beta(a)$ is considered, which simplifies the scheme variation, the relation between schemes is simplified, and all terms $\beta_{\geq 2}$ in Eq. (2.94) vanish.

3 Decay of the Higgs into Two Gluons

In the context of the Standard Model, the Higgs boson predominantly decays into bottom quarks $h \to b\bar{b}$. Another significant hadronic decay channel occurs through $h \to gg$, where the interaction between the Higgs and gluons is mainly mediated by the top quark within the SM framework. To compute higher-order QCD corrections for this process, an effective theory known as the heavy-top limit is employed, integrating out the top quark. The use of this effective theory is justified by the hierarchy $m_t \gg m_h$.

In perturbative QCD, the decay width $\Gamma(h \to gg)$ begins at α_s^2 and is currently known up to order α_s^6 (15) in the heavy-top limit. This represents corrections up to the next-to-next-to-next-to-next-to-leading order (N4LO). However, despite efforts to obtain the result at N4LO, the perturbative series in α_s exhibits instabilities due to the choice of renormalization scale, and the hierarchy of different terms is not very well understood. In fact, this series is possibly one of the most problematic series known in perturbative QCD. It has an intrinsic uncertainty of approximately 1%, related to the truncation at α_s^6 (15, 49). This uncertainty is highly significant and needs to be reduced for a future collider, such as the FCC-ee.

In the scenario where the top-quark mass is significantly larger than the Higgs mass ($m_t \to \infty$) and there are n_f massless flavors, the decay process of the Higgs boson into two gluons can be computed using the effective Lagrangian formalism

$$\mathscr{L} = \mathscr{L}_{\text{QCD}}(n_f) - 2^{1/2} G_F^{1/2} C_1 h \, G^a_{\mu\nu} G_a^{\mu\nu}. \tag{3.1}$$

In this expression, G_F represents the Fermi constant, and the second term on the right-hand side of the equation is responsible for the effective coupling between the Higgs boson and gluons. The effective coupling C_1, or Wilson coefficient, accounts for the dependence on the top-quark mass and short-distance α_s corrections. We can extract the formula for the decay width of the Higgs into two gluons from the Eq. (3.1), employing the optical theorem, resulting in (15)

$$\Gamma(H \to gg) = \frac{\sqrt{2} G_F}{m_h} \, |C_1|^2 \; \text{Im}\Pi_{G^2}(-s - i\delta), \tag{3.2}$$

where δ represents an infinitesimal parameter and the decay is evaluated at $s = m_h^2$. It is essential to mention that the standard method for deriving the Wilson coefficient is through a Low-Energy Theorem (LET). The imaginary part of the two-point correlation function of gluons is scrutinized in Ref. (15) through the optical theorem. Both of these theorems will be discussed in the next section.

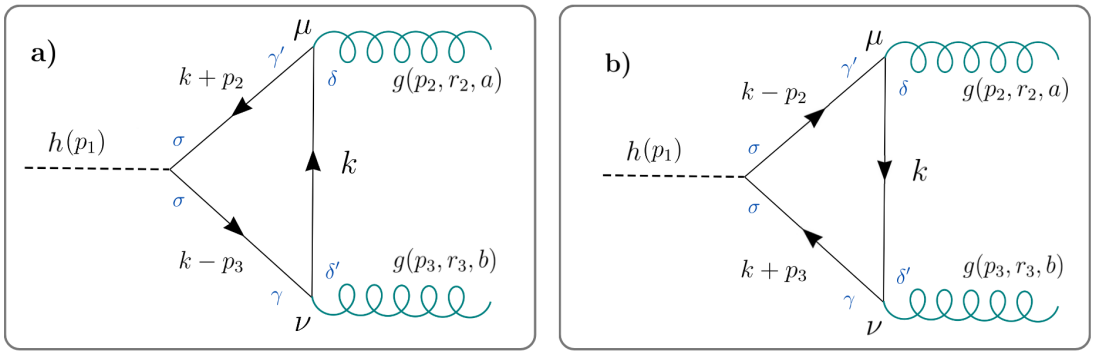

Figure 3.1 – Feynman diagrams for the $h \to gg$ process in leading order.

Source: By the author.

3.1 Higgs Decay into Two Gluons at LO

When studying the decay process of the Higgs boson into two gluons, it is crucial to note that the interaction between the Higgs boson and gauge fields is determined by the mass of the involved field. As a result, at the tree level, the Higgs boson does not directly interact with gluons, as we already mentioned. In the leading order of this decay, a loop involving quarks occurs, as depicted in the diagrams shown in Figure 3.1.

It is important to note, however, that the inclusion of identical particles as final states requires considering another diagram that we need to consider the u-channel contribution as well. This can be achieved by reversing the direction of quarks in the loop. To calculate the decay width of diagram **a)** seen in Figure 3.1, it is necessary to write the amplitude using Feynman rules (50), resulting in

$$\mathcal{M} = -g_s^2 i \frac{m_q}{v} \varepsilon^a_{\mu,r_2} \varepsilon^b_{\nu,r_3} \left(\frac{\lambda^a}{2}\right)_{\delta'\gamma'} \left(\frac{\lambda^b}{2}\right)_{\gamma\delta'} \delta_{\delta\delta'}\delta_{\gamma'\sigma}\delta_{\sigma\gamma} \int \frac{d^4k}{(2\pi)^4} \frac{\mathrm{Tr}[(k-p_3+m_q)\gamma^\nu(k+m_q)\gamma^\mu(k+p_2+m_q)]}{[(k-p_3)^2-m_q^2+i\varepsilon](k^2-m_t^2+i\varepsilon)[(k+p_2)^2-m_q^2+i\varepsilon]}. \tag{3.3}$$

Here, the variables ε^i, and λ^i represent, respectively, the polarization of gluons, and the generators of the su(3) algebra in this equation. The Kronecker deltas included in the amplitude correspond to the conservation constraint of quark color charge in the absence of any interaction. When all deltas are collectively imposed, what remains is just a color charge conservation delta δ_{ab}

$$\begin{aligned}\mathcal{M} &= -g_s^2 i \frac{m_q}{2v} \varepsilon^a_{\mu,r_2} \varepsilon^b_{\nu,r_3} \delta_{ab} \int \frac{d^4k}{(2\pi)^4} \frac{\mathrm{Tr}[(k-p_3+m_q)\gamma^\nu(k+m_q)\gamma^\mu(k+p_2+m_q)]}{[(k-p_3)^2-m_q^2+i\varepsilon](k^2-m_q^2+i\varepsilon)[(k+p_2)^2-m_q^2+i\varepsilon]} \\ &= -g_s^2 i \frac{m_q}{2v} \varepsilon^a_{\mu,r_2} \varepsilon^b_{\nu,r_3} \delta_{ab} I^{\mu\nu},\end{aligned} \tag{3.4}$$

where $I^{\mu\nu}$ is the integral over the momentum k. At this point, certain procedures need to be taken into account. The first one involves simplifying the complicated form of the

numerator of the integrand. Solving the trace of the numerator can be tedious. In the case of Eq. (3.3), handling the trace is not very difficult. However, in general, computations involving higher-order loops are performed with the help of FORM (51–54). The FORM code for our calculation is displayed in Appendix C, and the final result for the numerator can be expressed as

$$n^{\mu\nu} = 4m_q[p_3^\mu p_2^\nu + 4k^\mu k^\nu - 2k^\mu p_3^\nu + 2p_2^\mu k^\nu - p_2^\mu p_3^\nu + g^{\mu\nu}(m_q^2 - p_2 p_3) - g^{\mu\nu}k^2]. \tag{3.5}$$

The second step is to employ Feynman parametrization (55). This parametrization of the denominator terms A_j, where $j = 1,2,3$, in terms of new variables x, y, and z is given by

$$\frac{1}{A_1 A_2 A_3} = \int_0^1 dx \int_0^1 dy \int_0^1 dz\, \delta(x+y+z-1) \frac{2}{[A_1 x + A_2 y + A_3 z]^3}. \tag{3.6}$$

For simplicity, we can denote the denominator as $D = [A_1 x + A_2 y + A_3 z]$, where $A_1 = k^2 - m^2$, $A_2 = (k+p_2)^2 - m^2$, and $A_3 = (k-p_3)^2 - m^2$. This allows us to simplify the denominator terms as

$$D = (k^2 - m^2)x + (k^2 + 2kp_2 + \underbrace{p_2^2}_{0} - m^2)y + (k^2 - 2kp_3 + \underbrace{p_3^2}_{0} - m^2)z. \tag{3.7}$$

The vanishing terms occur because the gluons in the final states are on-shell. Therefore, considering the constraint imposed by the parametrization, $x + y + z = 1$, it suffices to factor out $k^2 - m^2$ in Eq. (3.7), denote $2(p_2 \cdot p_3)yz - m^2 \to -a^2$, and finally perform a change of variable from $k \to k - p_2 y + p_3 z$, reducing the problem to the calculation of the following integral

$$I^{\mu\nu} = \int_0^1 dy \int_0^{1-y} dz \int \frac{d^4k}{(2\pi)^4} \frac{8m_q n^{\mu\nu}}{(k^2 - a^2)^3}. \tag{3.8}$$

An important consideration at this point is that the change of variable in the denominator must also have an effect on the numerator

$$\begin{aligned} n^{\mu\nu} = {} & 4k^\mu k^\nu - g^{\mu\nu}k^2 + p_3^\mu p_2^\nu(1 - 4yz) + p_2^\mu p_3^\nu(-1 - 4yz + 2y + 2z) + p_3^\mu p_3^\nu(4z^2 - 2z) \\ & + p_2^\mu p_2^\nu(4y^2 - 2y) + g^{\mu\nu}(m^2 - p_2 \cdot p_3 + 2p_2 \cdot p_3 yz). \end{aligned} \tag{3.9}$$

Taking this change into account, the first two terms of $n^{\mu\nu}$ show signs of potentially leading to ultraviolet divergences in the final result. Despite these divergences "canceling out" after Passarino-Veltman reduction (56), which essentially states that the loop integral of terms involving $k^\mu k^\nu$ is proportional to $g_{\mu\nu}k^2$, regularization becomes necessary. In this work, dimensional regularization will be used, which isolates the divergence in the $\varepsilon \to 0$ limit and allows us to apply renormalization, in this case, the minimal subtraction scheme. Thus, for integrals exhibiting the aforementioned divergence, we will solve them as

$$G(D,\alpha,\beta,a^2) \equiv \int \frac{d^Dk}{(2\pi)^D} \frac{(k^2)^\alpha}{(k^2 - a^2)^\beta}. \tag{3.10}$$

Then, after doing the computations in Appendix D, we arrive at the master integral (34)

$$G(D,\alpha,\beta,a^2) = \frac{i(-a^2)^{\alpha-\beta}(a^2)^{D/2}}{(4\pi)^{D/2}} \frac{\Gamma(\beta-\alpha-D/2)\Gamma(\alpha+D/2)}{\Gamma(\beta)\Gamma(D/2)}. \tag{3.11}$$

At this point, by solving the integral of the first two terms of Eq. (3.8), which are the integral of the terms $k^\mu k^\nu - g^{\mu\nu}k^2$, we simply need to use the condition required by Lorentz invariance to arrive at

$$I_m = \int \frac{d^Dk}{(2\pi)^D} \frac{4k^\mu k^\nu - g^{\mu\nu}k^2}{(k^2-a^2)^3} = \frac{g^{\mu\nu}}{D} G(D,\alpha,\beta,a^2) - g^{\mu\nu}G(D,\alpha,\beta,a^2). \tag{3.12}$$

Here, the index m in Eq. (3.12) refers to the *master*, due to the use of the Eq. (3.11), and it is possible to identify $\alpha = 1$ and $\beta = 3$ from the integral (3.8). Therefore, by directly substituting the master integral structure (3.11) into the relation (3.12) and utilizing the fact that $\Gamma(D/2+1) = (D/2)\Gamma(D/2)$, we arrive at

$$I_m(D,1,3,a^2) = \left(\frac{4}{D} - 1\right) g^{\mu\nu} \frac{i}{(4\pi)^{D/2}} (a^2)^{D/2} \left(\frac{D}{4}\right) \Gamma(2-D/2). \tag{3.13}$$

Next, we proceed with the expansion around $D = 4 + 2\varepsilon$ in order to combine the terms of Eq. (3.13) and take the limit $\varepsilon \to 0$, leading to the cancellation of the divergence. Additionally, it is important to note that all terms in $n^{\mu\nu}$ that do not depend on k^μ contribute a finite value, $G(4,0,3,a^2)$. Thus, the remaining terms in the momentum integral (3.8) are as follows

$$G(4,0,3,a^2) = \frac{-i}{32\pi^2}\frac{1}{a^2} \quad \text{and} \quad \int \frac{d^Dk}{(2\pi)^D} \frac{4k^\mu k^\nu - g^{\mu\nu}k^2}{(k^2-a^2)^3} = \frac{i}{32\pi^2} g^{\mu\nu}.$$

Resuming the discussion of the integral (3.8) and proceeding to simplify the terms, the subsequent step involves solving this integral with respect to the Feynman parameters

$$\begin{aligned} I^{\mu\nu} = \frac{i8m_q}{32\pi^2} \int_0^1 \int_0^{1-y} dydz(-\alpha^{-2}) \Big[& p_3^\mu p_2^\nu (1-4yz) + p_2^\mu p_3^\nu (-1-4yz+2y+2z) \\ & + p_3^\mu p_3^\nu (4z^2-2z)] + p_2^\mu p_2^\nu (4y^2-2y) + g^{\mu\nu}(-p_2p_3 + 4p_2p_3yz) \Big]. \end{aligned}$$

At this stage, we use the on-shell condition for the transversality of gluons ($\varepsilon^a_{\mu,r_i} p_i^\mu = 0$), resulting in the simplification of the expression to the following remaining term

$$I^{\mu\nu} = \frac{i8m}{32\pi^2} [p_3^\mu p_2^\nu - g^{\mu\nu} p_2 p_3] \int_0^1 \int_0^{1-y} \frac{dydz}{-a^2} (1-4yz),$$

where we will denote the double integrals as

$$S = \int_0^1 \int_0^{1-y} \frac{dydz}{-a^2} (1-4yz). \tag{3.14}$$

With this definition, we can arrive at the following conclusion

$$\mathcal{M}^{(1)} = g_s^2 \frac{m_q^2}{8\pi^2 v} \varepsilon^a_{\mu,r_2} \varepsilon^b_{\nu,r_3} \delta_{ab} \left(p_3^\mu p_2^\nu - g^{\mu\nu} p_2 \cdot p_3\right) S.$$

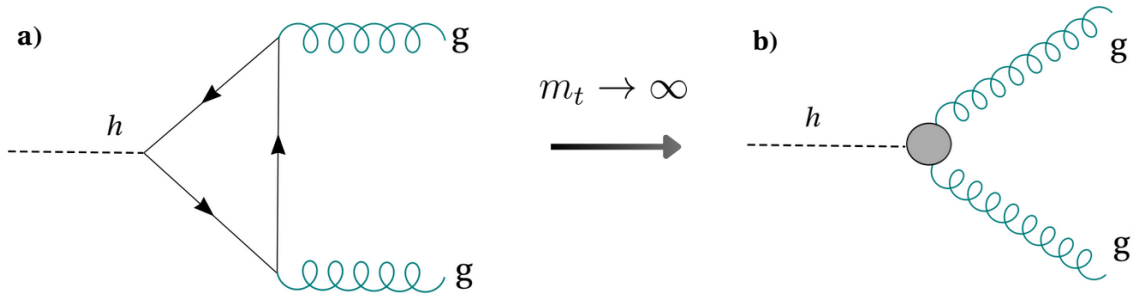

Figure 3.2 – a) A Feynman diagram of leading order for the decay $h \to gg$, where the top-quark is dominant in the loop. **b)** Diagram in effective theory, where the top quark is considered very heavy.

Source: By the author.

However, as mentioned before, it is necessary to consider a second contribution that takes into account the exchange of gluon momenta in the final state, resulting in a new amplitude $\mathcal{M}^{(2)}$ with the same structure as Eq. (3.3), but with the corresponding sign changes in the quark momenta in the propagators as shown by the Figure 3.1. To evaluate the integral for this new case, it is possible to employ the same methods described earlier. Upon calculating the numerator, we obtain the following result

$$n^{\mu\nu} = 4m_q(p_3^\mu p_2^\nu + 4k^\mu k^\nu + 2k^\mu p_2^\mu k^\nu) - p_2^\mu p_3^\nu + g^{\mu\nu}(m_q^2 - p_2 \cdot p_3 - k^2),$$

which has the same structure as Eq. (3.5), but with some signs flipped. However, it is important to note that the flipped signs accompany the odd terms in k^μ, which would result in a vanishing integral. Therefore, the results of the second diagram of Figure 3.1**b** are the same, and all we get is a factor of 2.

To obtain the decay width, we need to square the amplitude, considering the sum over all colors and polarizations

$$\sum_{a,b}\sum_{r_2,r_3} 4|\mathcal{M}^{(1)}|^2 = 4g_s^4\left(\frac{m_q^2}{8\pi^2 v}\right)^2 g_{\mu\lambda}g_{\nu\rho}\left(p_3^\mu p_2^\nu - g^{\mu\nu}p_2\cdot p_3\right)\left(p_3^\lambda p_2^\rho - g^{\lambda\rho}p_2\cdot p_3\right)|S|^2. \quad (3.15)$$

With the relation (3.15) in mind, it suffices to use the fact that the sum multiplied by color delta square, equals eight, and the orthogonality relation between gluon polarizations, when summed over r_1 and r_2, should be $g_{\mu\lambda}g_{\nu\rho}$. Consequently, in the end, we end up with an expression for the amplitude in terms of the integral S

$$|A_q|^2 = \sum|\mathcal{M}^{\text{total}}|^2 = g_s^4\frac{m_q^2}{v^2\pi^4}(p_2\cdot p_3)^2|S|^2, \quad (3.16)$$

where $p_2 \cdot p_3 = m_h^2/2$. In the Eq. (3.16) we will only consider the top-quark mass m_t, since the top has the biggest mass and consequently the largest contribution to the S integral defined as

$$S = \frac{1}{m_t^2}\int_0^1\int_0^{1-y} dydz\frac{1-4yz}{\frac{m_h^2}{m_t^2}yz - 1},$$

so that defining $\tau = (m_h/m_t)^2$ and expanding the integrand for a large top-quark mass, the integral S can be written as

$$S = \frac{1}{m_t^2}\left(-\frac{1}{3} - \frac{7}{360}\tau - \frac{1}{504}\tau^2 - \frac{13}{50400}\tau^3 + \mathcal{O}(\tau^4)\right). \tag{3.17}$$

Based on this result, the decay $h \to gg$ is obtained by employing $|A_q|^2$ in the expression for the two-body decay width. Therefore, in the limit where the top-quark mass is considered infinite and expanding in m_t^{-1}, we arrive at

$$\Gamma(h \to gg) = \frac{m_h^3}{8\pi v^2}\left(\frac{\alpha_s}{\pi}\right)^2 \frac{1}{9}\left(1 + \frac{7}{60}\tau + \frac{1543}{100800}\tau^2 + \frac{113}{50400}\tau^3 + \cdots\right) \tag{3.18}$$

$$= \Gamma_0(1 + 0.061 + 0.0058 + 0.0042 + \cdots), \tag{3.19}$$

where the first order τ correction terms in Eq. (3.18) accounting for only 6% of the leading-order result. The Eq. (3.18) represents a transition from **a)** to **b)** in Figure 3.2, since the first term of the expansion (3.18) is the first term of the Wilson coefficients, which is shown in part **b)** of this figure. In the limit where $\tau = 0$, we can define the leading-order $h \to gg$ coefficient as

$$\Gamma_0 = \frac{m_h^3}{72\pi v^2}\left(\frac{\alpha_s}{\pi}\right)^2, \tag{3.20}$$

which depends on α_s^2 and, consequently, on the renormalization scale.

3.2 The Low-Energy Theorem: A Higher-Order Perspective

The Wilson coefficient C_1, associated with the effective coupling of the Higgs with the two gluons, can be determined using a method widely explored in the literature, known as the Low-Energy Theorem (LET) (57). This theorem can be derived from the decoupling relation that connects the strong coupling value in a theory with n_f light flavors to the coupling with $n_f + 1$ flavors through the decoupling relation ζ_g (43, 57), as follows

$$\zeta_g^2(\mu, m_Q, \alpha_s^{(n_f)}) = \frac{\alpha_s^{(n_f+1)}}{\alpha_s^{(n_f)}(\mu)} = 1 + \sum_{k=2} d_k [\alpha_s^{(n_f)}(\mu)]^{k-1}, \tag{3.21}$$

where the coefficients d_k contain powers of logarithmic, such as $\log^k(\mu/m_Q^2(\mu))$, with the quark mass $m_Q(\mu)$ obtained in the $\overline{\text{MS}}$ renormalization scheme. Then, one way to obtain the Wilson coefficient based on the decoupling relation is through the derivative of the decoupling relation with respect to mass. This implies that the most complicated part of ζ_g^2, the constant terms implicit in coefficients d_k, does not contribute to the Wilson coefficients (43). This is possible due to the LET which, although not proven here, can be motivated as shown below.

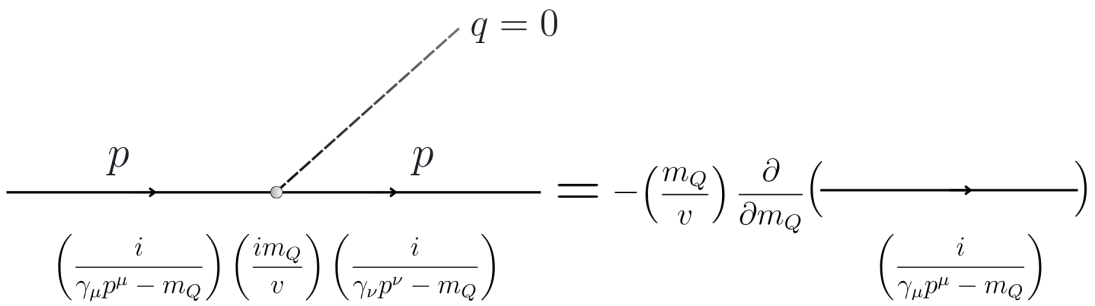

Figure 3.3 – Schematic representation of the Low-Energy Theorem for the Yukawa coupling example.

Source: By the author.

The low-energy theorem addresses loop contributions from the top quark by constructing an effective Lagrangian in which the top quark is integrated out. This integration can be approached by considering either a massless Higgs boson or, equivalently, an immensely heavy top quark. The theorem, initially proposed in Refs. (58–60), relates amplitudes of processes that differ solely due to the emission of a Higgs boson with zero momentum. One example motivated by the Yukawa coupling involves the coupling of a Higgs boson to a fermion with mass m_f and modifies the Lagrangian by considering the following substitution of the fermion mass

$$m_Q^0 \to m_Q^0 \left(1 + \frac{h^0}{v^0}\right), \tag{3.22}$$

where the quantities in the bare Lagrangian are represented with indices 0. This substitution leads to a relationship between two diagrams, as shown in Figure 3.3, where it is possible to see on the left-hand side of the equation a fermion emitting a Higgs boson with momentum q equal to zero. This condition for the Higgs boson does not change the structure propagator × vertices × propagator, and this can be written as the derivative of the fermion propagator with respect to mass times a constant. In Figure 3.3, the relation between the condition with and without the coupling of a Higgs field with zero momentum q is (30)

$$\lim_{q\to 0} \mathcal{M}(X \to Y + h) = \frac{m_Q^0}{v_0} \frac{\partial}{\partial m_Q^0} \mathcal{M}(X \to Y). \tag{3.23}$$

Nonetheless, when investigating higher orders, a subtlety arises. When renormalizing the $hf\bar{f}$ interaction, a problem emerges that demands correction: the counterterm for the Yukawa coupling is not the vertex with a subtraction at zero momentum transfer. Instead, it is determined by the counterterms for the fermion mass Z_m and the quark wave function

renormalization constant Z_2, according to (30)

$$\mathscr{L}_0 = -m_0\bar{Q}_0Q_0\frac{h}{v} = -m_Q\bar{Q}Q\frac{h}{v} + Z_{hQQ}m_Q\bar{Q}Q\frac{h}{v}, \tag{3.24}$$

with $Z_{hQQ} = 1 - Z_2Z_m$ as detailed in the references (36, 37). The correction involves replacing the differentiation with respect to the bare mass with differentiation with respect to the renormalized mass, considering the mass relation between the renormalized and non-renormalized masses (32)

$$m_0\frac{\partial}{\partial m_0} = \frac{m_Q}{(1+\gamma_m)}\frac{\partial}{\partial m_Q}, \tag{3.25}$$

where γ_m is the anomalous dimension of the fermion mass defined in Chapter 2.

The LET approach (43) allows us to evaluate how the decay of the Higgs into two gluons depends on the renormalization scale through $C_1(\mu)$. This dependence involves the top-quark mass $m(\mu)$ and also the coupling $\alpha_s(\mu)$. A first step to achieve this evolution is the determination of the Wilson coefficients themselves, obtained through decoupling

$$C_1 = -\frac{1}{2}m_t^2\frac{\partial}{\partial m_t^2}\ln\zeta_g^2(\mu,\alpha_s^{(n_f)},m_t), \tag{3.26}$$

where ζ_g^2 can be obtained from the Eq. (3.21), and as we will see in Chapter 3.1, the dominant quark in this process is the top quark, with mass m_t.

The analytic expression for C_1 up to N4LO has been provided in Ref. (15) as a function of the renormalization scale $\mu = \mu_t$, where $\mu_t = m_t(\mu_t)$ is the scale-invariant (SI) top-quark mass, i.e., the $\overline{\text{MS}}$ mass evaluated at the scale μ_t. These coefficients for the top-quark mass on-shell, called the OS scheme, were also presented. The series for the coefficient C_1 can be written as follows

$$C_{1,X} = -\frac{1}{3}a_s\left(1 + \sum_{n=1} c_{n,X}a_s^n(\mu^2)\right), \tag{3.27}$$

where $a_s = \alpha_s/(4\pi)$, and X represents the mass scheme employed. The series coefficients for these quantities can be found in (15). In this dissertation, we will use the coefficients

$$c_1 = 11, \quad c_2 = \frac{2777}{18} + 19L_t + n_f\left(-\frac{67}{6} + \frac{16}{3}L_t\right);$$

which is not explicitly dependent on the scheme; the dependence is only introduced in the logarithm $L_t = \ln(\mu^2/m_t^2)$. The N3LO and N4LO terms depend on the adopted scheme. The next coefficients in the SI scheme are

$$\begin{aligned} c_3^{(\text{SI})} = &-\frac{2892659}{648} + \frac{897943}{144}\zeta_3 + \frac{4834}{9}L_t + 209L_t^2 \\ &+ n_f\left(\frac{40291}{324} - \frac{110779}{216}\zeta_3 + \frac{2912}{27}L_t + 46L_t^2\right) \\ &+ n_f^2\left(-\frac{6865}{486} + \frac{77}{27}L_t - \frac{32}{9}L_t^2\right); \end{aligned}$$

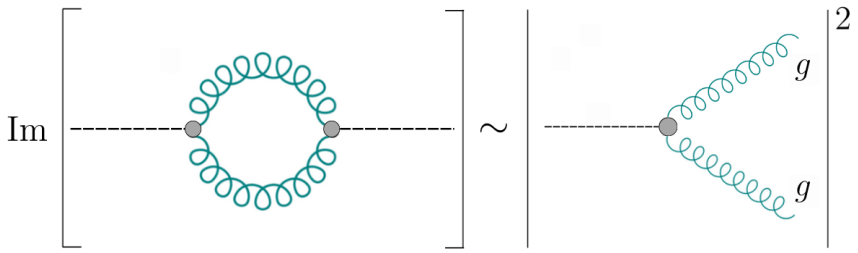

Figure 3.4 – Schematic representation, in the limit $m_t \to \infty$, of the optical theorem.

Source: By the author.

and the coefficient $c_4^{(\mathrm{SI})}$ can be found in Appendix B. Here, the a_n function is defined as $a_n = \mathrm{Li}_n(1/2) = \sum_{k=1}^{\infty}(2^k k^n)^{-1}$, while ζ represents the Riemann ζ-function. Furthermore, we will explore the OS scheme. The coefficients in this prescription are (15)

$$c_3^{(\mathrm{OS})} = c_3^{(\mathrm{SI})} + \frac{608}{3} + n_f\left(\frac{512}{9}\right); \tag{3.28}$$

$$\begin{aligned} c_4^{(\mathrm{OS})} = c_4^{(\mathrm{SI})} &+ \frac{297587}{27} + \frac{1216\zeta_2}{3} - \frac{304}{3}\zeta_3 + \frac{1216}{3}\zeta_2\ln 2 + 6688L_t \\ &+ n_f\left(\frac{189238}{81} + \frac{416}{3}\zeta_2 - \frac{256}{9}\zeta_3 + \frac{1024}{9}\zeta_2\ln 2 + 1472L_t\right) \\ &+ n_f^2\left(-\frac{4352}{81} - \frac{512}{9}\zeta_2 - \frac{1024}{9}L_t\right). \end{aligned} \tag{3.29}$$

The decay of the Higgs into two gluons contains the imaginary parts of the two-point scalar gluonium correlator. To understand this fact one uses the optical theorem. This theorem can assume distinct expressions if we consider, for example, two particles in the initial state. The theorem takes the form of scattering. On the other hand, for the $h \to gg$ process, we are dealing with one particle in the initial state. Thus, considering this initial particle as a, the optical theorem simply states (34)

$$-2\mathrm{Im}\left(\overline{\sum_n}\mathcal{M}_{i\to i}\right) = 2\sqrt{k^2}\sum_n \Gamma(a \to n) = 2\sqrt{k^2}\,\Gamma(a \to all), \tag{3.30}$$

where k is the four-momentum and $\Gamma(a \to all)$ is the total decay width. The $\sqrt{k^2}$ in Eq. (3.30) is necessary because the left-hand side of this equation has the self-energy amplitude of a given particle a, which in general is off-shell, i.e., $k^2 \neq m_a^2$.

In our specific case of interest, it is possible to say that $\Gamma_{h\to gg} \propto \mathrm{Im}\Pi_{G^2}$, as depicted in Figure 3.4, linking a Higgs self-energy diagram through a gluon loop to the squared amplitude of the decay $h \to gg$. It is essential to emphasize at this point that the coupling between the Higgs and gluons in the figure is already the effective coupling C_1.

In Ref. (15), the method used to compute the imaginary part of the gluonium correlator involves the use of the following relation

$$\mathrm{Im}\Pi_{G^2}(-s - i\delta) = \mathrm{Im}e^{i\pi\varepsilon L}\Pi_{G^2} = \sin(\pi\varepsilon L)\Pi_{G^2}(s), \tag{3.31}$$

where L is the number of loops and $\varepsilon = (4-D)/2$. Thus, the finite part of $\Pi_{G^2}(s)$ is proportional to $1/\epsilon$, since the Taylor expansion of $\sin(\pi\varepsilon L)$ is indicated by

$$\sin(\pi\varepsilon L) = L\pi\varepsilon\left(1 - \frac{1}{3!}(L\pi\varepsilon)^2 + \frac{1}{5!}(L\pi\varepsilon)^4 + \cdots\right). \tag{3.32}$$

In general terms, computing Π_{G^2} entails a higher computational cost due to the presence of diagrams with quartic divergence. To rearrange the infrared divergences, the superficial degree of divergence discussed in Chapter 2 must be logarithmic. This is achieved by considering the fourth coefficient in the Taylor expansion of all diagrams in terms of the external momentum q and by employing the operator

$$\frac{1}{4!}q^{\mu_1}q^{\mu_2}q^{\mu_3}q^{\mu_4}\frac{\partial}{\partial q^{\mu_1}}\frac{\partial}{\partial q^{\mu_2}}\frac{\partial}{\partial q^{\mu_3}}\frac{\partial}{\partial q^{\mu_4}}(\text{Diagrams})\bigg|_{q=0}. \tag{3.33}$$

The computational implementation, realized in references (15, 53), carried out in this work involves the use of QGRAF (61), which is subsequently processed in a FORM (51–54) program that automatically classifies the color factor and the topology of the diagram. This is very useful for computational optimization because diagrams with the same color factor, topology, and maximum power n_l are classified into a category of diagrams called meta-diagrams. In the context of Π_{G^2}, employing this method results in 1 meta diagram at the one-loop level, 5 at the two-loop level, 38 at the three-loop level, 394 at the four-loop level, and 6405 at the five-loop level. This illustrates the challenge of obtaining the coefficients for this decay at high orders in perturbation theory.

The imaginary part of the gluonium correlator can be written in perturbation theory up to N4LO in terms of the coefficients g_n (15)

$$\frac{4\pi}{N_A q^4}\text{Im}\Pi_{G^2}(q^2) \equiv G(q^2) = 1 + \sum_{n=1} g_n a_s^n, \tag{3.34}$$

where $N_A = 8$ is the number of generators for the SU(3) group. The coefficients g_n in the $\overline{\text{MS}}$ scheme are (15):

$$g_1 = +\frac{73}{3}C_A - \frac{14}{3}n_f; \tag{3.35}$$

$$\begin{aligned} g_2 = {} & +\frac{37631}{54}C_A^2 - \frac{242}{3}C_A^2\zeta_2 - 110C_A^2\zeta_3 + n_f\bigg(-\frac{6665}{27}C_A \\ & + \frac{88}{3}C_A\zeta_2 - 4C_A\zeta_3 - \frac{131}{3}C_F + 24C_F\zeta_3\bigg) + n_f^2\left(\frac{508}{27} - \frac{8}{3}\zeta_2\right); \end{aligned} \tag{3.36}$$

$$\begin{aligned} g_3 = {} & +\frac{15420961}{729}C_A^3 - \frac{45056}{9}C_A^3\zeta_2 - \frac{178156}{27}C_A^3\zeta_3 + \frac{3080}{3}C_A^3\zeta_5 \\ & + n_f\left(-\frac{2670508}{243}C_A^2 + \frac{8084}{3}C_A^2\zeta_2 + \frac{9772}{9}C_A^2\zeta_3 - \frac{80}{3}C_A^2\zeta_5 - \frac{23221}{9}C_FC_A\right. \\ & \left. + \frac{572}{3}C_FC_A\zeta_2 + 1364C_FC_A\zeta_3 + 160C_FC_A\zeta_5 + \frac{221}{3}C_F^2 + 192C_F^2\zeta_3 - 320C_F^2\zeta_5\right) \\ & + n_f^2\left(\frac{413308}{243}C_A - \frac{1384}{3}C_A\zeta_2 + \frac{56}{9}C_A\zeta_3 + 440C_F - \frac{104}{3}C_F\zeta_2 - 240C_F\zeta_3\right) \\ & + n_f^3\left(-\frac{57016}{729} + \frac{224}{9}\zeta_2 + \frac{64}{27}\zeta_3\right); \end{aligned} \tag{3.37}$$

and the coefficient g_4 can be found in Appendix B. In this context, C_A and C_F represent the Casimir operators of the adjoint and fundamental representations of the Lie algebra, $C_A = N_c$ and $C_F = (N_c^2 - 1)/2N_c$, respectively. They are related as follows: $[T^a, T^b]_{ij} = C_F \delta_{ij}$ and $f^{acd} f^{bcd} = C_A \delta^{ab}$.

The quartic Casimir dependences are denoted as d_A^{abcd} and d_F^{abcd}. To obtain $\Gamma_{h\to gg}(\mu)$ in perturbation theory in terms of n_f, it is necessary to combine the coefficients of the Wilson coefficients C_1 with $\mathrm{Im}\Pi_{G^2}$ according to Eq. (3.2). To achieve this, we use the numerical values of the coefficients at each power of α_s^n and re-expand the result. Keeping this in mind, the fully symmetrical tensors (62)

$$d_F^{abcd} = \frac{1}{6}\mathrm{Tr}\Big[T^a T^b T^c T^d + T^a T^b T^d T^c + T^a T^b T^c T^d + T^a T^c T^d T^b + T^a T^d T^b T^c + T^a T^d T^c T^b\Big], \tag{3.38}$$

must be employed. In the case of d_A^{abcd}, only the matrices in Equation 3.38 change. Instead of the fundamental representation, the adjoint generators must be employed, defined by the matrices $[C^a]_{bc} \equiv -if^{abc}$.

It is useful to evaluate the numerical values of the coefficient g_4 given the product between fully symmetric tensors. For this purpose, we employ properties for SU(N_c) that basically state that (62)

$$\frac{d_A^{abcd} d_A^{abcd}}{N_A} = \frac{N_c^2(N_c^2 + 36)}{24}, \tag{3.39}$$

$$\frac{d_F^{abcd} d_A^{abcd}}{N_A} = \frac{N_c^2(N_c^2 + 6)}{48}, \tag{3.40}$$

$$\frac{d_F^{abcd} d_F^{abcd}}{N_A} = \frac{N_c^4 - 6N_c^2 + 18}{96N_c^2}. \tag{3.41}$$

In QCD, where $N_c = 3$, possessing these relationships (3.41) allows us to explore the decay $h \to gg$ numerically in perturbation theory by explicitly outlining the dependence on n_f of the series. This will be useful for our work later on.

3.3 Current Status of the Decay $h \to gg$ in Perturbation Theory

In reference (15), the Higgs decay into two gluons is determined up to order α_s^6, exactly, for different values of n_f and different renormalization scale values for the quark top mass, combining the Wilson Coefficients (3.27) and the imaginary part of Π_{G^2} (6.7) according to (3.2), which can be evaluated analytically. However, here it will be presented numerically in terms of each n_f power through

$$\Gamma_{h\to gg}^{(n_f)}(\mu_i) = \Gamma_0 \sum_{n=0}^{\infty} c_n \alpha_s^n = \Gamma_0 K_{\mu_i}^{(n_f)}, \tag{3.42}$$

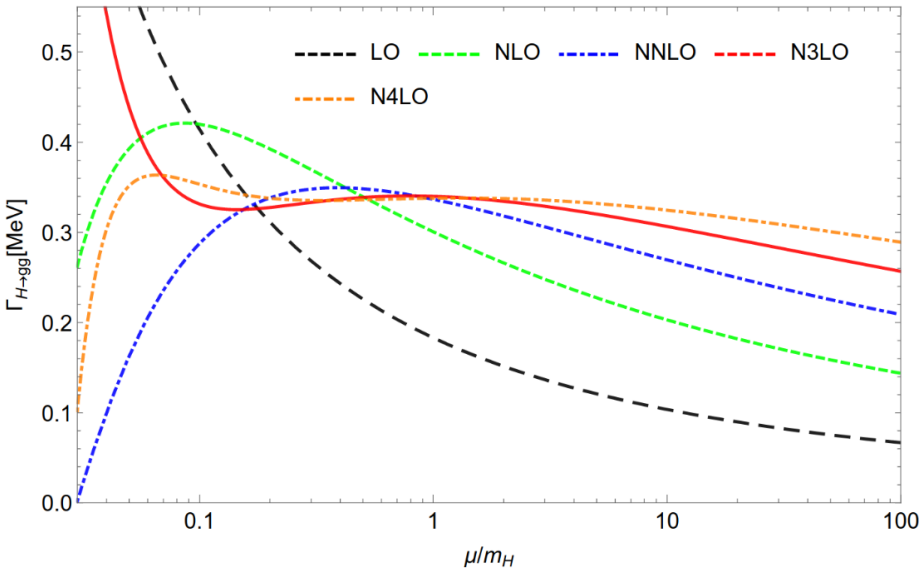

Figure 3.5 – Evolution of the Higgs decay into two gluons as a function of the renormalization scale for $n_f = 5$ in the $\overline{\text{MS}}$ and On-Shell top-quark mass.

Source: By the author.

where μ_i is the renormalization scale value of $m_t(\mu_i)$. Two cases were evaluated here; the first is for SI top-quark mass

$$\begin{aligned}\Gamma^{(n_f)}_{h\to gg}(\mu_t) = \Gamma_0[1 &+ \alpha_s(7.55986 - 0.371362n_f) + \alpha_s^2\left(0.0913684n_f^2 - 4.81767n_f + 37.378\right) + \\ &+ \alpha_s^3\left(-0.017346n_f^3 + 1.70814n_f^2 - 34.5769n_f + 144.901\right) \\ &+ \alpha_s^4\left(0.00258089n_f^4 - 0.440084n_f^3 + 16.5497n_f^2 - 178.799n_f + 461.56\right) \\ &+ \mathcal{O}(\alpha_s^5)],\end{aligned}$$

and the second one is for the on-shell quark top $m_t = 173$ GeV

$$\begin{aligned}\Gamma^{(n_f)}_{h\to gg}(m_t) = \Gamma_0[1 &+ \alpha_s(7.55986 - 0.371362n_f) + \alpha_s^2\left(0.0913684n_f^2 - 4.82489n_f + 37.3523\right) + \\ &+ \alpha_s^3\left(-0.017346n_f^3 + 1.71005n_f^2 - 34.5639n_f + 144.903\right) \\ &+ \alpha_s^4\left(0.00258089n_f^4 - 0.440714n_f^3 + 16.554n_f^2 - 178.466n_f + 462.628\right) \\ &+ \mathcal{O}(\alpha_s^5)].\end{aligned} \tag{3.43}$$

The evolution of Eq. (3.43), for $n_f = 5$, on the renormalization scale is indicated by the plot in Figure 3.5 order by order in perturbation theory. This plot was generated using the `RunDec` (63, 64) Wolfram Mathematica package and reproduces the same result obtained in Ref. (65).

In Chapter 6, we will explore the dependence on the number of flavors, as detailed in Ref. (15), to estimate the first unknown coefficient of this decay in terms of n_f.

4 Gluonium Correlator: A Borel Space Perspective

In this chapter, general properties of perturbative series in QCD are discussed, mainly in the context of the two-gluon correlator. The calculation of the correlator in the large-β_0 limit is presented in the Borel plane. Additionally, methods for performing estimates of higher-order coefficients are introduced.

4.1 Divergent Series

In QCD at high energies, physical quantities $f(\alpha)$ can be described using perturbation theory, expressed as an expansion in terms of the coupling constant α of the theory. Conceptually, this means constructing an interacting universe $\alpha \neq 0$ from a non-interacting one $\alpha = 0$. With each order in perturbation theory, more information about fundamental interactions is revealed (66). However, knowing a quantity to all orders does not guarantee exact knowledge of the observable. These series are divergent. The divergent behavior was demonstrated by Dyson for QED (67), and it can also be extended to QCD. In addition to being divergent, there is a conjecture regarding these series, essentially stating that such series are asymptotic, meaning they must be truncated at a certain order in perturbation theory corresponding to a good approximation of real value.

Despite this conjecture, the behavior of perturbative series is not completely understood, as calculations at high orders come with a significant computational cost; thus, only the first few coefficients are known. Increasing the order in perturbation theory leads to an increase in the number of loops to be considered, as well as the number of diagrams. The description of an asymptotic quantity $f(\alpha)$ in a region C of the complex α plane is given by (22)

$$\left| f(\alpha) - \sum_{n=0}^{N} r_n \alpha^n \right| < K_{N+1} \alpha^{N+1}, \tag{4.1}$$

where for all α in C, the truncation error at order N must be of the order α^{N+1}. In this context, the coefficients of the series increase with $K_N \sim N!$ the factorial growth is not suppressed by the α^N power, and consequently, for large enough N this series diverges. In other words, a series of this type must have a physical meaning up to a certain order N^*, that is the minimal increment of the series, where the series should be truncated. Generally this point is called of optimal truncation, and the numerical value of N^* is proportional to α^{-1}, assuming that the coupling $\alpha > 0$. In fact, for the QED where $\alpha \approx 1/137$ correspond to a small number the divergence will dominate the series for $N^* \approx 140$. In QCD, the coupling evaluated at the tau mass $\alpha_s(m_\tau) \approx 0.3$, which leads to an optimal truncation at $N^* \approx 3$.

In dealing with series whose coefficients grow factorially, one viable approach is the application of Borel summation. Consider a power series

$$f(\alpha_s) = f(0) + \sum_{n=0}^{\infty} f_n \alpha_s^{n+1}, \tag{4.2}$$

which generally has a convergence radius equal to zero. The Borel transform of a series, $B[f]$, can be defined as follows

$$B[f] = f(0)\delta(t) + \sum_{n=0}^{\infty} f_n \frac{t^n}{n!}, \tag{4.3}$$

where t is referred to as the Borel variable. In the $t-$plane, the factorial growth of coefficients is mitigated by the presence of $n!$ in the denominator. The original series can be recovered from the Borel transform through the inverse Borel transform, which is essentially a Laplace transform of $B[f]$. Typically, this transformation can be written as

$$\tilde{f}(\alpha_s) = \int_0^{\infty} dt\, e^{-t/\alpha_s} B[f](t), \tag{4.4}$$

where generally it can be expressed in terms of the variable $u = \beta_0 t$ as follows

$$\tilde{f}(\alpha_s) = \left(\frac{1}{\beta_0}\right) \int_0^{\infty} du\, e^{-u/\beta_0 \alpha_s} B[f](u). \tag{4.5}$$

Here we can divide the series of type f into two classifications. The first consists of series that are Borel summable, meaning that the integral is well defined, without singularities along the path $u > 0$, and the equation for $B[f]$ results in a real value. The second type consists of series whose Borel transform has singularities along the integral path, and these singularities introduce ambiguities in the Borel sum. Furthermore, to compute the inverse of $B[f]$ in this case, it is necessary to choose an integration path, and this choice of path affects the result of the integral.

In general, singularities in the Borel transform arise due to the factorial growth of the coefficients f_n, known as renormalons. An example is considering a growth of the form (22)

$$f_n \sim K(\tilde{p}/\beta_0)^{-n} n^b n!, \tag{4.6}$$

whose Borel transform can be written as

$$B[f] = \frac{K\Gamma(1+b)}{1 - u/(\beta_0 p)^{1+b}} = \frac{K\Gamma(1+b)2^{1+b}}{(\tilde{p} - u)^{1+b}}, \tag{4.7}$$

which has a pole of multiplicity $1 + b$ at $u = \tilde{p}$, with $\tilde{p} = \beta_0 p$. Suppose that the transform has singularities at $\tilde{p}_1$ and $\tilde{p}_2$. These poles contribute to the asymptotic series as $(1/\tilde{p}_1^{n+1} + 1/\tilde{p}_2^{n+1})$, where $n + 1$ is the perturbative order. As a direct consequence, if $|\tilde{p}_2| > |\tilde{p}_1|$, $\tilde{p}_1$ has more effect on the series at higher orders. For this reason, the nearest origin pole is the dominant renormalon. In this context, note that if $\tilde{p} < 0$, the

singularities appear on the negative real axis of the Borel plane are ultraviolet renormalons. Consequently, in this regime the integral (4.5) exists and the series is Borel summable. However, for $\tilde{p} > 0$, the singularity introduces the aforementioned ambiguity, arising from infrared renormalons. These ambiguities follow a power law proportional to the transferred momentum Q^2. To visualize this, suppose the Borel transform has a pole at $u_0 = \beta_0 t_0 > 0$. The prescription adopted for the contour integral defines the value of the integral, but the difference between the two contour prescriptions around the pole, although it has not been demonstrated here, follows the rule (68)

$$\delta\tilde{f} \sim \left(\frac{1}{\beta_0}\right) \oint_C du\, e^{-u/\beta_0 \alpha_s(Q)} B[f] \sim \left(\frac{\Lambda_{QCD}}{Q}\right)^{2u_0}, \tag{4.8}$$

where the contour C encloses the pole u_0.

However, despite the result of Eq. (4.8), which essentially states that the singularity u_0 produces an ambiguity in $\tilde{f}$ of $(\Lambda_{QCD}/Q)^{2u_0}$, there are nonperturbative sector ambiguities that should produce a cancellation of this term (68).

4.2 Analytic Structure of Π_{G^2}

We start our investigation of higher-order terms in the decay of the Higgs boson into two gluons by examining the perturbative expansion of the two-gluon correlator Π_{G^2}. As discussed in Chapter 3, the calculations of the $h \to gg$ decay are expressed in terms of the imaginary part of this correlator. The main advantage of starting with this study is that, in this case, the result in the large-β_0 limit of QCD is known, providing valuable information about the renormalons in the perturbative series. We can then use these results as a laboratory for the methods we will employ later in the complete results for Higgs decay into two gluons.

The investigation of the two-gluon correlator has revealed several theoretically interesting aspects and has been explored in recent literature (69). One concrete case arises when considering that the current behind in the correlator is associated with the gluonic component of the QCD Lagrangian. This, in turn, is related to the energy-momentum tensor of this theory, which in certain cases exhibits significant sensitivity to the variation of the renormalization scale due to truncation (70). It is worth noting that this current constitutes the gluonic contribution to the anomalous trace of the QCD energy-momentum tensor, one of the factors responsible for the breaking of the theory's conformal symmetry (71). Finally, the expected value of these currents with respect to the nonperturbative QCD vacuum (Ω) represents the gluon condensate, one of the fundamental parameters within QCD sum rules, which has been recently investigated in the literature (72–74). Furthermore, the two-gluon correlator plays a crucial role in investigating QCD sum rules for glueballs, one of the yet-to-be-confirmed predictions of QCD, where it is possible to form a bound state of gluons, giving rise to a new massive particle.

The structure of the two-gluon correlator is given by

$$\Pi_{G^2}(q^2) = i \int d^4x e^{iq\cdot x} \langle \Omega | T\{J_G(x) J_G(0)\} | \Omega \rangle \,, \tag{4.9}$$

where $J_G(x) = G_{\mu\nu}G^{\mu\nu}(x)$ corresponds to the gluonic current, and q denotes the external momentum, which in this case is associated with the Higgs boson mass. It is essential to emphasize that the treatment employed in this work for this correlator from the perspective of perturbative QCD (pQCD) involves investigating the asymptotic nature of the quantity (4.9) encoded in its dominant renormalons. In general, as we discussed previously, the renormalons associated with low-energy (IR) regions of Feynman diagrams are responsible for introducing ambiguities in the Borel space, which require the choice of a prescription for performing the Borel summation. These ambiguities are related to higher-dimensional power corrections in the operator product expansion (OPE).

However, valuable information about the structure of the correlator and its behavior at high orders in perturbation theory can be obtained from the large-β_0 limit, which has been recently employed in (17,19) to investigate higher-order terms in the Higgs decay into quarks ($b\bar{b}$) and two photons, where the quark correlator was explored. Thus, to investigate the structure of the renormalons and the efficiency of the methods employed in this work, the physical correlator or the Adler-type function, according to Eq. (4.12), will be employed. Here we follow closely Ref. (71).

The significant difference compared to the QCD Adler function is that it is necessary to employ three derivatives to eliminate the subtraction constants from $\hat{\Pi}_{G^2}(s)$, which must be considered in the spectral approach as (71)

$$\hat{\Pi}_{G^2}(s) = \hat{\Pi}_{G^2}(0) + s\hat{\Pi}'_{G^2}(0) + \frac{s^2}{2}\hat{\Pi}''_{G^2}(0) + s^3 \int \frac{\hat{\rho}_{G^2}(s')}{(s')^3(s'-s-i0)} \mathrm{d}s', \tag{4.10}$$

where $\hat{\Pi}_{G^2}$ represents an RGI (renormalization group invariant) quantity

$$\hat{\Pi}^{\beta_0}_{G^2} = \left(\frac{\beta(a_s)}{\beta_1 a_s}\right)^2 \Pi^{\beta_0}_{G^2}, \tag{4.11}$$

and $\hat{\rho}_{G^2}$ is the spectral function itself, obtained through the imaginary part of the correlator. In this sense, to eliminate the subtraction constants and work with a physical quantity, we will employ the physical correlator

$$\hat{D}_{G^2}(s) \equiv -s\frac{\mathrm{d}^3}{ds^3}\hat{\Pi}_{G^2}(s), \tag{4.12}$$

known to all orders in the large-β_0 limit, this will be further discussed in the next section.

In order to reproduce the results in the dominant order for $\hat{D}_{G^2}(s)$ obtained in Ref. (71), it is possible to consider only the abelian terms of the QCD field tensor, giving rise to an "abelian" current denoted as $J^A_G(x)$.

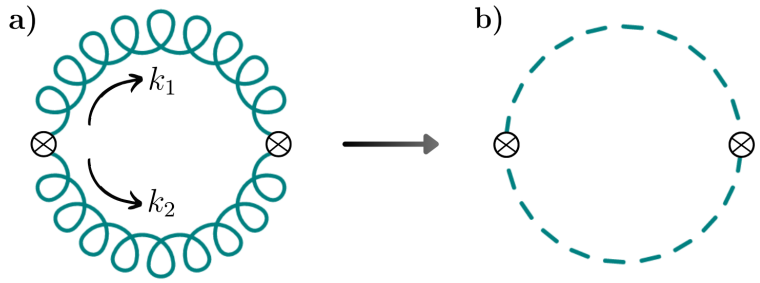

Figure 4.1 – a) A representation of the gluon-gluon correlator, showing a loop of gluonic currents in the non-perturbative QCD vacuum, where $k_1 = -k$ and $k_2 = -(k+q)$.
b) Diagram of the correlator in the large-β_0 limit, where the gluon propagator is replaced by the resummed propagator.

Source: By the author.

This current, although not yet renormalization group invariant (RGI), is positioned in the correlator

$$\Pi_{G^2} = i \int d^4x e^{iq\cdot x} \langle \Omega | T J_G^A(x) J_G^A(0) | \Omega \rangle \,, \tag{4.13}$$

which corresponds to the diagram in Figure (4.1) **a)**. In this way, by writing J_G^A in terms of the gluonic field, we arrive at

$$J_G^A(x) = [\partial\mu A_\nu^a \partial^\mu A^{\nu a} - \partial_\mu A_\nu^a \partial^\nu A^{\mu a} - \partial_\nu A_\mu^a \partial^\mu A^{\nu a} + \partial_\nu A_\mu^a \partial^\nu A^{\mu a}](x). \tag{4.14}$$

Hence, it is possible to simplify Eq. (4.14) by a simple index exchange and maintaining the signs of the terms, which in this case are symmetric, arriving at the equations

$$J_G^A(x) = [2\partial_\mu A_\nu^a \partial^\mu A^{\nu a} - 2\partial_\mu A_\nu^a \partial^\nu A^{\mu a}](x), \tag{4.15}$$

$$J_G^A(0) = [2\partial_\rho A_\sigma^b \partial^\rho A^{\sigma b} - 2\partial_\rho A_\sigma^b \partial^\sigma A^{\rho b}](0). \tag{4.16}$$

After that, the procedure consists of expanding the product of the gluonic currents in terms of derivatives of the gluon field, so that both currents have the same structure. Nevertheless, it is necessary to implement the temporal ordering of the expansion of the product of the mentioned currents and perform all possible Wick's contractions of the operators, yielding multiplicity factors for some terms that must be taken into account. After considering all the summed contributions, the result is

$$\Pi_{G^2} = -i(N_c^2 - 1) \int \frac{d^4k}{(2\pi)^4} \frac{1}{D_1 D_2} [8(d-2)(k\cdot(k+q))^2 + 8k^2(k+q)^2], \tag{4.17}$$

where k and q represent the loop and external momenta, respectively. Additionally, the denominators are written as $D_1 = -k^2$ and $D_2 = -(k+q)^2$, and the numerator will be denoted as

$$I(k,q) = [8(d-2)(k\cdot(k+q))^2 + 8k^2(k+q)^2]. \tag{4.18}$$

Furthermore, one must remember that

$$k \cdot q = \frac{1}{2}(-D_2 + D_1 - q^2). \tag{4.19}$$

Then, after writing the numerator in terms of $D_1 = k_1^2 = -k^2$ and $D_2 = k_2 = -(k+p)^2$, it is possible to perform the scalar one-loop integral by the master integrals method. So that solving the integral (4.17) using the α-parametrization method developed in Appendix D, one arrives at

$$\Pi_{G^2} = 2i(N_c^2 - 1)(d-2)s^2 \left(\mu^2 \frac{e^\gamma}{4\pi}\right)^{-\varepsilon} \frac{i\pi^{d/2}}{(2\pi)^d}(-s)^{-\varepsilon} \frac{2\Gamma(1+\varepsilon)\Gamma^2(1-\varepsilon)}{\Gamma(1-2\varepsilon)(d-3)(d-4)}, \tag{4.20}$$

which can be expanded around $\varepsilon = 0$ to arrive at

$$\Pi_{G^2} = -\frac{(N_c^2-1)}{4\pi} s^2 \left[-\frac{1}{\varepsilon} - 1 + \ln(-s/\mu^2)\right]. \tag{4.21}$$

The result (4.21) represents the LO correlator in QCD at the α_s-plane.

4.3 Result for Π_{G^2} in the Large-β_0 Limit

To work within the framework of the Borel transform employed in perturbative series, the investigation of the asymptotic behavior of the two-gluon correlator can be performed through the large-β_0 limit (75). This limit is an extension of the large-n_f limit. To elucidate how things work, we can rewrite the aforementioned, Eq. (4.2), quantity $f(\alpha_s)$ as

$$\begin{aligned} f(\alpha_s) &= 1 + \sum_{n=0}^{\infty}\sum_{k=0}^{n} r_{n,k} n_f^k \alpha_s^{n+1} \\ &= 1 + r_{0,0}\alpha_s + (r_{1,1}n_f + r_{1,0})\alpha_s^2 + \\ &+ (r_{2,2}n_f^2 + r_{2,1}n_f + r_{2,0})\alpha_s^3 + \cdots, \end{aligned} \tag{4.22}$$

where the coefficients with large power in the number of flavours is given by $r_{n,n}$ coefficient.

In the large-n_f limit, the number of flavors, n_f, is considered infinite, $n_f \to \infty$, while the product $\alpha_s n_f \sim \mathcal{O}(1)$, so that $\alpha_s \sim 1/n_f$. In this limit, infinite bubbles of $q\bar{q}$ are evaluated. An individual fermion bubble contributes to the gluon with (22)

$$\Pi_1(k^2) = \beta_{0f}\alpha_s \left[\log\left(\frac{-k^2}{\mu^2}\right) + C\right], \tag{4.23}$$

where $\beta_{0f} = -n_f/6\pi$ is the fermionic contribution to the leading β function coefficient, and C is the same renormalization parameter already discussed in Chapter 2. The gluon-gluon and ghost interactions are not considered in the large-n_f limit since we only obtain terms $(\alpha_s n_f)^n$, as other terms are suppressed by α_s. In this limit, we can disregard the subleading n_f terms in Eq. (4.22), retaining only the coefficients $r_{n,n}$ in Eq. (4.22). The large-β_0 limit can be achieved after replacing the only fermionic contribution with the complete β_0 term

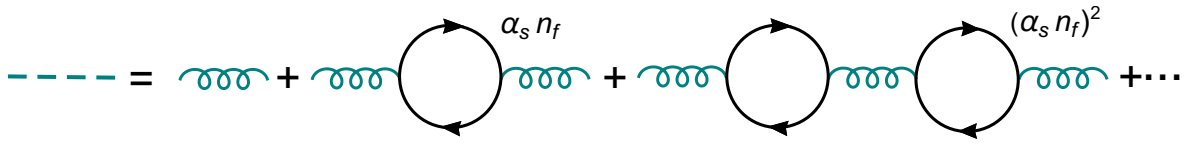

Figure 4.2 – Modification of the gluon propagator for the large-n_f limit, considering only higher-order terms in n_f.

Source: By the author.

defined in Eq (2.84): $\beta_{0f} \to \beta_{0f} + \beta_{0A}$, where now the non-abelian term β_{0A} is considered, so that $\beta_0 > 0$, and the features of QCD running coupling are recovered. This can be done by replacing

$$n_f \to n_f - \frac{33}{2}, \tag{4.24}$$

in the coefficient β_{0f}. This change directly affects the series coefficients, where the terms $r_{n,n}$ are reproduced exactly at all orders in perturbation theory, while the non-abelian terms are predicted. For example, considering the second-order coefficient in the large-n_f, the non-abelianization procedure yields

$$r_{1,1} n_f \alpha_s^2 \to (r_{1,1} n_f + r_{1,0})\alpha_s^2, \tag{4.25}$$

where the large-β_0 limit makes the prediction of $r_{1,0} = -(33/2)r_{1,1}$. Then, the large-β_0 limit is obtained by expanding in large-n_f and employing the naive non-Abelianization procedure, where n_f dependence is replaced by the full QCD β_0 term. This limit will be used as a kind of laboratory to test our estimation methods. The higher-order coefficients of $D_{G^2}^{\beta_0}$ will be estimated using Padé approximants, which will be discussed later.The accuracy of the estimates can provide the best method for the $h \to gg$ investigation.

In the large-β_0 limit, the strategy for the calculation involves replacing the usual gluon propagators with chains of quark bubbles with momentum k flowing through the gluon (in addition to using the Ward-Takahashi identity $q_\mu \Pi^{\nu\mu} = 0$ and employing the Landau gauge $\xi = 0$), as indicated in Figure 4.2, which is the resummed gluon propagator

$$D_{\mu\nu}^{ab}(k^2) = -\frac{i\,\delta^{ab}}{k^2}\left(g_{\mu\nu} - \frac{k_\mu k_\nu}{k^2}\right)\frac{1}{1+\Pi_1(k^2)} + (-i)\xi\frac{k_\mu k_\nu}{k^4}, \tag{4.26}$$

discussed in Chapter 2. To investigate how this replacement is done, we can start by the development of the bubble chain in Eq. (4.26) times the QCD coupling $\alpha_s(\mu)$, which leads to (68)

$$\alpha_s(k^2) D_{\mu\nu}^{ab}(k^2) = -\frac{i\delta^{ab}}{k^2}\left(\frac{k_\mu k_\nu}{k^2} - g_{\mu\nu}\right)\frac{\alpha_s(\mu^2)}{1+\beta_{0f}\alpha_s(\mu^2)\ln(-k^2/\mu^2 e^{-C})}. \tag{4.27}$$

Then, it is possible to replace

$$\frac{\alpha_s(\mu^2)}{1+\beta_0\alpha_s\ln(-k^2/\mu^2 e^{-C})} = \sum_{n=0}^{\infty}(\alpha_s)^{n+1}(-\beta_0)^n \ln^n\left(-\frac{k^2}{\mu^2 e^{-C}}\right), \tag{4.28}$$

and taking the Borel transform of Eq. (4.27) taking into account the expansion of Eq. (4.28), we arrive at

$$B[\alpha_s D^{ab}_{\mu\nu}] = -\frac{i\delta^{ab}}{k^2}\left(\frac{k_\mu k_\nu}{k^2} - g_{\mu\nu}\right)\exp\left[\ln\left(\frac{\mu^2 e^{-C}}{-k^2}\right)^{-u}\right]$$
$$= -\frac{i\delta^{ab}}{(k^2)^{1+u}}\left(\frac{k_\mu k_\nu}{k^2} - g_{\mu\nu}\right)\left(\mu^2 e^{-C}\right)^{-u}, \tag{4.29}$$

which basically states that the transition between the gluon-gluon correlator in QCD and the large-β_0 limit can be done simply by taking into account the change

$$\frac{-g_{\mu\nu}}{k^2 + i\eta} \to (-\mu^2 e^{-C})^u \frac{-g_{\mu\nu}}{(k^2 + i\eta)^{1+u}}, \tag{4.30}$$

where u is the Borel plane variable. Moreover, upon examining Eq. (4.26) in comparison with the outcome of Eq. (4.29), it can be observed that

$$B\left[\frac{\alpha_s}{(1 + \Pi(k_j^2))}\right] = \left(-\frac{\mu^2}{k^2}e^{-C}\right)^{u_j}, \tag{4.31}$$

which we will employ later in the calculation of the gluonic correlator. In this way, through Eq. (4.30), the form of $\Pi^{\beta_0}_{G^2}$ in the Borel plane is obtained with the modification in the powers of the denominators, effectively transitioning from Figure 4.1 **a)** to 4.1 **b)**.

Then, after writing the numerator in terms of D_1 and D_2 and the denominator with modified exponents, it is possible to perform the one-loop integral of $B[\Pi^{\beta_0}_{G^2}]$ using the method of master integrals (76).

This procedure can be demonstrated in more detail by decomposing each current after employing contributions from infinite quark bubbles. Considering a case with two gluonic currents, the modification of the correlator is

$$\hat{\Pi}^{\beta_0}_{G^2} = -\frac{i}{\pi^2}(N_c^2 - 1)\int \frac{d^4k}{(2\pi)^4}\frac{I(k,q)}{D_1 D_2}\left[\frac{\alpha_s}{(1 + \Pi_1(k_1^2))}\right]\left[\frac{\alpha_s}{(1 + \Pi_1(k_2^2))}\right]. \tag{4.32}$$

In this context, we are considering a correlator invariant under the renormalization group, denoted as $\hat{\Pi}^{\beta_0}_{G^2}$. As mentioned earlier, in the large-β_0 limit, only the first coefficient of the beta function, β_0, is taken into account. Therefore, in this case, a correlator invariant under the renormalization group can be expressed as

$$\hat{\Pi}^{\beta_0}_{G^2} = \left(\frac{\beta(a_s)}{\beta_0 a_s}\right)^2 \Pi^{\beta_0}_{G^2} = a_s^2\, \Pi^{\beta_0}_{G^2}. \tag{4.33}$$

Note that each α_s has been strategically positioned in Eq. (4.32) to facilitate the development of the integral later. To perform the Borel transform of Eq. (4.32), it is necessary to have the relationship between the Borel transform of the products of two currents (77)

$$B\left[\prod_{j=1}^{2}\frac{\alpha_s}{1 + \Pi(k_j^2)}\right] = \frac{2\pi}{\beta_{0f}}\int_0^u du_1 du_2\, \delta(u - u_1 - u_2)\prod_{j=1}^{2} B\left[\frac{\alpha_s}{1 + \Pi_1(k_j^2)}\right](u_j). \tag{4.34}$$

Thus, by substituting (4.34) into Eq. (4.32), one obtains

$$B[\Pi^{\beta_0}_{G^2}] = \frac{-2\,i(N_c^2-1)}{\pi\beta_{0f}}\int_0^u du_1\,du_2\,\delta\,(u-u_1-u_2)\int\frac{d^4k}{(2\pi)^4}\prod_{j=1}^{2}\frac{I(k,q)}{D_1D_2}B\left[\frac{\alpha_s}{1+\Pi_1(k_j^2)}\right].$$

As mentioned previously, the first term of the β function carries an index f indicating fermionic contributions, and it is necessary to substitute it with the complete QCD β_0, as discussed at the beginning of this section. After that, one obtains

$$B[\Pi^{\beta_0}_{G^2}] = \frac{-i(N_c^2-1)}{\beta_0}\left(\mu^2e^{-C}\right)^{u_1+u_2}\int_0^u du_1du_2,\delta(u-u_1-u_2)\int d^4k\frac{I(k,q)}{D_1^{1+u1}D_2^{1+u_2}}. \quad (4.35)$$

This integral shows how the change in the power of D_1 and D_2 arises naturally after applying the large-n_f limit. Moving forward, dimensional regularization will be used to solve the loop integrals, where each component of the integral encodes different powers of the denominators with respect to u_1 and u_2. The next step is to expand the numerator $I(k,q)$, leading to

$$\begin{aligned}\int d^Dk\frac{I(k,q)}{D_1^{1+u1}D_2^{1+u_2}} = (D-2)[&2G(u_1-1,1+u_2)+4G(u_1,u_2)+2G(u_1+1,u_2-1)\\&+4G(u_1,1+u_2)+4G(u_1+1,1+u_2)\\&+2G(u_1+1,1+u_2)]+8G(u_1,u_2).\end{aligned} \quad (4.36)$$

Here, each component of the integral (4.36) can be obtained from the next integral

$$G(n_1,n_2) = \int\frac{d^dk}{D_1^{n_1}D_2^{n_2}} = i\pi^{d/2}(-p^2)^{d/2-n_1-n_2}\tilde{G}(n_1,n_2), \quad (4.37)$$

where the demonstration of this relation can be found in Appendix D.

Following the same prescription shown in detail in Ref. (76), after solving an integral through the application of the delta function $\delta(u-u_1-u_2)$, the result is

$$B[\Pi^{\beta_0}_{G^2}] = \frac{(N_c^2-1)}{(2\pi)^4\beta_{1f}}\left(\mu^2e^{-C}\right)^u\int_0^u du_1\,\sigma_k(u_1,u,s), \quad (4.38)$$

where $\sigma_k(u_1,u,s)$ carries all contributions from the integral concerning the loop momentum.

Then, employing master integrals for the one-loop case and expanding around the dimension $D=4-2\varepsilon$, for $\varepsilon\to 0$, one reaches the following result

$$\sigma_k(u,u_1,s) = 6i\pi^2(-s)^{\frac{1}{2}(4-2u)}f(u,u_1)\frac{\Gamma(u-2)\Gamma(2-u_1)\Gamma(-u+u_1+2)}{\Gamma(4-u)\Gamma(u_1+1)\Gamma(u-u_1+1)}, \quad (4.39)$$

where the function $f(u,u_1)$ is

$$f(u,u_1) = 4[u_1(u-u_1)+u]-8(u+1)+16.$$

Furthermore, to work with the physical correlator $\hat{D}_{G^2}$, one must take the third derivative of Eq. (4.38) according to the definition in (4.12), taking advantage of the property of the

Borel transform that allows acting directly on the structure of the transformation, in this case, on Π_{G^2} itself. Then, the Borel transform is given by

$$B[D_{G^2}] = -\frac{3(N_c^2-1)}{\pi^3\beta_1}\left(\frac{-s}{\mu^2}e^C\right)^{-u}\frac{\Gamma(1+u)}{\Gamma(4-u)}\int_0^u du_1 f(u,u_1)\frac{\Gamma(2-u_1)\Gamma(2-u+u_1)}{\Gamma(1+u_1)\Gamma(1+u-u_1)}. \tag{4.40}$$

Recalling that C represents a constant that encodes the renormalization scheme initially chosen as $C = -5/3$ for the $\overline{\text{MS}}$ scheme, we will employ this constant to explore the perturbative structure of the Adler-type function. This exploration involves expanding $B[D_{G^2}^{\beta_0}]$ within the framework of perturbation theory

$$B[D_{G^2}^{\beta_0}] = \frac{(N_c^2-1)}{\pi^3\beta_1}\sum_{n=0}^{\infty} a_n u^{n+1}. \tag{4.41}$$

The relationship between the Borel transform $B[D_{G^2}^{\beta_0}]$ and the Adler-type function $D_{G^2}^{\beta_0}$ is given by the Borel sum (22), which is essentially the Laplace transform of Eq. (4.41). This finally gives the result in the α_s-plane

$$D_{G^2}^{\beta_0}(s) = \frac{(N_c^2-1)}{2\pi^2}a_s^2(-s)\sum_{n=0}^{\infty}\frac{(n+1)!}{2^n}a_n[\beta_1 a_s(-s)]^n, \tag{4.42}$$

where the coefficients a_n are known to all orders in perturbation theory (71). The series (4.42) can be expanded as

$$D_{G^2}^{\beta_0}(s) = \frac{(N_c^2-1)}{2\pi^2}a_s^2\left(1+2a_{s,r}+3.46a_{s,r}^2+5.29a_{s,r}^3+8.55a_{s,r}^4+12.57a_{s,r}^5+\cdots\right), \tag{4.43}$$

where the expansion was realized in terms of the reduced coupling, defined here as $a_{s,r} = \beta_1 a_s$.

4.3.1 Renormalons

The singularities of the Borel plane exhibit distinct effects depending on their proximity to the origin of the plane. As was mentioned previously, renormalons in close proximity to the origin are referred to as sub-dominant renormalons, whereas the closest one is termed the dominant renormalon. The knowledge of the $B[D_{G^2}^{\beta_0}]$ behavior when the dominant and sub-dominant renormalons are acting is important because these renormalons determine the asymptotic behavior of that series. In the present case, the factor $\Gamma(1+u)$ in Eq. (4.40) shows ultraviolet renormalons for all negative integers u, as discussed in the Ref. (71). The dominant UV renormalon at $u = -1$ generates a signal alternation for larger orders in the perturbative series when we consider a general scheme parameter C, according to the equation

$$B[D_{G^2}^{\beta_0}](u) \overset{u\to -1}{=} -\frac{(N_c^2-1)}{\pi^3\beta_0}\frac{\frac{493}{3360}e^C}{(1+u)}. \tag{4.44}$$

Furthermore, it is possible to write down the behavior in the vicinity of other UV renormalons

$$B[D^{\beta_0}_{G^2}](u) \overset{u\to UV}{=} -\frac{(N_c^2-1)}{\pi^3\beta_0}\left[\frac{\frac{493}{3360}e^C}{(1+u)}+\frac{\frac{172}{1575}e^{2C}}{(2+u)}+\frac{\frac{3723}{49280}e^{3C}}{(3+u)}+\cdots\right]. \tag{4.45}$$

On the other hand, the IR singularities are connected to power corrections in the OPE and bring ambiguities to the Borel transform. When we take the limit $\lim_{u\to 3} B[\hat{D}] = -\infty$, although the Borel plane in the large-β_0 limit generally shows an IR renormalon at $u = 2$, here the dominant UV renormalon is at $u = 3$. Given that the gluonium correlator is itself of dimension four, the first contribution comes from the dimension-six operator $\langle\Omega|g_s f^{abc}G^a_{\mu\nu}G^{\nu,b}_{\lambda}G^{\lambda\mu,c}|\Omega\rangle$. Exploring the Eq. (4.40) around dominant IR renormalon, we have a logarithmic behavior (71)

$$B[D^{\beta_0}_{G^2}](u) \overset{u\to 3}{=} 3\frac{(N_c^2-1)}{\pi^3\beta_0}e^{-3C}\ln\left[1-\frac{u}{3}\right]. \tag{4.46}$$

Furthermore, it is important to highlight that the Borel transform of $B[\hat{D}]$ has no singularity for $p \geq 4$; it only has branch cuts. This occurs due to the factor $1/\Gamma(4-u)$ in Eq. (4.40), which suppresses the logarithms $\ln[1-u/p]$ by a factor of $(p-u)$ (71).

4.4 Variation of the Renormalization Scheme

With the aim of probing the behavior of the two-gluon correlator in the large-β_0 limit with the variation of the renormalization scheme, which is encoded in C, we can explicitly decompose $B[\hat{D}]$ into a component dependent on the renormalization scheme and another independent of it, denoted as $b(u)$, via the following relation (20)

$$B[\hat{D}_{G^2}] = e^{-u\,C}b(u), \tag{4.47}$$

this highlights the fact that the residues depend on the renormalization scheme parameter C, while the positions of the renormalons remain invariant. Writing the Borel transform of the physical correlator as in Eq. (4.47), it is observed that by performing the Borel summation, the following relation can be obtained

$$\hat{D} = \int_0^\infty dt\ \exp\left[-t\left(\frac{1}{\alpha_s^C}+\frac{\beta_1 C}{2\pi}\right)\right] b\left(\frac{\beta_1 t}{2\pi}\right), \tag{4.48}$$

if we denote $\alpha_s^C = \hat{\alpha}$, it is possible to write the relationship between the coupling constant as a function of the scheme in terms of its value in the $\overline{\text{MS}}$ scheme

$$\frac{1}{\hat{\alpha}} = \frac{1}{\alpha_s^{\overline{\text{MS}}}} - \frac{\beta_1 C}{2\pi}. \tag{4.49}$$

In light of the foregoing discussion in chapter 2, we can now explore the possibility of adjusting the renormalization scheme to make our series more perturbative or less

perturbative. The change of scheme in the large-β_0 limit is simpler since the parameter to be varied, C, is evident in the Borel space expansion given the exponencial dependence in Eq. (4.47).

According to the definition adopted in (19) for the modification of the coupling, using the $\overline{\text{MS}}$ scheme, it is sufficient by setting $C = -5/3$. However, to align with the definitions employed in Chapter 2, a shift must be performed to parameterize the change of renormalization scheme around $C = 0$, as indicated by Figure (2.6). This change is specifically $C \to (\delta + C)$, where $\delta = 5/3$, and has already been done in the literature, as outlined in Ref. (20). This results in

$$\frac{1}{\hat{\alpha}_s} = \frac{1}{\alpha_s^{\overline{\text{MS}}}} - (\delta + C)\,\frac{\beta_1}{2\pi}, \tag{4.50}$$

which can be rewritten as

$$\frac{1}{\hat{a}_{s,r}} = \frac{1}{a_{s,r}^{\overline{\text{MS}}}} - \frac{(\delta + C)}{2}. \tag{4.51}$$

At this point, we are using the convention $a_s = \alpha_s/\pi$ and introducing the reduced coupling $a_{s,r} = \beta_1 a_s$. With this in mind, one of the possibilities to be explored is finally to use more positive or more negative values for C to assess the sensitivity of the series analyzed.

4.5 Conformal Mapping of the Borel Plane

Besides the variation of the renormalization scheme, the conformal mapping method is also investigated in this work. The conformal mapping of the Borel plane has been extensively explored in the context of both perturbative and non-perturbative QCD in the references (66, 73, 78). These works provide discussions and various applications for the conformal mapping of the Borel space, including the use of Padé approximants. Additionally, as briefly discussed in the introduction, infrared renormalons are responsible for introducing ambiguities in the Borel integral, which is related to the need for incorporating new terms due to non-perturbative corrections. These corrections, exponentially suppressed by the strong coupling, are referred to as power corrections and must be considered in the expansion in the product of operators. However, conformal mapping may serve as an alternative method to handle such power corrections (66). One of the most effective techniques for improving the convergence of perturbative series in QCD is the use of conformal mapping, previously applied to the Borel plane of the Adler function in the reference (66). In this reference, it is demonstrated that there exists a transformation that maps the singularities of the Borel plane onto a unit disk in the complex plane. This arrangement places dominant renormalons on the real axis and the boundary of the disk, creating a situation where none of them are privileged, this arrangement is called optimal conformal mapping. The resulting expression for the transformation, given the positions

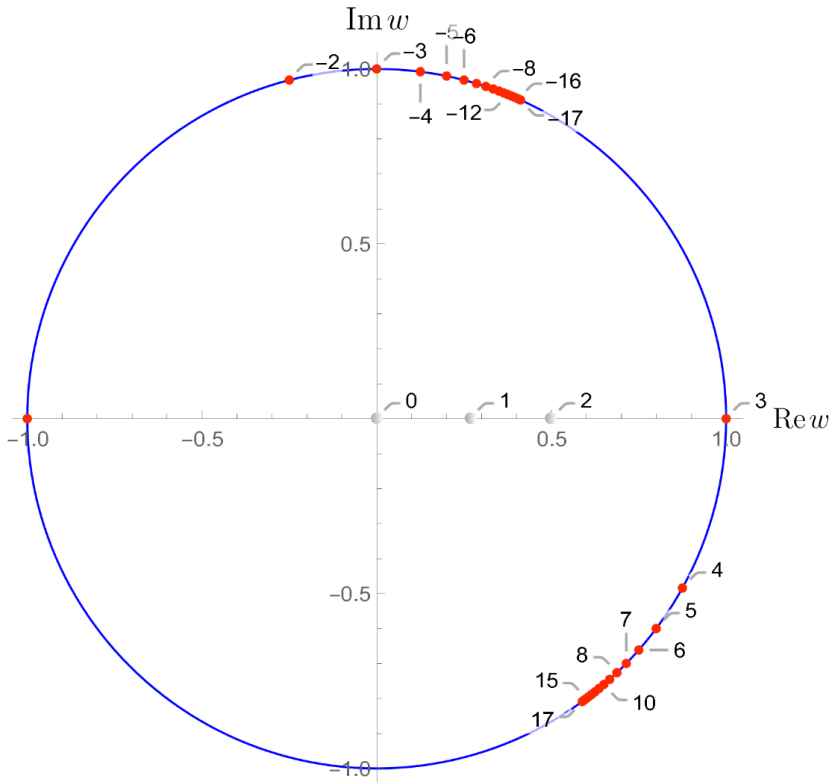

Figure 4.3 – Position of renormalons after optimal mapping onto a unit circle in the w-plane. Here, each red point represents the renormalons of $B[\hat{D}^{\beta_0}_{G^2}]$.

Source: By the author.

of the dominant renormalons p_{UV} and p_{IR}, closest to the origin of the u-plane, is

$$\tilde{w}(u) = \frac{\sqrt{1-u/p_{\mathrm{UV}}} - \sqrt{1-u/p_{\mathrm{IR}}}}{\sqrt{1-u/p_{\mathrm{UV}}} + \sqrt{1-u/p_{\mathrm{IR}}}}, \tag{4.52}$$

where w is the variable in the mentioned complex plane, and u is the Borel variable. This mapping can significantly enhance the convergence of the perturbative expansion of an observable by reducing the influence of renormalons. Not only the dominant renormalons but all renormalons are mapped onto the unit circle and equidistant from the origin.

The inverse of the optimal conformal mapping for the unit circle is given by

$$\tilde{u}(w) = \frac{3w}{(w-\xi_1)(w-\xi_2)}, \tag{4.53}$$

where the poles are at $\xi_1 = (-1)^{\frac{1}{3}}$ and $\xi_2 = -(-1)^{\frac{2}{3}}$. Through this inverse (4.53), we can rewrite the Borel transform in terms of w instead of u. The procedure involves substituting the Borel variable with the Taylor expansion of $\tilde{u}(w)$ and truncating at a certain order. After this variable change, the original series must be expanded again up to the last order before truncation.

By rewriting the Borel Transform in terms of w, we can express the Borel transform of the physical correlator function as a series in powers of w

$$B[\hat{D}] = \sum_{n=0}^{\infty} c_n w^n. \tag{4.54}$$

The power series in w is less affected by renormalons, making it more stable than the series in powers of u. In some cases, this may allow for better estimates of the coefficients of the perturbative series.

4.6 Padé Approximants

To make predictions for the coefficients at high orders of $D^{\beta_0}_{G^2}$, both the variation of the renormalization scheme and the conformal mapping will be evaluated in conjunction with Padé approximants (PAs). The approximant P^M_N is obtained through the ratio of two polynomials of order M and N, given by

$$P^M_N(u) = \frac{Q_M(z)}{R_N(z)} = \frac{a_0 + a_1 z + \cdots + a_M z^M}{1 + b_1 z + \cdots + b_N z^N}, \tag{4.55}$$

a rational approximant that makes contact of order $M+N$ with the Taylor series expansion of a function in the complex plane around $z = 0$, for example

$$f(z) = 1 + \sum_{n=0}^{\infty} f_n z^{n+1}. \tag{4.56}$$

For the sake of clarity, we can make an example to illustrate how this method works, i.e., applying a simple PA, P^1_1, to a toy function $f(z)$, that can be expanded in a Taylor series as

$$f(z) = \frac{\sqrt{1-z^2}}{(1+4z)^2} \approx 1 - 8z + \frac{95}{2}z^2 - 252z^3 + \frac{10047}{8}z^4 + \mathcal{O}(z^5). \tag{4.57}$$

The Padé approximant idea is that the Eq. (4.55) can be expanded and the coefficients of expansion in each perturbative order can be matched with the same order coefficient of Eq. (4.57) such that the coefficients of Padé approximants are determined. Expanding the approximant P^1_1 in a Taylor series, we arrive at

$$P^1_1 = \frac{a_0 + a_1 z}{1 + b_1 z} \approx a_0 + (a_1 - a_0 b_1)z + (a_0 b_1^2 - a_1 b_1)z^2 + (a_1 b_1^2 - a_0 b_1^3)z^3 + \mathcal{O}(z^4). \tag{4.58}$$

When the Eq. (4.58) is matched to Eq. (4.57), it is possible to determine the coefficients of P^1_1 as

$$a_0 = 1, \quad a_1 = -\frac{33}{16}, \quad b_1 = \frac{95}{16}. \tag{4.59}$$

Consequently, we can construct the PA in terms of the computed coefficients

$$P^1_1 = \frac{1 - \frac{33}{16}z}{1 + \frac{95}{16}z} \tag{4.60}$$

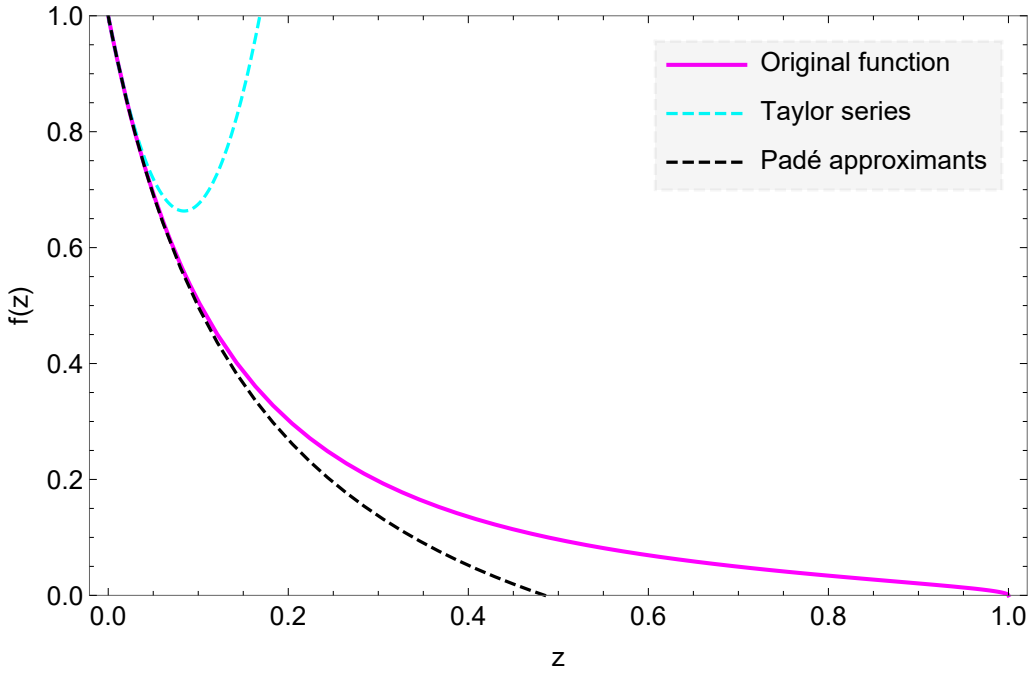

Figure 4.4 – Graph depicting a comparison between the Padé approximants and the Taylor series to approximate the function $f(z) = \sqrt{1-z^2}/(1+4z)^2$, using the same amount of information of $f(z)$.

Source: By the author.

and compare the coefficients not used to construct the PA, producing predictions for the next unknown coefficients

$$f(z) \approx 1 - 8z + 47.50z^2 - 252.00z^3 + 1255.88z^4 + \cdots, \tag{4.61}$$

$$P_1^1 \approx 1 - 8z + 47.50z^2 - 282.03z^3 + 1674.56z^4 + \cdots. \tag{4.62}$$

In this case, the order z^3 coefficient in Eq. (4.62) was predicted with approximately just 11% error, and the next-order coefficient was predicted with a 25% error. Another important feature of PAs to be discussed here is the pole predictions of the $f(z)$ function. This function has a pole at $z = -0.25$, and analyzing the denominator of the approximant P_1^1 it is possible to see that this function has a pole at $z = -0.168$, reproducing the pole with a 33.6% error.

In Figure (4.4), it is possible to see how the PA, the dashed black curve, adjusts to the original function $f(z)$, represented by the purple curve, in contrast with the truncated Taylor expansion of $f(z)$ (the dashed cyan curve), where it is clear that the Padé approximant presents a better adjustment to the original $f(z)$ than the Taylor expansion, relying on exactly the same amount of information.

Furthermore, in this work, a variant of the Padé approximant was employed, which is the partial Padé approximants, which is defined as

$$\mathbb{P}_{N,K}^{M}(z) = \frac{Q_M}{R_N(z)T_K(z)}, \tag{4.63}$$

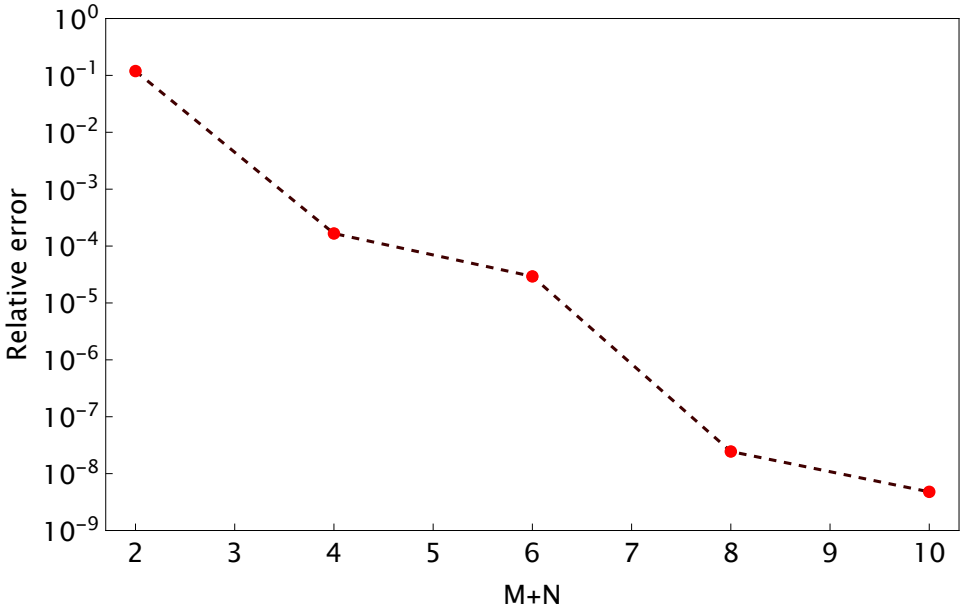

Figure 4.5 – Graph illustrating the relative error of the coefficients of $f(z)$ estimated by $P_N^N(z)$ concerning the number of coefficients $M+N$ used for the estimates.

Source: By the author.

where the coefficients R_N and Q_M are determined in the same way as explicitly explained by Eq. (4.55), and the T_K is a polynomial that encodes K zeros at the first K poles of the function we are applying the method. The explicit structure of this approximant after using the polynomial T_k form is

$$\mathbb{P}_{N,K}^{M}(z) = \frac{Q_M}{R_N(z)(z+z_1)(z+z_2)...(z+z_K)}, \tag{4.64}$$

where z_i, with $i = 1,2...K$, are the first zeros of $T_K(z)$. One way to analyze the estimates made by Padé approximants is through the convergence of the approximant to the approximated function $f(z)$. An important theorem in this context is Pomerenke's theorem (79).

Pomerenke's Theorem: *Let $f(z)$ be an analytic function at the origin and throughout the entire z-plane except for a finite number of isolated poles and essential singularities. Then we have:*

$$\lim_{N\to\infty} P_N^{\lambda N} = f(z), \tag{4.65}$$

provided that a compact set in the z-plane is taken and $\lambda \neq 0$ and $\lambda \neq \infty$.

It is still important to note that in light of Pomerenke's theorem, it is possible in some cases that even with the increase in the magnitude of $M+N$, there may be an increase in the relative error. This behavior can occur because some zeros of the numerator and denominator of the PA are close, which effectively acts as a reduction of order. This effect is called *defects* or *Froissart doublets* (18).

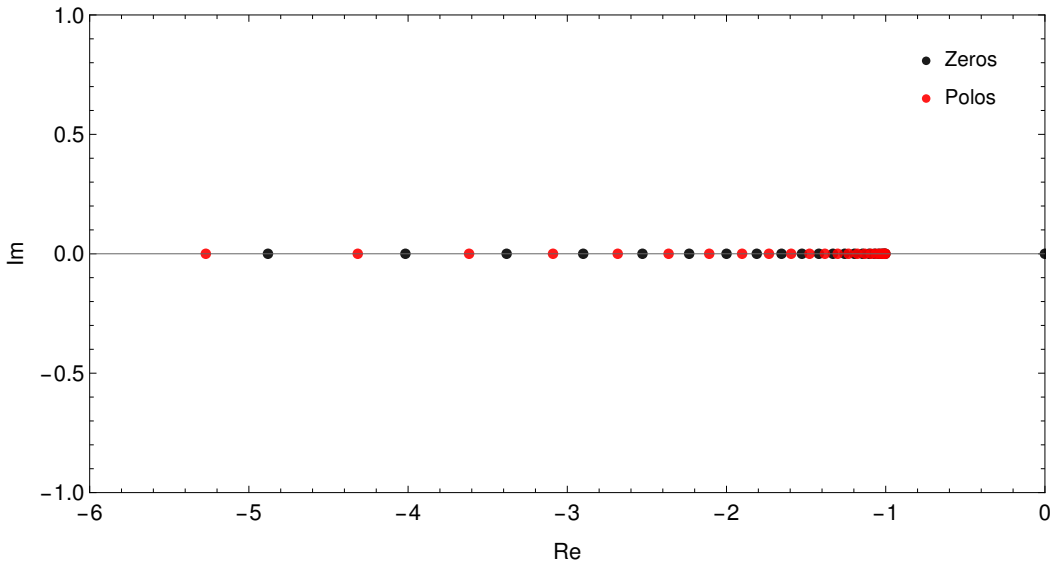

Figure 4.6 – Graph depicting that the PA P_{30}^{30} reproduce cuts by accumulations of poles and zeros. In this case, the approximants were employed for the function $f(z) = \log(1 - z)$.

Source: By the author.

In the case of interest in this work, in the large-β_0 limit, the first $(M + N)$ coefficients must be known to allow for the prediction of the coefficient of order $(M + N + 1)$ or higher. Considering that the series shown by Eq. (4.41) starts at u, we can set a_0 equal to zero for any PA calculated in this work. By applying PAs to the Borel transform of Eq. (4.41), we can obtain predictions for the higher-order coefficients of the two-gluon correlator in the large-β_0 limit. The results obtained from PAs are analyzed through the relative errors, according to

$$\sigma_{\text{rel}} = \left| \frac{a_n^P - a_n}{a_n} \right|, \tag{4.66}$$

where a_n^P refers to the estimated coefficient, while a_n represents the exact coefficient. This will be investigated for all the estimation methods at the large-β_0 limit used in this work, both for the first and the second unknown coefficients.

Dlog Padé Approximant

As we mentioned, the investigation of the renormalon structure of the Borel transform of the physical correlator shown in Eq. (4.41) reveals a cut for $u \geq 4$ due to the suppression of singularities in this region as discussed in (71). In order to investigate functions that have cuts using Padé approximants, it is necessary to explore how these approximants reproduce functions. A practical example involves applying the approximants to the function $\log(1 + z)$, which exhibits a branch cut for $z < -1$. Figure (4.6) illustrates the results for the polos and zeros of the Padé approximants for $M = N = 30$, based on matching to the first 32 coefficients, many more than in the previously used examples at the

beginning of the chapter. In the Figure (4.6), the poles and zeros of the Padé approximant are shown overlaid, where it can be observed that Padé attempts to reproduce the branch cut of the function through the accumulation of polos and zeros. A strategy to deal with this structure is to employ Dlog Padé approximants (18). For instance, considering a function that has cuts (18)

$$f(u) = \frac{A(u)}{(p-u)^{\gamma}} + B(u), \tag{4.67}$$

where $A(u)$ and $B(u)$ are analytic functions at $u = \mu$, but there are cuts resulting from the singular structure of the denominator when γ is a non-integer number. According to the method discussed in (18), instead of applying Padé approximants to the function $f(u)$, it is convenient to define another function, which for u close to p behaves as

$$F(u) = \frac{d}{du}\log[f(u)] \sim \frac{\gamma}{p-u}. \tag{4.68}$$

The Padé approximants P_N^M applied to the function $F(u)$ produce an approximation for the function $f(u)$ that is not necessarily rational. Here, we denote this approximation as $\mathrm{Dlog}_N^M(u)$ having the following structure

$$\mathrm{Dlog}_N^M(u) = f(0)\exp\left[\int du\, \mathrm{P}_N^M(u)\right], \tag{4.69}$$

where the normalization constant $f(0)$ must be reintroduced due to the loss of a constant in the differentiation process.

5 Large-β_0 Results

In this chapter, we will explore the accuracy of estimates for the physical correlator in the large-β_0 limit, $D^{\beta_0}_{G^2}$, using the Padé-Borel method, conformal mapping, and the change of renormalization scheme. Here, several sequences of Padés were initially investigated in the $\overline{\text{MS}}$ scheme with the purpose of finding an optimal method for making estimates in QCD, beyond the large-β_0 limit. As seen, in this limit, the quantity $D^{\beta_0}_{G^2}$ was computed at all orders in perturbation theory; nevertheless, the predictions of the sixth and seventh coefficients will be denoted as the first and second unknown coefficients, respectively, with reference to the challenges we encounter in complete QCD, where we know five coefficients of the Higgs decay into two gluons — that is the range of known coefficients —, so that this range corresponds to $M + N = 5$ coefficients necessary to make these predictions. In addition, quantitative analyses were performed using relative error for our predictions of $D^{\beta_0}_{G^2}$ coefficients employing Padé approximants, allowing exploration of the error of estimates in the α_s-space.

5.1 Padé Approximants Results in the $\overline{\text{MS}}$ Scheme

In the present case, the constant in the numerator of the Padé approximant (a_0) is always zero because the series $\hat{D}_{G^2}$ starts at α_s^2, and thus the series in the Borel space starts at u, as previously discussed in Chapter 4. Starting our investigation with Padés of the family P_N^{N+1}, which, since $a_0 = 0$, requires $2N + 1$ coefficients from the known series to predict the $2N + 2$ term. Then, a possible approximant to be considered in the final estimates in the Borel space is P_2^3, where it is necessary to fix a_1, a_2, a_3, b_1, and b_2, that is, five coefficients to realize predictions of the "missing" coefficients. The structure of $P_2^3(u)$ applied to $B[\hat{D}^{\beta_0}_{G^2}]$ is

$$P_2^3(u) = \frac{u + 0.999777u^2 + 0.575925u^3}{(u - 1.84668 + 0.531324i)(u - 1.84668 - 0.531324i)}, \tag{5.1}$$

which makes possible the quantitative analysis through the comparison of the series

$$B[D^{\beta_0}_{G^2}] \approx u + 2u^2 + 2.30556u^3 + 1.76444u^4 + 1.14045u^5 + 0.55870u^6 + 0.30433u^7 + \cdots,$$
$$P_2^3(u) \approx u + 2u^2 + 2.30556u^3 + 1.76444u^4 + 1.14045u^5 + 0.662866u^6 + 0.354161u^7 + \cdots.$$

In which it is possible to see through the expansion of the approximant P_2^3 the predictions in the Borel space, highlighted in blue, for the coefficients of order u^6 and u^7. After returning to the α_s-plane, it is possible to see that the approximant (5.1) provided an estimate in the α_s-plane for the coefficient $c_5 = 14.9145$ compared to 12.5708 from the exact series of the physical correlator in large-β_0, while the prediction for the second

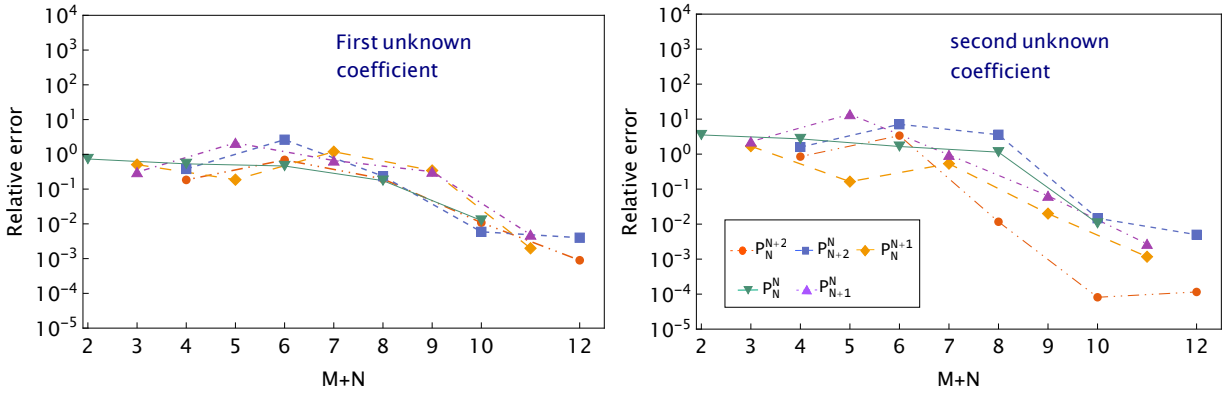

(a) (b)

Figure 5.1 – a) Relative error using the usual Padés in the $\overline{\text{MS}}$ scheme for the first unknown coefficient. **b)** The same types of Padés are used, but for the second unknown coefficient.

Source: By the author.

Table 5.1 – Estimates of the high-order coefficients of the physical correlator $\hat{D}(s)$ in the large-β_0 limit.

	c_5	c_6	c_7	c_8
Large-β_0	12.5708	23.9659	29.4801	111.206
P_3^2	39.5066	354.986	2835.48	19399.8
P_2^3	14.9145	27.8902	55.0385	111.773
P_4^1	31.6985	223.809	1474.4	8227.42
P_1^4	16.5855	37.5203	97.0054	282.149

Source: By the author.

unknown coefficient was $c_6 = 27.8902$ compared to 23.9659 from the original series, which represents a good estimate. However, in this case, the renormalons are not reproduced accurately, given that the poles of Eq. (5.1) are complex at $u = 1.847 \pm 0.531i$.

A final estimate should be made considering the parameters estimated by various families of Padés to avoid any kind of bias in the final estimate. Thus, it is necessary to compare our estimates with the exact result in large-β_0 to define an optimal method. In this range of known coefficients, we should only consider the approximants P_2^3, P_3^2, P_4^1, and P_1^4. As we have already shown the structure of P_2^3, we will also analyze the structure of the next approximant

$$P_3^2(u) = \frac{u - 0.800011u^2}{(u - 0.516271 \pm 0.694675i)(u - 0.703407)}. \tag{5.2}$$

Note that despite P_3^2 presenting a pole at $u = 0.703407$, the dominant IR renormalon of the series is at $u = 3$, as a consequence, this approximant does not capture the dominant renormalons. This behavior may occur because Padés do not very well reproduce functions

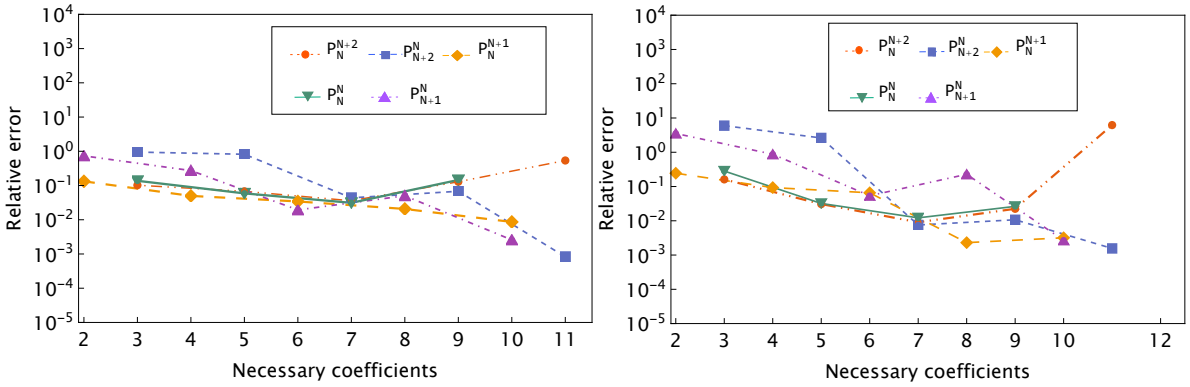

(a) (b)

Figure 5.2 – a) Relative error using the Dlog Padé approximants as indicated in the legend. **b)** The same type of approximants, but for the second unknown coefficient.

Source: By the author.

with cuts for low-order approximants, as the cut reproduction mechanism of Padés occurs through the reproduction of nearby poles, as indicated by Figure (4.6). Therefore, better reproduction of IR dominance should be expected employing Dlog Padé approximants. On the other hand, there are still two remaining cases, P_1^4 and P_4^1. In comparison with P_1^4, which only presents complex poles, P_4^1 predicts the unknown coefficients better, as indicated by Table 5.1. In this table, it is possible to see that the approximants P_3^2 and P_4^1 do not perform very well in terms of coefficient estimates. Furthermore, the results obtained for the relative errors of the first unknown coefficient are shown in Figure (5.1), further the result for the second unknown coefficient. Note that even with increasing $M + N$ magnitude there may be an increase in error, indicating a presence of Froissart doublets.

5.2 Dlog Padé Approximants Results in the $\overline{\text{MS}}$ Scheme

Considering that the estimates by rational methods used in the previous section showed considerable inaccuracies in estimating the first and second unknown coefficients, one possibility is to employ other methods, such as the Dlog Padé presented earlier, since $B[\hat{D}^{\beta 0}_{G^2}]$ has a cut for $u \geq 4$. Thus, for this range of interest, we have only a few contributions for the diagonal and closest-to-diagonal approximants.

Here, it is important to emphasize the number of coefficients needed to make predictions, since Dlog_N^M requires $M + N + 2$ coefficients from the series in the Borel space. However, considering that here the first term of the series is always zero, we can state that Dlog_N^M needs $M + N + 1$ coefficients from the original series, implying that in the case of Dlog_N^M we have $M + N = 4$, since the range of interest already mentioned is equal to five. The

Table 5.2 – Estimates, employing Dlog Padé, of the high-order coefficients of the physical correlator $\hat{D}(s)$ in the large-β_0 limit.

	c_5	c_6	c_7	c_8
Large-β_0	12.5708	23.9659	29.4801	111.206
Dlog_2^2	11.8297	23.198	13.7274	137.399
Dlog_3^1	22.8522	86.6234	289.498	848.03
Dlog_1^3	11.7195	23.2299	11.3268	146.509

Source: By the author.

starting point for our analysis in this limit is the following approximant

$$\text{Dlog}_1^3(u) = \frac{e^{0.0984417u^2+2.31774u}u}{(u+0.76706)^{0.243724}}, \tag{5.3}$$

which makes possible the quantitative analysis through the comparison of the series

$$B[D_{G^2}^{\beta_0}] \approx u + 2u^2 + 2.30556u^3 + 1.76444u^4 + 1.14045u^5 + 0.55870u^6 + 0.30433u^7 + \cdots,$$
$$\text{Dlog}_1^3(u) \approx u + 2u^2 + 2.30556u^3 + 1.76444u^4 + 1.14045u^5 + 0.52085u^6 + 0.294983u^7 + \cdots;$$

where it is clear that it requires 5 known coefficients from the original series for predictions when using Dlog_N^M, with $M+N=4$. Furthermore, it is noted that the estimates highlighted in blue, carried out by $\text{Dlog}_1^3(u)$, present a relative error of approximately 6.8% in the order of u^6 and 3.1% in the order of u^7, representing very good estimates.

In addition to approximant (5.5), we also investigated other sequences

$$\text{Dlog}_2^2(u) = \frac{u}{(13.3261\ -u)^{31.2172}(u+0.786904)^{0.26956}}, \tag{5.4}$$

$$\text{Dlog}_3^1(u) = \frac{e^{1.16494\tan^{-1}(0.498765(2u+0.0799489))}u}{(1.17918\ -u)^{0.990687}\,(u^2+0.0799489u+1.00656)^{0.00465629}}; \tag{5.5}$$

where the results of predictions can be found in Table 5.2. In this case, the approximants $\text{Dlog}_2^2(u)$ and $\text{Dlog}_1^3(u)$ show superior estimates to all presented so far, while the poor behavior of Dlog_1^3 can be justified by the absence of reproduction of dominant renormalons, as it shows a pair of complex poles and a pole at $u = 1.17918$ that does not reproduce the main IR renormalon, On the other hand, Dlog_3^1 brings, for the first time, a partial reproduction of the dominant UV renormalon, presenting branch point at $u = -0.76706$. The same occurs with Dlog_2^2, which has a pole at $u = -0.786904$. Thus, a superiority is detected in relation to the estimates in Table (5.3), especially in the approximants that partially reproduce the pole at $u = -1$. In Figure (5.2), it is possible to see how the relative error behaves with the variation of the number of coefficients needed to perform the estimates. It can be noted that both for the prediction of the first and the second coefficient, there is an increase in relative error for the number of necessary coefficients equal to eleven. After scrutinizing the structure of Dlog_4^6, a Froissart doublet was spotted, with a zero at $u = -4.84681$ and a branch point at the u value.

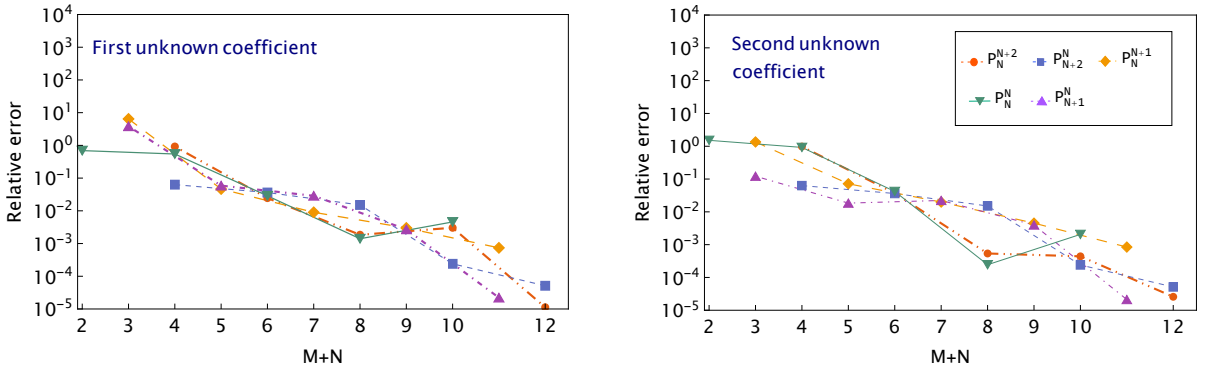

(a) (b)

Figure 5.3 – a) Relative error using the indicated Padés, with $C = 0$, for the first unknown coefficient. **b)** The same types of Padés are investigated, but for the second unknown coefficient.

Source: By the author.

5.3 Variation of Renormalization Scheme

In the light of the formalism presented in Section 4.4 for the change of renormalization scheme, one of the most interesting cases for investigation is to eliminate the exponential dependence that accompanies the residues of the renormalons, which in this case should be $C = 0$, resulting in the modification

$$\hat{D}^{C=0}_{G^2} \approx \hat{a}^2_{s,r}(1 + 0.333\hat{a}_{s,r} + 0.542\hat{a}^2_{s,r} - 0.216\hat{a}^3_{s,r} + 1.351\hat{a}^4_{s,r} - 3.028\hat{a}^5_{s,r} + \cdots),$$

and as a consequence of this variation, the series assumes an oscillatory character in the sign starting from $\hat{a}^3_{s,r}$. However, for the purpose of comparison with the results obtained in the $\overline{\text{MS}}$ scheme, it is necessary to modify the value of $\hat{a}_{s,r}$ according to the Eq. (4.51). In this case, a Taylor expansion is required to connect with the original result

$$\hat{a}_{s,r} = a_{s,r} + a^2_{s,r}\left(\frac{C+\delta}{2}\right) + a^3_{s,r}\left(\frac{C+\delta}{2}\right)^2 + a^4_{s,r}\left(\frac{C+\delta}{2}\right)^3 + a^5_{s,r}\left(\frac{C+\delta}{2}\right)^4 + \cdots,$$

and later it is necessary to realize a re-expansion of the series, obtaining a new series in terms of $a_{s,r}$; in addition, truncate this new series at the same order as the considered series $\hat{D}^{C=0}_{G^2}$. The results of the approximants with a change of scheme show better estimates for the coefficients of high orders of the series, which can be visualized in Figure 5.3, in contrast with Figure 5.1. Through the comparison of these figures, one notes better results for $C = 0$ when compared with $\overline{\text{MS}}$. No longer are there just a few exceptions of Padé sequences, but rather a general behavior of all the approximants. Additionally, as can be observed in the previous results, in some cases, a competition between the first and second unknown coefficients, since sometimes the prediction of the second unknown coefficient is better than the first. Furthermore, analyzing the results, it can be concluded that the sequences

Table 5.3 – Estimates, employing Padé approximants, of the high-order coefficients of the physical correlator $\hat{D}_{G^2}(u)$ in the large-β_0 limit using $C = 0$ (C_0) in comparison with the $\overline{\text{MS}}$ scheme.

	c_5	c_6	c_7	c_8
Large-β_0	12.5708	23.9659	29.4801	111.206
$P_2^3[\overline{\text{MS}}]$	14.9145	27.8902	55.0385	111.773
$\text{P}_2^3[C_0]$	12.7113	23.9243	31.6375	105.424
$P_3^2[\overline{\text{MS}}]$	39.5066	354.986	2835.48	19399.8
$\text{P}_3^2[C_0]$	12.3925	23.1475	25.5251	100.432
$P_4^1[\overline{\text{MS}}]$	31.6985	223.809	1474.4	8227.42
$\text{P}_4^1[C_0]$	15.8487	42.3433	129.497	444.289
$P_1^4[\overline{\text{MS}}]$	16.5855	37.5203	97.0054	282.149
$\text{P}_1^4[C_0]$	5.45188	59.3355	-440.64	5170.61
$\text{Dlog}_2^2[\overline{\text{MS}}]$	11.8297	23.198	13.7274	137.399
$\text{Dlog}_2^2[C_0]$	12.0088	23.2941	17.4774	127.71
$\text{Dlog}_3^1[\overline{\text{MS}}]$	22.8522	86.6234	289.498	848.03
$\text{Dlog}_3^1[C_0]$	10.6654	20.3775	-16.5231	149.013
$\text{Dlog}_1^3[\overline{\text{MS}}]$	11.71950	23.2299	11.3268	146.509
$\text{Dlog}_1^3[C_0]$	11.71953	23.2299	11.3268	146.509

Source: By the author.

of approximants P_{N+1}^N and P_N^{N+1} provide good estimates for the complete $M + N = 5$ and also show competitive estimates for the first and second unknown coefficients.

In this way, through a case analysis, some results stand out and should be highlighted, for example

$$P_2^3[C_0] = \frac{u + 0.890676u^2 + 0.15905u^3}{(u + 1.04064)(u - 2.47768)}, \tag{5.6}$$

$$P_3^2[C_0] = \frac{u + 0.746445u^2}{(u + 0.999403)(u - 3.29969 \pm 0.587629i)}; \tag{5.7}$$

where the notation C_0 refers to $C = 0$. This time, the results are better than the Padé approximants for the $\overline{\text{MS}}$ scheme because eliminating the exponential dependence of $B[\hat{D}(s)] = e^{-uC}b(u)$ results in a modification of the residues of the poles but does not change their positions. This change allows the approximants to more easily capture the dominant renormalons. In the case of P_3^2, despite having complex poles, the approximant showed great success in estimates, as shown in Table 5.3, due to the excellent reproduction of the pole at $u = -0.999403$. This is also demonstrated by P_2^3, presenting a pole at $u = -1.04064$. However, unlike the previous case, the IR renormalon is partially reproduced by the pole at $u = 2.47768$, effectively resulting in insufficient performance for estimating the second unknown coefficient of this series due to the competition between renormalons.

Another possibility is to implement a scheme variation for the Dlog Padés to explore the sensitivity of estimates to the variation of C. To do this, initially adopting the

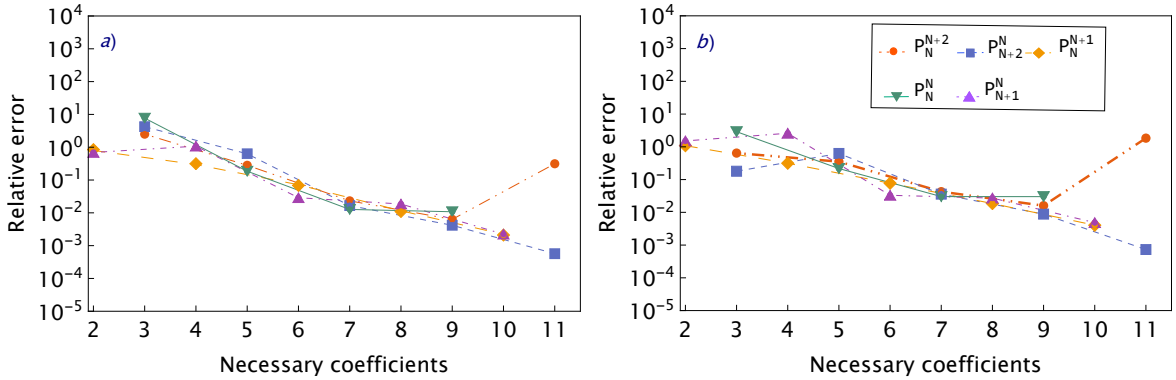

Figure 5.4 – a) Relative error using the indicated Dlog Padés, with $C = 0$, for the first unknown coefficient. **b)** The same types of Padés are investigated, but for the second unknown coefficient.

Source: By the author.

same procedure of eliminating the exponential dependence and analyzing Dlog_2^2, Dlog_3^1, and Dlog_1^3, similar to the previous case, a difference in estimates is observed due to the modification in capturing renormalons. For instance, Dlog_2^2 presented a pole at $u = -0.816492$, being more faithful to the dominant UV renormalon than the estimate made in the $\overline{\text{MS}}$ scheme

$$\text{Dlog}_2^2(u) = \frac{u}{(4.89044 - u)^{3.48797}(u + 0.816492)^{0.310177}}.$$

On the other hand, Dlog_3^1 reproduced exactly the same pole at $u = -0.76706$, while Dlog_1^3 also shows a profile modification, maintaining the two complex poles. However, unlike the previous case, it manages to provide an approximation for the dominant UV with the pole at $u = -0.702426$. The general behavior at higher order can be visualized in Figure 5.4, where it is possible to see that the Froissart doublet is still present for the approximant Dlog_4^6, with the number of necessary coefficients equal to eleven.

5.4 Conformal Mapping Results

Through the series in terms of a new variable, w, and employing the conformal mapping defined by the Eq. (4.52), the Padé approximants can be constructed similarly to what was done previously. However, the main interest in this procedure is to make estimates for $M + N = 5$ in the α_s space, which requires returning to this space after making estimates in the w-plane.

One point to highlight in this part is that the best results for prediction in the w space for the first unknown coefficient were obtained through P_{N+1}^N with $M + N = 3$, showing a relative error of 0.53% for the fourth unknown coefficient of the series. However, the same family of approximants exhibits a significant worsen for $M + N$ equal to five. In

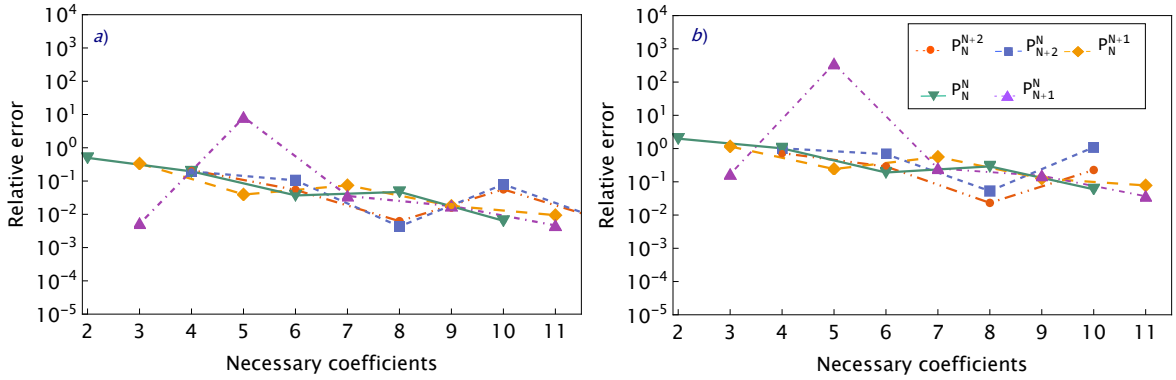

Figure 5.5 – a) Relative error using the indicated Padés with $C = 0$ and optimal conformal mapping for the first unknown coefficient. **b)** The same types of Padés are investigated, but for the second unknown coefficient.

Source: By the author.

Figure (5.5), it is possible to see that the same general behavior can be observed for the second unknown coefficient. The reduced accuracy of these estimates for $M+N=5$ can be explained by the presence of Froissart doublets, as $P_3^2(w)$ has a zero at $w=-0.00947251$ and a pole exactly at the same value, effectively reducing the order of the Padé.

On the other hand, the optimal behavior of P_2^1 can be explained by its structure being the same as the inverse transformation $\tilde{u}(w)$, leading its Taylor expansion to more accurately reproduce the series in the w space, as its derivatives have the same structure. The relative error is not invariant between the conformal plane and the Borel space; consequently, relative errors in w do not, at first, correspond to a directly proportional accuracy of estimates in the α_s space.

To verify the mentioned behavior, it is sufficient to analyze the series produced as the final result. Note that the blue coefficients represent the estimates initially done in the conformal space. The first unknown coefficient has an absolute error of 96.61 and a relative error of 3.94%, while the second unknown coefficient shows a significant deterioration compared to the differences in estimates.

- The exact series $B[\hat{D}_{G^2}](w)$ and the approximated $P_2^3(w)$ in the conformal space

$$B[\hat{D}](w) = 3w + 21w^2 + 98.25w^3 + 344.669w^4 + 996.557w^5 + 2453.96w^6 + 5287.38w^7 + \cdots,$$

$$P_2^3(w) = 3w + 21w^2 + 98.25w^3 + 344.669w^4 + 996.557w^5 + 2357.35w^6 + 4008.89w^7 + \cdots.$$

To return to the Borel space, one must employ the transformation $\tilde{w}(u)$, expand in Taylor series, and couple this expansion at each order of the previous series. This procedure requires a coherent re-expansion, i.e., a coefficient of a certain order will affect another order of the series. As a direct consequence of this, the relative error between the Borel space and the conformal space is not invariant.

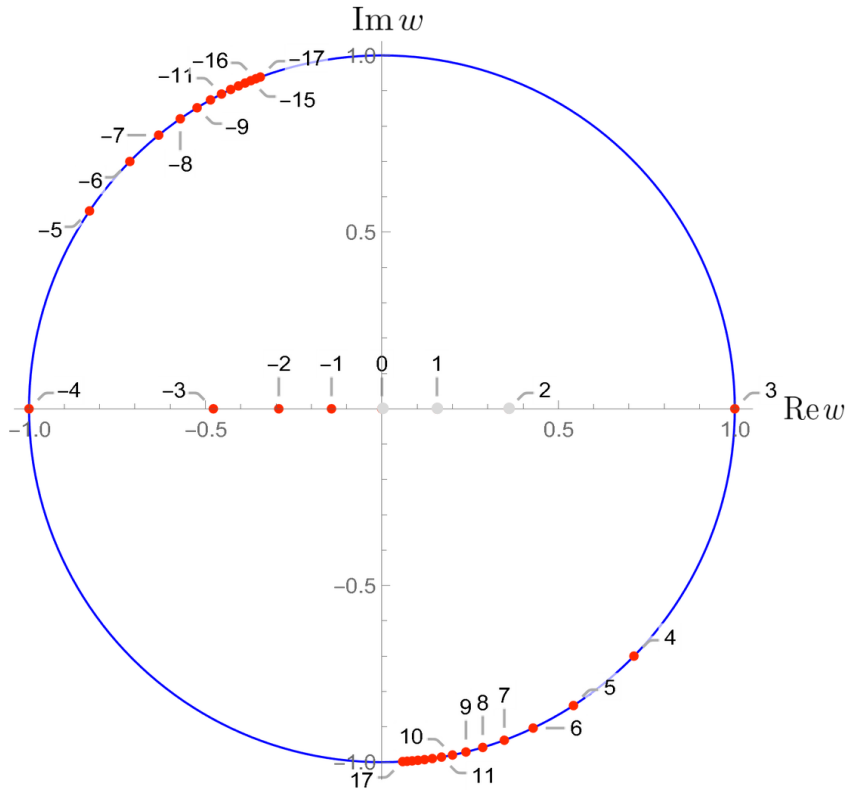

Figure 5.6 – Position of renormalons after modifying the structure of mapping onto a unit circle in the w-plane. Here, each red point represents the renormalons of $B[\hat{D}^{\beta_0}_{G^2}]$.

Source: By the author.

- The exact series $B[\hat{D}_{G^2}](u)$ and the approximated $\tilde{B}[\hat{D}_{G^2}](u)$, in the Borel space

$$B[\hat{D}](u) = u + 2u^2 + 2.30556u^3 + 1.76444u^4 + 1.14045u^5 + 0.558704u^6 + 0.304329u^7 + \cdots,$$

$$\tilde{B}[\hat{D}](u) = u + 2u^2 + 2.30556u^3 + 1.76444u^4 + 1.14045u^5 + 0.426184u^6 - 0.0152191u^7 + \cdots.$$

On the other hand, to re-establish the connection with the original series $a_{s,r}$, we must employ Borel transformation, where the coefficients of the Borel transform a_n are multiplied by $(n+1)!/2^n$. This leads to the invariance of the relative error between the two spaces.

- Exact series $B[\hat{D}]$ and approximated P^3_2 in the space $a_{s,r}$

$$\hat{D}_{G^2} = a^2_{s,r}(1 + 2a_{s,r} + 3.458a^2_{s,r} + 5.293a^3_{s,r} + 8.553a^4_{s,r} + 12.571a^5_{s,r} + 23.966a^6_{s,r} + \cdots),$$

$$\tilde{D}_{G^2} = a^2_{s,r}(1 + 2a_{s,r} + 3.458a^2_{s,r} + 5.293a^3_{s,r} + 8.553a^4_{s,r} + 9.589a^5_{s,r} - 1.199a^6_{s,r} + \cdots).$$

Note that the first unknown coefficient in the $\overline{\text{MS}}$ scheme was not reproduced with sufficient accuracy compared to the predictions in the Borel plane, presented using $C = 0$ as shown in Table 5.3. However, it exhibited comparable precision to the usual Padé applied directly in Borel space, evaluated in the $\overline{\text{MS}}$ scheme. This indicates that the conformal mapping, despite yielding extremely precise results in the range of $M + N$ equal to 3, did not provide more accurate results than the previous ones for $M + N = 5$.

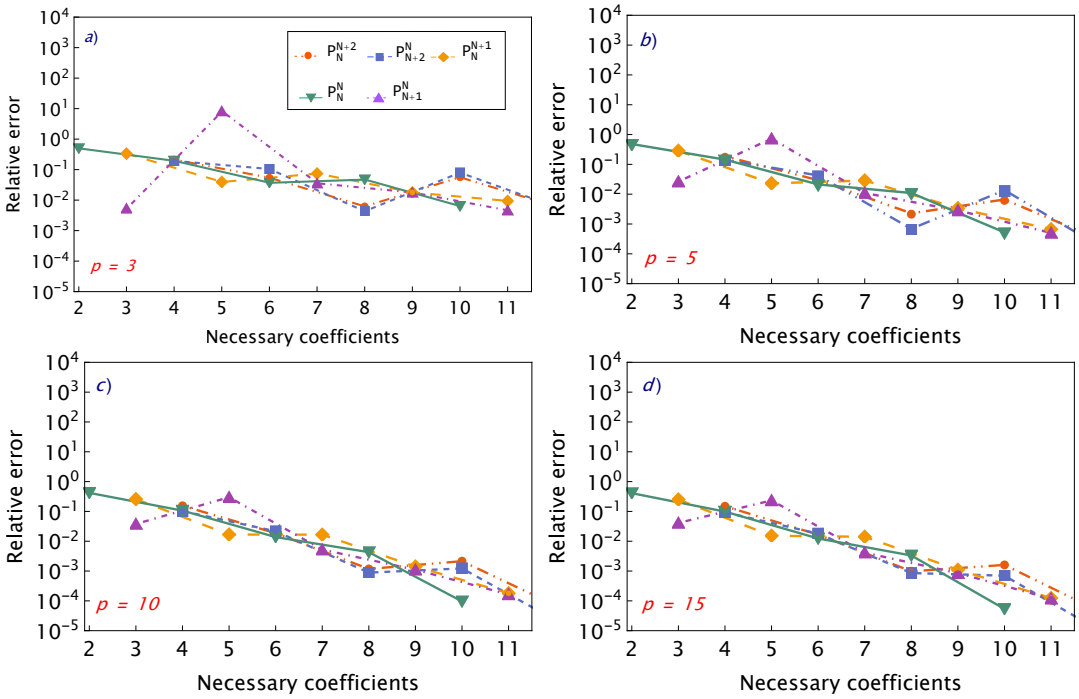

Figure 5.7 – Graphs showing the modification of the relative error with the variation of p, approximating the IR renormalon from the origin.

Source: By the author.

One of the paths to follow in this case is to consider a modification of the structure of the conformal mapping presented by the Eq. (5.8), in addition to the possibility of changing the renormalization scheme as done previously, which leads us to a problem with three parameters already introduced before in Eq. (4.52): C, p_{IR}, and p_{UV}. In principle, following the prescription of Ref. (73), which practically maps the IR renormalons inside the unit circle in the w space, the value of p indicates which value will be on the edge of the disc. The implemented values for p are $(3, 5, 10, 15)$ while $p_{\mathrm{UV}} = -1$, with the caveat that the absence of IR renormalons beyond the dominant one is already known in the present case. Then, the structure of this new conformal mapping is

$$\tilde{w}(u,p) = \frac{\sqrt{1+u} - \sqrt{1-u/p}}{\sqrt{1+u} + \sqrt{1-u/p}}. \tag{5.8}$$

In the pursuit of improving the obtained results, one approach is to adopt various values of C and p and analyze the relative error concerning the estimates. One of the most interesting cases shown in Figure 5.7 refers to the successful estimation of the coefficient for $\mathcal{O}(w^4)$ and consequently for order $\mathcal{O}(\alpha_s^5)$ as mentioned. Based on this behavior, the relative errors for this coefficient were analyzed, for $C = 0$ in conjunction with the variation the structure of the conformal mapping to assess the sensitivity of our results in this range for such variations, as indicated by Figure 5.7.

Analyzing the profile of results for the variation of p for $C = -5/3$, it is clear that

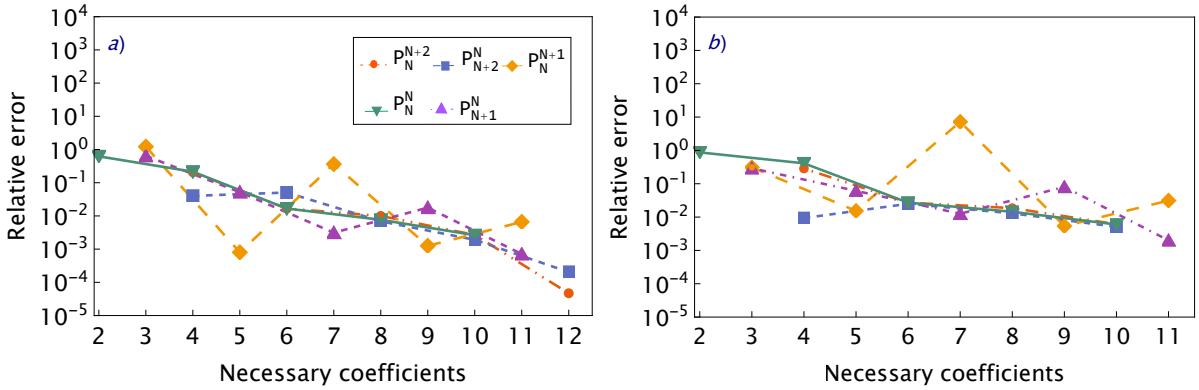

Figure 5.8 – a) Relative error for the first unknown coefficient in the w-space for various Padé families, using $C = 0.26$ with $p_{\text{UV}} = -1$ and $p_{\text{IR}} = 3$. **b)** The same prescription, but for the second unknown coefficient.

Source: By the author.

the precision decreases for the coefficient of $\mathcal{O}(\alpha_s^6)$ with the increase of p. However, in compensation, a significant improvement is observed for the approximant P_{N+1}^N with $N = 2$, P_2^3, due to the elimination of the Froissart doublet present at $p = 3$. However, the reduction reaches a saturation, varying very little between Figure 5.7 c) and Figure 5.7 d), leading us to conclude that there are not significant advantages of this method in contrast with the others already implemented in this chapter. Furthermore, P_2^3 provided assessments for the terms of order $\mathcal{O}(w^4)$ with approximately 1.5% uncertainty. However, for the α_s-plane, the first unknown coefficient demonstrates a relative error of 22%, suggesting a significant loss of precision between these spaces.

Another possibility is to prioritize the UV poles, given the cuts in the positive real part in the Borel plane for $B[\hat{D}_{G^2}]$, in order to set $p_{\text{UV}} = p' = -4$ (lying on the edge of the unit circle) while $p_{\text{IR}} = 3$ is maintained fixed, according to equation

$$\tilde{w}(u) = \frac{\sqrt{1 - u/p'} - \sqrt{1 - u/3}}{\sqrt{1 - u/p'} + \sqrt{1 - u/3}}. \tag{5.9}$$

As such, the outcomes of this variation in mapping can be found in Table 5.4.

To define an optimal method to be used, one possibility is the variation of C, which can provide better estimates by more easily capturing the essence of dominant singularities in the Borel space, masterfully reproducing the dominant UV renormalon as in the case of P_3^2 and P_3^2, according to equations (5.6) and (5.7), by eliminating the exponential dependence ($C = 0$). Based on this, we explore the behavior of estimates in the space of $\hat{a}_{s,r}$ using $p_{\text{IR}} = 3$ with small variations around $C = 0$ to search for precise estimates in the range of $M + N$ equal to five.

5.5 Final Large-β_0 Results

With the purpose of assigning a final result in the large-β_0 limit, it is important to illustrate the possible traps that can appear when we are analyzing the sensitivity to the renormalization parameter C. For example, Figure 5.8 indicates the results of the Padé approximants employing the optimal conformal mapping and a very specific C value: $C = 0.26$. The first coefficient corresponds to an estimate of $c_5 = 12.5675$ with only 0.027% error. Furthermore, analogous to the case of conformal mapping in the $\overline{\text{MS}}$ scheme for different values of p, there is the presence of a Froissart doublet in the next order after an optimal estimate, in this case at $M + N = 7$. Such estimates are visualized in Table 5.4. This case is ideal to demonstrate that despite estimates for a range of approximants providing very low relative errors, it does not mean that we should exclusively use them in the final estimates for complete QCD to avoid biased final results.

Table 5.4 – Estimates, employing Pade approximants, of the high-order coefficients of the physical correlator $\hat{D}^{\beta_0}_{G^2}$ in the large-β_0 limit using $C = 0$.

	c_5	c_6	c_7	c_8
Large-β_0	12.5708	23.9659	29.4801	111.206
$\text{P}^3_2(u)$	12.7113	23.9243	31.6375	105.424
$\text{P}^2_3(u)$	12.3925	23.1475	25.5251	100.432
$\text{P}^1_4(u)$	15.8487	42.3433	129.497	444.289
$\text{P}^4_1(u)$	5.45188	59.3355	-440.64	5170.61
$\text{Dlog}^2_2(u)$	12.0088	23.2941	17.4774	127.71
$\text{Dlog}^3_1(u)$	10.6654	20.3775	-16.5231	149.013
$\text{Dlog}^1_3(u)$	11.7195	23.2299	11.3268	146.509
$\text{P}^3_2(w)$	12.9731	24.2721	35.7199	104.54
$\text{P}^2_3(w)$	12.0595	22.3369	17.7071	95.0747
$\text{P}^4_1(w)$	13.0785	24.5051	37.5133	106.374
$\text{P}^1_4(w)$	12.1161	22.5123	19.0653	97.039
$\text{P}^3_2(w)$	12.6538	23.7763	30.5381	104.274
$\text{P}^2_3(w)$	12.1669	22.3384	19.9979	89.3471
$\text{P}^4_1(w)$	11.8357	22.8947	16.2494	121.942
$\text{P}^1_4(w)$	17.5705	58.5073	232.145	947.541

Source: By the author.

In order to determine the ultimate result for the large-β_0 limit, the methodology employed for assigning a definitive value to the estimates involves utilizing the arithmetic mean as the central value. In this analysis, estimates through Padé approximants and Dlog's in Borel space were incorporated, in addition to optimal conformal mapping. Furthermore, the mapping was still performed, emphasizing UV renormalons, which can be found in Table 5.4. Additionally, the final systematic uncertainty is calculated as half of the interval between the largest and smallest estimates.

This results in a final estimate for the first and second "unknown" coefficients of

$$c_5 = (12 \pm 6), \qquad c_6 = (29 \pm 20); \tag{5.10}$$

which provides good estimates when compared to the exact value of the coefficient. However, from Table 5.4, we notice that estimates using the conformal mapping do not show significant advantages over other estimates. Then, in full QCD, the renormalization change is more complicated than the large-β_0 limit. Then, one possibility also explored here is to evaluate the estimates directly in the α_s-plane along with the Padé-Borel method.

6 Full QCD Results

In this chapter, we will present the results for the prediction of the first unknown coefficient in perturbation theory of Higgs decay into two gluons. To illustrate how the methods work, we will employ the PAs in the last known coefficient of $\mathrm{Im}\Pi_{G^2}$. We also conducted a postdiction of the last known coefficient of $\Gamma_{h\to gg}$ to reiterate the validity of our prediction methods. Finally, we investigate the sensitivity of the Higgs decay into two gluons with respect to the renormalization parameter and its truncation error.

At this point in the study, we determine the error directly by estimating the first unknown coefficient of the series through the use of Padé approximants and Dlog Padé approximants, instead of scrutinizing the truncation error through the variation of the renormalization parameter. To elucidate this choice, consider a physically meaningful quantity in perturbation theory, evaluated at the scale $\mu = \mu_0$ and starting at a power k_0, which can be written as

$$\Gamma(\mu) = \sum_{n=0}^{\infty} \alpha_s^{n+k_0}(\mu) \sum_{i=0}^{n-1} c_{n,i} \ln^i \left(\mu^2/Q^2\right). \tag{6.1}$$

Often, this quantity is evaluated for $\mu^2 = Q^2$, i.e., in this case, the logarithms are resummed and the perturbative coefficients become independent of μ. The scale dependence can be recovered by writing the coupling at a given scale $\alpha_s(\mu_0)$ in terms of an expansion in powers of $\alpha_s(\mu)$ using the beta function, so that after replacing each power of $\alpha_s(\mu_0)^{n+k_0}$ in Eq. (6.1), it is necessary to re-expand. For $k_0 = 0$, one obtains the following recursive relation for the coefficients (80)

$$c_{n,l}(Q,\mu) = \frac{1}{l} \sum_{j=0}^{n-1} j\beta_{n-1-j} c_{j,i-1}, \tag{6.2}$$

where one notes that only $c_{0,n}$ are scale-independent, while the others are linear combinations of coefficients of the type $c_{0,n}$ and the coefficients of the beta function. Therefore, the $c_{0,n}$ are the independent coefficients that must be determined in loop calculations, while the others are generated by the renormalization group. This is presented in Ref. (80) and discussed in detail for different k_0 values in Ref. (65).

Considering the behavior of perturbative series, as discussed in Chapter 4, the series in Eq. (6.1) must be truncated at a certain order due to the Missing Higher-Order coefficients (MHO). Assuming a scenario where non-perturbative effects are negligible, we can write

$$\Gamma(Q) = \sum_{n=0}^{k} c_n(Q) \alpha_s^{n+k_0} + \Delta_{\mathrm{MHO}}, \tag{6.3}$$

where the trucation error is

$$\Delta_{\mathrm{MHO}} = \sum_{n=k+1}^{k'} c_n(Q) \alpha_s^{n+k_0}. \tag{6.4}$$

Under the assumption that $|c_{k+1}| \approx |c_k|$, it is possible to write (80)

$$\Delta_{\text{MHO}} \simeq |c_{k+1}|\alpha_s^{k_0+k+1}. \tag{6.5}$$

The prescription used here to evaluate the impact of Δ_{MHO} on the observable, Γ, calculated exactly up to order k (Γ_k), is as follows

$$\Gamma_k^{\pm} = \Gamma_k \pm \frac{\Delta_{\text{MHO}}}{2}, \tag{6.6}$$

where it is expected that the true value of this quantity is inside the range $[\Gamma_k^+, \Gamma_k^-]$. In other words, estimating the coefficient c_{k+1} means estimating, within the mentioned approximation, the effects of MHOs. In this chapter, we will show this estimation of truncation error for the decay $h \to gg$ using Padé approximants, analogous to what was done in large-β_0. In addition to testing the methods used in this part on the last known coefficient of the decay of interest, a good estimate of the last known coefficient suggests promising prospects for predicting unknown coefficients.

6.1 The Illustration of the Prediction Method

To elucidate the application of Padé approximants used in the final estimates for the first unknown coefficient, we will exemplify a practical scenario by estimating the last known coefficient of the two-gluon correlator in full QCD, as indicated in Eq. (6.7), since this correlator is one of the ingredients in the description of the Higgs decay into two gluons, as discussed in Chapter 3. As we already discussed, the coefficients of $\text{Im}\Pi_{G^2}$ exhibit a dependence on n_f. After testing the methods discussed in the previous chapter in the case of full QCD, and given the fact that only limited information about the renormalons are available in this case, it turned out that the optimal strategy involves the use of the n_f dependence of the perturbative coefficients. In this part of the work, the method that we employ involves the estimation of coefficients at each power of n_f^n, where n ranges from 0 to k, with k representing the highest exactly known power. Additionally, the method has proven useful in predicting coefficients of the $\beta(a_s)$ function, as shown in the Ref. (21).

Eq. (6.7) that describes the imaginary part of the gluonium correlator times a factor of $4\pi/N_A q^4$, which is called $G(q^2)$, can be written as a function of n_f through the numerical calculation of coefficients $g_1, \ldots, g_4$ in a series

$$G(q^2) = 1 + \sum_{n=1} g_n \alpha_s^n, \tag{6.7}$$

given in Eq. (3.36) to (3.37), such that the result is (15)

$$\begin{aligned} G(q^2) = 1 &+ (5.80916 - 0.371362n_f)\alpha_s + (24.6184 - 3.98941n_f + 0.0913684n_f^2)\alpha_s^2 \\ &+ (82.3393 - 24.899n_f + 1.49889n_f^2 - 0.017346n_f^3)\alpha_s^3 + (218.615 - 112.977n_f + \\ &+ 12.7653n_f^2 - 0.397864n_f^3 + 0.00258089n_f^4)\alpha_s^4 + \mathcal{O}(\alpha_s^5). \end{aligned} \tag{6.8}$$

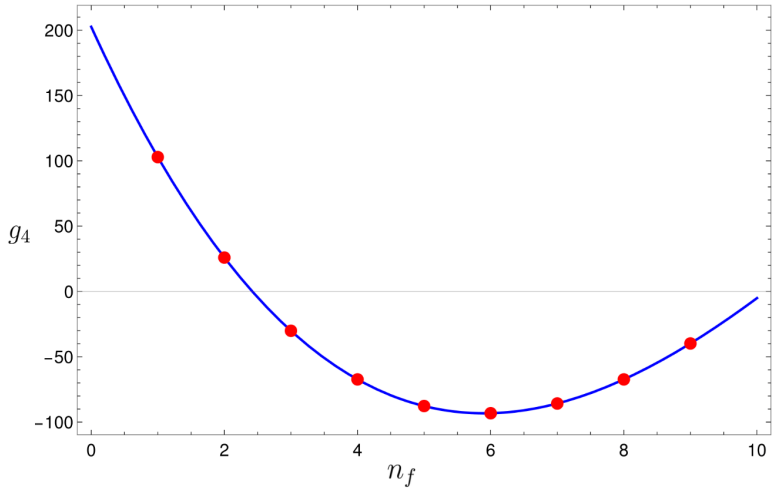

Figure 6.1 – Polynomial fit (blue) to the results of g_4 obtained with the PA P_2^1 in the range $1 \leq n_f \leq 9$.

Source: By the author.

Here, we are interested in showing how it is possible to predict each monomial of the coefficient

$$\begin{aligned} g_4 &= g_4^{(0)} + g_4^{(1)} n_f + g_4^{(2)} n_f^2 + g_4^{(3)} n_f^3 + g_4^{(4)} n_f^4 \\ &= 218.615 - 112.977 n_f + 12.7653 n_f^2 - 0.397864 n_f^3 + 0.00258089 n_f^4, \end{aligned} \tag{6.9}$$

where the $g_k^{(n)}$ denote the coefficient associated with the n-th power in n_f of g_4.

In Ref. (15), a fixed range is considered for the variation of the number of flavors including values outside the physical limit $n_f \leq 6$, which is $1 \leq n_f \leq 9$, where n_f is an integer. The idea is to assume that we do not know the coefficient of the order α_s^4 and then assess the robustness of our predictions. To do this, it is necessary to calculate the function $G(n_f)$ within the mentioned interval and then apply the Padé approximant for the following n_f values

$$G(n_f = 1): \quad 1 + 5.438\alpha_s + 20.720\alpha_s^2 + 58.922\alpha_s^3 + 118.008\alpha_s^4 + \cdots \tag{6.10}$$

$$G(n_f = 3): \quad 1 + 4.695\alpha_s + 13.472\alpha_s^2 + 20.664\alpha_s^3 - 15.9616\alpha_s^4 + \cdots \tag{6.11}$$

$$G(n_f = 5): \quad 1 + 3.952\alpha_s + 6.956\alpha_s^2 - 6.852\alpha_s^3 - 75.2574\alpha_s^4 + \cdots \tag{6.12}$$

$$G(n_f = 7): \quad 1 + 3.210\alpha_s + 1.170\alpha_s^2 - 24.458\alpha_s^3 - 76.9949\alpha_s^4 + \cdots \tag{6.13}$$

$$G(n_f = 9): \quad 1 + 2.467\alpha_s - 3.885\alpha_s^2 - 32.987\alpha_s^3 - 37.2983\alpha_s^4 + \cdots; \tag{6.14}$$

where the coefficients highlighted in blue will be postdicted. These postdictions make it possible to assess each power of n_f within the g_4 coefficient. For the sake of simplicity, we will consider for the moment the specific case of the Padé P_2^1 applied directly to the α_s series. Then, the first step is to build the Padé approximant, P_2^1, for each of these series.

Table 6.1 – Estimates for the monomials $g_4^{(n)}$ from the results of the polynomial fit displayed in Fig. 6.1

	$g_4^{(0)}$	$g_4^{(1)}$	$g_4^{(2)}$	$g_4^{(3)}$	$g_4^{(4)}$
g_4	218.6149	-112.9771	12.7653	-0.3979	0.0026
P_2^1	202.6296	-111.9088	12.4642	-0.3435	0.0008

Source: By the author.

For example, for $n_f = 1$, we have

$$P_2^1(n_f = 1) = \frac{1 - 0.636248\alpha_s}{1 - 6.07404\alpha_s + 12.3091\alpha_s^2}$$
$$\approx 1 + 5.438\alpha_s + 20.720\alpha_s^2 + 58.922\alpha_s^3 + 102.846\alpha_s^4 + \cdots. \quad (6.15)$$

The coefficient in red in Eq. (6.15) provides a postdiction for the last known coefficient of $G(n_f = 1)$ in Eq. 6.10. By following the same procedure for other values of n_f, we obtain the red points on the graph in Figure (6.1). The next step consists in fitting a polynomial in powers of n_f to these red points in order to extract the coefficients $g_4^{(n)}$ of the polynomial dependence on n_f of Eq. (6.9), as shown in Table (6.1), of $\mathrm{Im}\Pi_{G^2}$ in terms of n_f. The first three powers are very well estimated, while the n_f^4 power has an error of 70%. Certainly, this method has its advantages:

1. The exact calculations of observable quantities at higher orders are typically carried out for each power of n_f, as demonstrated in (15). Due to the complexity of the exact calculation, the results of perturbative coefficients may be presented partially in terms of powers of n_f, e.g., the quantities evaluated in the large-β_0 limit. This allows our estimates to be used to fill this potential gap.

2. Enables the realization of a final estimate, for a given value of n_f, with statistically meaningful errors. It is possible to provide estimates with a Gaussian error, in contrast to the estimates presented with flat distributions in Chapter 5.

In this context, it is important to note that the fit shown in Figure 6.1 passes almost exactly through the points, and therefore, the intrinsic error is very small and can be disregarded since it will be much smaller then the systematic error associated with the PAs[1].

6.2 Postdiction of the Last Known Coefficient of $\Gamma(h \to gg)$

Here perform the postdiction of the last unknown coefficient associated with the process $h \to gg$ in the OS scheme for the top-quark mass, utilizing various sequences of Padé

[1] We are neglecting the potential correlation between $g_4(n_f)$.

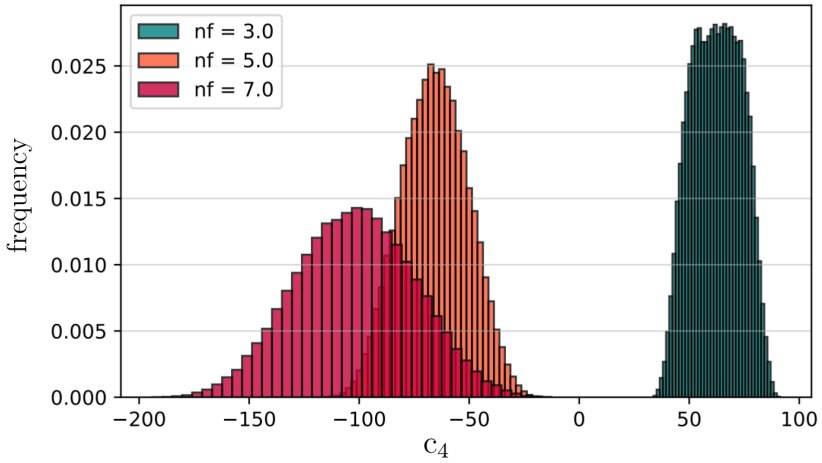

Figure 6.2 – Histogram of the distribution of the coefficient c_4 for $n_f = 3, 5, 7$.

Source: By the author.

approximants. This method is performed in a similar way to the one used for estimating the last known coefficient of $\mathrm{Im}\Pi_{G^2}(s)$ for determining the coefficient of $\mathcal{O}(\alpha_s^4)$ in Eq. (3.43). A successful estimation will enhance confidence in applying the same procedure to the first unknown coefficient in this decay process. Here, the shape of the fit performed on the estimates corresponds to that depicted in Figure 6.1; hence, we will omit it.

Padé approximants and Dlog Padés were used in the α_s plane (Despite not having information about the presence of cuts in α_s-plane), but only Dlogs were applied in the Borel space, since we expect the presence of branch cuts in the Borel space. The usual PAs applied to Borel space are not taken into account in the final results since they provide unstable estimates when compared with Dlog PAs, which are more trustworthy in estimates in Borel space. The results of the estimates are shown in Table (6.2), and in each power of n_f, the approximants provide good estimates, except for Dlog_2^1 in the n_f^4 power, which exhibits a relative error of approximately 580%. Despite this large relative error, to assign a final value for the estimate in each column of Table 6.2, the adopted prescription to analyze the result in each n_f power was to use as the mean as the central value, resulting in mean ± error, where this error was obtained by using the maximum spread divided by two, which represents a flat distribution. From there, we employ a Monte Carlo simulation to produce estimates for the last known coefficient with a Gaussian error, as we will discuss later.

Through the results indicated in Table 6.2, it is observed that it is not always the approximants that yield optimal estimates for one or two powers of n_f that will generate highly accurate estimates for the remaining powers. For instance, $\mathrm{Dlog}_2^1(\alpha_s)$ estimates very well the coefficients $c_4^{(0)}$ and $c_4^{(1)}$, while from $c_4^{(2)}$ to $c_4^{(4)}$, the approximant $\mathrm{P}_3^2(\alpha_s)$ proves to be superior.

Table 6.2 – Estimates of $c_4^{(n)}$ for $\Gamma_{h\to gg}$ in the direct OS scheme from the α_s plane with dependence on n_f.

	$c_4^{(0)}$	$c_4^{(1)}$	$c_4^{(2)}$	$c_4^{(3)}$	$c_4^{(4)}$
exact: $\mathcal{O}(\alpha_s^4)$	462.628	-178.466	16.554	-0.440714	0.00258089
$P_3^2(\alpha_s)$	448.160	-176.024	16.5298	-0.427476	0.00244874
$P_2^3(\alpha_s)$	440.527	-179.164	16.1610	-0.373381	0.00134397
$\mathrm{Dlog}_2^1(\alpha_s)$	464.098	-178.251	16.2964	-0.382359	0.00060855
$\mathrm{Dlog}_1^2(u)$	476.800	-176.054	16.8122	-0.366454	0.00021309
$\mathrm{Dlog}_2^1(u)$	482.224	-175.046	15.6677	-0.297499	0.01754420
Mean	462.362	-176.908	16.2934	-0.369434	0.00457879
Error	20.8485	2.0590	0.57225	0.0649885	0.00866555

Source: By the author.

Then, with the purpose of analyzing our final estimates, we can expand the factor K in $\Gamma_{h\to gg}^{(n_f)}(\mu_i) = \Gamma_0 K_{\mu_i}^{(n_f)}$, since

$$\Gamma_{h\to gg}^{(n_f)}(\mu_i) = \Gamma_0 \sum_{n=0}^{\infty} c_n \alpha_s^n = \Gamma_0(c_0 + c_1\alpha_s + c_2\alpha_s^2 + c_3\alpha_s^3 + c_4\alpha_s^4 + \cdots). \tag{6.16}$$

Here, we are specially interested in the last known coefficient c_4, in terms of the n_f

$$\begin{aligned} c_4 &= c_4^{(0)} + c_4^{(1)} n_f + c_4^{(2)} n_f^2 + c_4^{(3)} n_f^3 + c_4^{(4)} n_f^4 + c_4^{(4)} n_f^4 \\ &= 462.628 - 178.466 n_f + 16.554 n_f^2 - 0.440714 n_f^3 + 0.00258089 n_f^4. \end{aligned} \tag{6.17}$$

Setting $n_f = 3{,}5{,}7$ and OS top-quark mass $m_t = 164$ GeV in Eq. (6.16), one obtains (15)

$$K_{\mathrm{OS}}^{(3)} = 1 + 6.445775\alpha_s + 23.69992\alpha_s^2 + 56.1329\alpha_s^3 + 64.5259\alpha_s^4 + \cdots, \tag{6.18}$$

$$K_{\mathrm{OS}}^{(5)} = 1 + 5.703052\alpha_s + 15.51204\alpha_s^2 + 12.6660\alpha_s^3 - 69.3287\alpha_s^4 + \cdots, \tag{6.19}$$

$$K_{\mathrm{OS}}^{(7)} = 1 + 4.960329\alpha_s + 8.055116\alpha_s^2 - 19.2021\alpha_s^3 - 120.458\alpha_s^4 + \cdots. \tag{6.20}$$

The exact coefficients highlighted in blue in Eq. (6.18) to Eq. (6.20) will be postdicted with Gaussian error. This error was propagated using the interval obtained for each monomial in Table 6.2, evaluated with a flat distribution. Subsequently, the Monte Carlo simulation was applied, generating the random samples and producing the final results with Gaussian error for these coefficients

$$c_4(3) = (62 \pm 11), \tag{6.21}$$

$$c_4(5) = (-66 \pm 15), \tag{6.22}$$

$$c_4(7) = (-102 \pm 27); \tag{6.23}$$

which provides excellent estimates for the last known coefficients, $c_4 \equiv c_4(n_f)$, indicated in blue in Eq. (6.18) to Eq. (6.20). This offers promising prospects for predicting the first unknown coefficient through this method.

Furthermore, in Figure 6.2, it is observed that between $n_f = 5$ and $n_f = 7$, there is not only a change in the sign of the coefficient, but also the profile of the error distribution does not behave exactly like a Gaussian. Consequently, it is notable that the estimate from Eq. (6.23) is inferior compared to the other evaluated flavor number values. This can be explained by the greater uncertainty associated with the higher power of n_f, so that for larger values of the flavor number, the associated error is also greater.

6.3 Predictions for the Decay of the Higgs into Two Gluons.

Utilizing the methodologies established in the preceding sections, it becomes possible to carry out the prediction of the first unknown coefficient of the decay $h \to gg$ in full QCD. This process starting at α_s^2 and is known up to the order of α_s^6, as detailed in Chapter 3. In Ref. (15), this observable is calculated exactly up to $\mathcal{O}(\alpha_s^6)$ for several values of n_f and varying renormalization prescriptions of the top-quark mass. Two specific cases were examined here: the first is for $m_t = m_t(\mu_t)$, also denominated as the Invariant Scale. The second is for the On-Shell top-quark mass.

Here, the dependence on the number of flavors, detailed in Ref. (15), will be explored to obtain an estimate of the first unknown coefficient of this decay in terms of n_f, as demonstrated in sections 6.1 and 6.2. In this case, the method involves performing a fit of $\mathcal{O}(n_f^5)$ to the coefficientes obtained from the Padé and Dlog Padé approximants used in each series for $1 \leq n_f \leq 9$ (15):

$$
\begin{aligned}
K_{\rm SI}^{(1)} &= 1 + 7.188498\alpha_s + 32.65167\alpha_s^2 + 112.015\alpha_s^3 + 298.873\alpha_s^4 + \cdots,\\
K_{\rm SI}^{(3)} &= 1 + 6.445775\alpha_s + 23.74728\alpha_s^2 + 56.0755\alpha_s^3 + 62.4363\alpha_s^4 + \cdots,\\
K_{\rm SI}^{(5)} &= 1 + 5.703052\alpha_s + 15.57384\alpha_s^2 + 12.5520\alpha_s^3 - 72.0916\alpha_s^4 + \cdots,\\
K_{\rm SI}^{(7)} &= 1 + 4.960329\alpha_s + 8.131350\alpha_s^2 - 19.3879\alpha_s^3 - 123.853\alpha_s^4 + \cdots,\\
K_{\rm SI}^{(9)} &= 1 + 4.217606\alpha_s + 1.419805\alpha_s^2 - 40.5769\alpha_s^3 - 110.998\alpha_s^4 + \cdots;
\end{aligned}
$$

where one can note the change in the sign of coefficients for the high n_f values. To predict the first unknown coefficient, the estimates were realized using PAs and Dlogs, resulting in the predictions in Table 6.3. With these estimates, we realized fits for several n_f values for each approximant highlighted in Table 6.3. It becomes possible to predict c_5 at each power of n_f according to Table 6.4. In this heavy-top limit, this n_f value has a phenomenological interest, since in this limit the top-quark decouples, resulting in an effective theory with five light quarks. We are presenting these two tables explicitly to enable a comparison between the prediction of c_5 with Gaussian error and with error following a flat distribution.

To extract an estimate of the first unknown coefficient of the Higgs decay into two gluons, we will initially use the mean as the central value and the maximum spread divided

Table 6.3 – Estimates of the first unknown coefficients of $\Gamma_{h\to gg}$ for the SI scheme and $n_f = 5$.

	c_5	c_6	c_7	c_8
$\mathrm{P}_3^3(\alpha)$	-282.884	-69.2993	2991.01	12188.1
$\mathrm{P}_4^2(\alpha)$	-283.644	-78.123	2940.87	12024.2
$\mathrm{P}_2^4(\alpha)$	-349.806	-701.351	131.018	5717.22
$\mathrm{Dlog}_2^2(\alpha)$	-306.838	-374.595	1129.76	5778.6
$\mathrm{Dlog}_3^1(\alpha)$	-306.366	-370.273	1146.45	5796.01
$\mathrm{Dlog}_3^1(u)$	-341.994	164.456	6265.12	23159.5
$\mathrm{Dlog}_1^3(u)$	-252.405	-22.2762	3426.09	673.295

Source: By the author.

Table 6.4 – Estimates of $c_5^{(n)}$ for $\Gamma_{h\to gg}$ for the SI scheme and with dependence on n_f.

	$c_5^{(0)}$	$c_5^{(1)}$	$c_5^{(2)}$	$c_5^{(3)}$	$c_5^{(4}$	$c_5^{(5)}$
$\mathrm{P}_4^2(\alpha)$	1185.98	-714.314	109.252	-5.46443	0.0872611	-0.00026407
$\mathrm{P}_2^4(\alpha)$	1149.18	-721.223	108.734	-5.47562	0.133105	-0.00317741
$\mathrm{P}_3^3(\alpha)$	1206.95	-723.111	110.856	-5.65435	0.100096	-0.00046349
$\mathrm{Dlog}_2^2(\alpha)$	1199.03	-723.733	109.152	-5.29382	0.0723541	0.00016264
$\mathrm{Dlog}_3^1(\alpha)$	1198.49	-723.231	109.042	-5.29168	0.0702081	0.00090767
$\mathrm{Dlog}_1^3(u)$	1199.12	-720.727	107.516	-4.58872	0.03438771	0.00522560
$\mathrm{Dlog}_3^1(u)$	986.315	-689.671	105.704	-4.52435	-0.0470713	0.02320370
Mean	1160.72	-716.573	108.608	-5.18471	0.0643344	0.00365638
Error	110.318	17.031	2.576	0.565	0.0900882	0.01319060

Source: By the author.

by two as the error. By doing this, we arrive at

$$c_5^{\mathrm{SI}} = (-303 \pm 48). \tag{6.24}$$

On the other hand, employing the average as the central value and maximum spread divided by two as the error at each power of n_f of the coefficients in Table 6.4, we perform the Monte Carlo method to obtain a prediction with a Gaussian error, which is

$$\tilde{c}_5^{\mathrm{SI}} = (-304 \pm 106), \tag{6.25}$$

in which the increase in error is evident, but still, it represents a reasonable increment in exchange for having errors with a much more precise statistical meaning and arguably a more conservative result. Hence, we will prefer to work with estimates that possess Gaussian error.

Having these estimates, we can calculate their impact on the Higgs boson decay width into two gluons through the truncation error estimation and its renormalization scale variation. To accomplish this, it is important to mention that physical quantities should not depend on the renormalization scale μ; however, since we deal with truncated series in perturbation theory, it is expected that there will be a residual scale dependence. Dealing

Table 6.5 – Estimates of the first unknown coefficients of Γ_{gg} for the OS scheme and $n_f = 5$.

	c_5	c_6	c_7	c_8
$\mathrm{P}_3^3(\alpha_s)$	-274.171	-69.2993	2991.01	12188.1
$\mathrm{P}_4^2(\alpha_s)$	-274.25	-78.123	2940.87	12024.2
$\mathrm{P}_2^4(\alpha_s)$	-336.639	-701.351	131.018	5717.22
$\mathrm{Dlog}_2^2(\alpha_s)$	-296.502	-374.595	1129.76	5778.6
$\mathrm{Dlog}_0^4(\alpha_s)$	-312.427	-370.273	1146.45	5796.01
$\mathrm{Dlog}_1^3(u)$	-250.957	-407.398	154.452	4009.26
$\mathrm{Dlog}_3^1(u)$	-302.14	-535.944	494.381	5308.12

Source: By the author.

Table 6.6 – Estimates of $c_5^{(n)}$ for $\Gamma_{h\to gg}$ for the OS scheme and with dependence on n_f.

	$c_5^{(0)}$	$c_5^{(1)}$	$c_5^{(2)}$	$c_5^{(3)}$	$c_5^{(4)}$	$c_5^{(5)}$
$\mathrm{P}_4^2(\alpha_s)$	1193.68	-713.079	109.107	-5.47292	0.0875461	-0.000264069
$\mathrm{P}_2^4(\alpha_s)$	1158.75	-719.432	108.74	-5.55621	0.14201	-0.00349669
$\mathrm{P}_3^3(\alpha_s)$	1210.37	-721.246	110.737	-5.66563	0.100782	-0.000480134
$\mathrm{Dlog}_2^2(\alpha_s)$	1205.83	-722.067	109.158	-5.36849	0.0812377	-0.000206527
$\mathrm{Dlog}_0^4(\alpha_s)$	1280.77	-729.095	106.412	-5.29845	0.0884474	-0.000317731
$\mathrm{Dlog}_1^3(u)$	1208.29	-720.11	107.687	-4.76849	0.0499473	0.00448315
$\mathrm{Dlog}_3^1(u)$	1137.74	-727.718	110.183	-4.75107	-0.0560376	0.0234065
Mean	1199.35	-721.821	108.861	-5.26875	0.0705618	0.0033035
Error	71.515	8.008	2.1625	0.45728	0.0990238	0.0134516

Source: By the author.

with the residual dependence of the renormalization scale in QFT analyzed through perturbation theory remains a current challenge. There are some methods in the literature intended to eliminate this dependence, such as the Principle of Maximum Conformality (PMC) method (81, 82). On the other hand, many authors argue that the dependence on μ cannot be removed in an entirely unambiguous way (83, 84).

The standard way to account for the effects of this dependence on physical quantities $\Gamma(\mu)$ is through the variation of the renormalization scale. Typically, this variation is done within an interval $[Q/2, 2Q]$, where Q is the hard scale of the process. Since the factor of 2 is somewhat arbitrary, a more reasonable interval would be to consider $[Q/\xi, \xi Q]$, as done in (85), with ξ being an integer greater than or equal to two. In a first moment, we are only interested in the series error, so that the $m_t(\mu)$ and $\alpha_s(\mu)$ errors will be considered later. Based on the forecast indicated in Eq. (6.25), it is possible to analyze the impact of this estimate on the decay of the Higgs into two gluons, resulting in

$$\Gamma_{h\to gg}^{\mathrm{SI}} = \Gamma_0(m_h)\left[1.8463 \pm (0.0028)_{\mathrm{series}} \pm (0.0010)_{\sigma}\right]. \tag{6.26}$$

This result can be rewritten in terms of the uncertainties combined in quadrature

$$\Gamma_{h\to gg}^{\mathrm{SI}} = \Gamma_0(m_h)\left[1.8463 \pm 0.0030\right]. \tag{6.27}$$

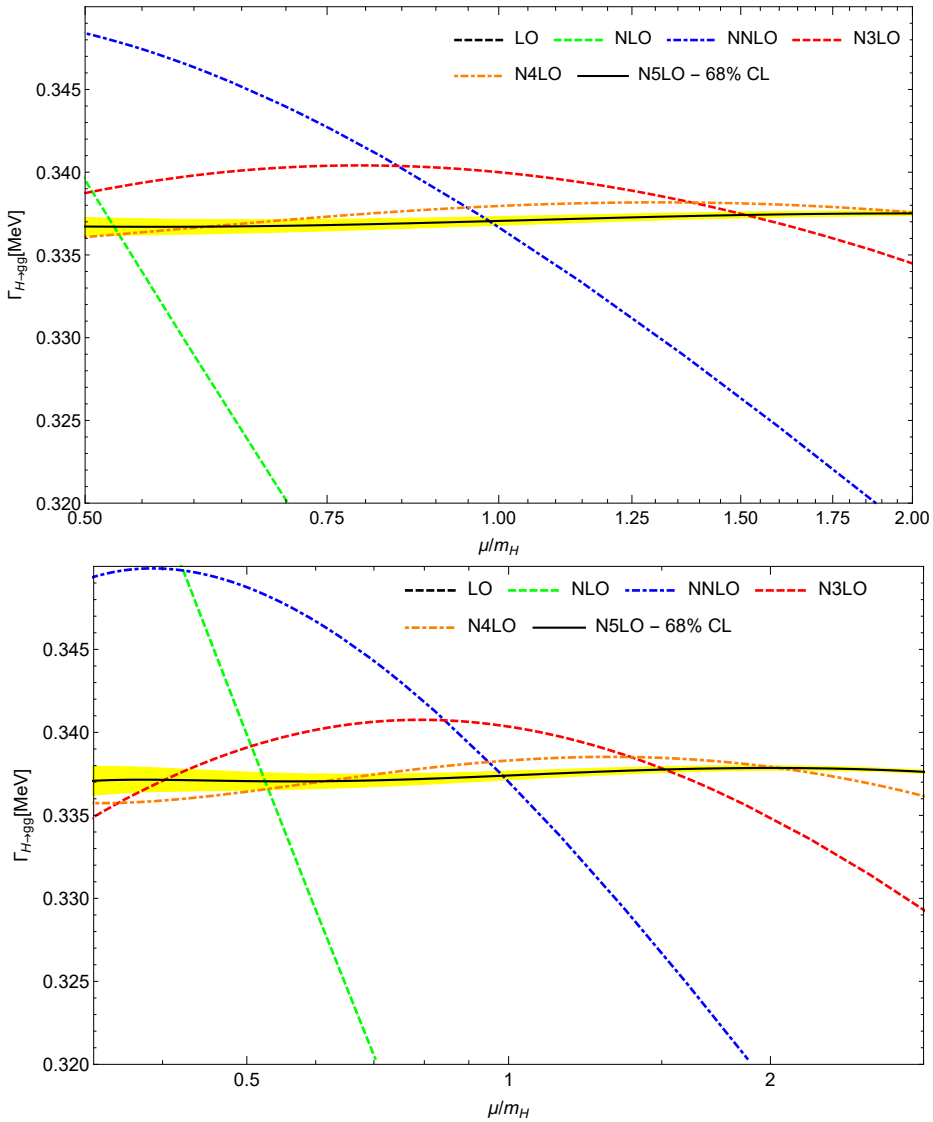

Figure 6.3 – The graph above represents the evolution of $\Gamma_{h\to gg}$ in the renormalization scale, presenting all orders known exactly currently, according to Ref. (15), and our estimates for the N5LO contribution, within the interval: $1/2 < \mu/m_H < 2$. The one below represents the same but within a more reliable interval: $1/3 < \mu/m_H < 3$.

Source: By the author.

Additionally, it is important to remember that the error associated with $\alpha_s(\mu)$ and $m_t(\mu)$ is not being taken into account in Eq. (6.26).

As mentioned in Chapter 3, we also investigated the OS scheme. The method employed here involves using the same prescription as that used for the SI scheme, i.e., by estimating the coefficients c_5 and $\tilde{c}_5$ are based on Tables 6.5 and 6.6. As a result, in this scheme, we obtain

$$c_5^{\rm OS} = (-292 \pm 42), \tag{6.28}$$

and the estimate with Gaussian error is

$$\tilde{c}_5^{\rm OS} = (-293 \pm 78). \tag{6.29}$$

Here, it is possible to note that the central values between Eq. (6.28) and (6.29) are practically the same, but the Gaussian error is larger than the error in Eq. (6.28). With these perspectives, it is possible to compare the estimates in the different schemes prescriptions. The first point is that both equations (6.29) and (6.25), have the same order of magnitude, showing that the PAs and Dlog's were not unstable in relation to small variations in the coefficients' magnitude due to changes in the top-quark mass scheme.

Furthermore, using the coefficient $\tilde{c}_5$ as an estimate of truncation error, the decay width is

$$\Gamma^{\rm OS}_{h\to gg} = \Gamma_0(m_h)\left[1.8462 \pm (0.0027)_{\rm series} \pm (0.0007)_{\sigma}\right], \tag{6.30}$$

where the uncertainties, as realized before, can be combined in quadrature

$$\Gamma^{\rm OS}_{h\to gg} = \Gamma_0(m_h)\left[1.8462 \pm 0.0028\right]. \tag{6.31}$$

Here, one can observe smaller errors than the decay within the SI scheme of Eq. (6.26).

Additionally, another possibility is to explore the case where the estimate $\tilde{c}_5$ is included as an N5LO coefficient in the Higgs decay into two gluons, in terms of renormalization scale evolution. In Figure 6.3, it is evident that the black solid line — representing the partial sum with the central value of $\tilde{c}_5$ — demonstrates a very weak dependence on the scheme variation, appearing almost flat. The yellow band in the figure represents the Gaussian error of the estimate.

Through the graph that considers the interval $1/3 < \mu/m_H < 3$, a higher error is observed due to the greater influence of the coefficient multiplying α_s^7. For values of μ/m_H close to three, the coupling is very small, and the associated error has little influence. With our estimate of the coefficient of order $\mathcal{O}(\alpha_s^7)$ it becomes clear that the renormalization scale dependence is reduced, as expected by the renormalization group.

7 Conclusion

In this work, we studied the perturbative series for $h \to gg$, with the objective of understanding its truncation error by employing a model-independent estimation of yet unknown higher-order coefficients. This was done with rational approximants, also known as Padé approximants, in combination with the Borel transform of the series. Dlog Padé approximants were also used in this context. In the present case, since in $h \to gg$ we do not have the large-β_0 result which serves as a laboratory to test the method, an intermediate step that was used was to analyze the corrections to the gluon-gluon correlator, initially obtained analytically at this limit in Ref. (71).

After the reproduction of the physical gluon-gluon correlator D_{G^2} in the large-β_0 limit (71), where we know the coefficients to all orders in perturbation theory, we were able to explore the behavior of renormalons. The divergent profile of the series sets in from the twelfth order in perturbation theory in powers of $a_{s,r} = \beta_1 a_s$, and therefore for any n_f. The poles identified in the Borel transform of $\hat{D}^{\beta_0}_{G^2}$ are located at all negative integers, except for the logarithmic singularity at $u = 3$. From $u \geq 4$, only cuts are found. We explicitly state the form of the UV renormalons along with their respective residues and verify that the dependence on the renormalization scheme affects only the values of the residues, but not the position of the renormalons.

To analyze the gluon-gluon correlator in the large-β_0 limit, we employed various methods firstly applied in $D^{\beta_0}_{G^2}$, including Padé-Borel approximants, Dlog Padés in Borel space, renormalization scheme change, and conformal mapping. Initially, the results obtained from Padé approximants and Dlog Padés in the $\overline{\text{MS}}$ scheme revealed unsatisfactory outcomes in the large-β_0 limit. However, as shown in chapter 5, these approximants attempt to reproduce UV renormalons. In this case, where $C = -5/3$, the residues of these renormalons are suppressed, while the dominant IR is favored. One way to address this issue is to eliminate the exponential dependence on C in the Borel transform through a change in the renormalization scheme, leading to a modification in the coupling constant. With this scheme change ($C = 0$), the results of Padé approximants and Dlog Padés showed a significant improvement in precision in the estimates.

In this limit, we investigated the optimal conformal mapping in conjunction with renormalization-scheme variation. We projected the Borel space onto a unit circle, where the renormalons are situated. However, we observed an anomalous behavior in the relative error in the w-space for estimates of the approximant P^1_2, yielding highly accurate estimates. Subsequently, we identified that the exceptional performance of P^1_2 stemmed from its structural alignment with the inverse transformation $\tilde{u}(w)$.

After adopting the prescriptions of varying the positions of the conformal mapping parameters p_{IR} and p_{UV} in the w-plane highlighted throughout Chapter 5, the final result for the estimates in the large-β_0 limit, considered Padé approximants and Dlog Padés in

the Borel space can be evaluated. These methods provided the estimate for the first and second unknown coefficients of the physical gluon-gluon correlator in the large-β_0 limit: $c_5 = (12 \pm 6)$ and $c_6 = (29 \pm 20)$, where the relative deviation of the central value with respect to the true value is approximately 5% for c_5, while for c_6 it is approximately 2%. However, the uncertainty associated with predicting the coefficient c_6 is higher than the uncertainty of c_5, as expected.

In the context of full QCD, where the decay $h \to gg$ is known up to the order of α_s^6 in perturbation theory, we also employ Padé approximants to investigate terms at high orders. However, even though the large-β_0 limit guides the methods used, the optimal strategy in this case turned out to rely on a different strategy, taking advantage of the n_f dependence of the coefficients. This involves making estimates of the coefficient at each power in the massless flavors number n_f. To achieve this, we start by evaluating the imaginary part of the correlator of two gluons in the $\overline{\text{MS}}$ scheme. It was analyzed to motivate and illustrate the methods employed in this stage of the work. The last known coefficient of $\text{Im}\Pi_{G^2}$ was estimated using the Padé approximant P_2^1 in the α_s-plane, considering its dependence on n_f. In this step, it was exemplified how the fit is performed, considering a range outside the physical limit: $1 \leq n_f \leq 9$, which provides estimates for the coefficients listed in Table 6.1. For each integer value of n_f in this range, an estimate is made, corresponding to the red points in Figure 6.1.

After illustrating the method, we estimated the last known coefficient of $\Gamma^{\text{SI}}_{h\to gg}$ for $n_f = 3,5,7$. The final result of the coefficients was evaluated with a Gaussian error. Furthermore, when compared to exact values, we observed that the estimates were excellent, suggesting promising prospects for estimating the first unknown coefficient of this decay. For example, consider the scenario that corresponds to the physical decay width for $n_f = 5$. The calculated coefficient is $c_4(5) = (-66 \pm 15)$, deviating slightly from the exact value of $c_4 = -69.33$, where the central value of estimates has a relative error of approximately 5%.

Finally, with this method, estimates for the first unknown coefficient were made for two different schemes of the top quark mass: the Scale Invariant (SI) scheme and the On-shell (OS) scheme. We obtained, respectively

$$\tilde{c}_5^{\text{SI}} = (-304 \pm 106), \qquad \tilde{c}_5^{\text{OS}} = (-293 \pm 78). \tag{7.1}$$

Thus, we analyzed the impact of these estimates on the decay width for the SI scheme, as our estimate is an evaluation of the truncation error for this quantity, according to

$$\Gamma^{\text{SI}}_{h\to gg} = \Gamma_0(m_h)\left[1.8463 \pm (0.0028)_{\text{series}} \pm (0.0010)_{\sigma}\right], \tag{7.2}$$

where "series" refers to the truncation error estimate, and σ represents the error of PAs. For the OS scheme we obtained

$$\Gamma^{\text{OS}}_{h\to gg} = \Gamma_0(m_h)\left[1.8462 \pm (0.0027)_{\text{series}} \pm (0.0007)_{\sigma}\right]. \tag{7.3}$$

Furthermore, another possibility that we explored was to consider the estimate of c_5, with its respective error, as the N5LO coefficient to analyze the evolution with the renormalization scale of the Higgs decay into two gluons. A very small variation of $\Gamma_{h\to gg}$ was observed in the interval $\xi < \mu/m_h < 1/\xi$, for $\xi = 2$; while for $\xi = 3$ the central value still varies very little, and the uncertainty associated with the estimate is more significant for low values of μ/m_h. This occurs because, in this regime, the value of $\alpha_s(\mu)$ is higher, and therefore, the influence of the perturbative coefficient value is greater. Therefore, our estimate is in accordance with what is expected physically for the quantity $\Gamma_{h\to gg}$ at high orders, regarding the variation of the renormalization scale.

Our results show that the truncation error of series and the stabilization with respect to variations in μ is under control. It is, however, important to increase the precision in the determination of $\alpha_s(\mu)$, since if if the α_s error is propagated ([15], [86]), it largely dominates the final theoretical uncertainty of the decay width.

References

1 SCHWARTZ, M. D. *Quantum field theory and the standard model*. Cambridge: Cambridge University Press, 2014.

2 DIRAC, P. A. M. Quantum theory of emission and absorption of radiation. *Proceedings of the Royal Society London A*, v. 114, n.767, p. 243, 1927.

3 TOMONAGA, S. On a relativistically invariant formulation of the quantum theory of wave fields. *Progress of Theoretical Physics*, v. 1, n. 2, p. 27–42, 1946.

4 SCHWINGER, J. S. Quantum electrodynamics. I a covariant formulation. *Physical Review*, v. 74, n. 10, p. 1439, 1948.

5 FEYNMAN, R. P. Space - time approach to quantum electrodynamics. *Physical Review*, v. 76, n. 6, p. 769–789, 1949.

6 GELL-MANN, M.; LOW, F. E. Quantum electrodynamics at small distances. *Physical Review,*, v. 95, n.5, p. 1300–1312, 1954.

7 NE'EMAN, Y. Patterns, structure and then dynamics: discovering unitary symmetry and conceiving quarks. 1981. Available at: //www.academy.ac.il/ShopEng/Entry.aspx?nodeId=1534entryId=21126. Accessible at: 15 Jan. 2023.

8 FRITZSCH, H.; GELL-MANN, M.; LEUTWYLER, H. Advantages of the color octet gluon picture. *Physics Letter B*, v. 47, p. 365–368, 1973.

9 GLASHOW, S. L. Partial Symmetries of weak interactions. *Nuclear Physics*, v. 22, p. 579–588, 1961. DOI: 10.1016/0029-5582(61)90469-2.

10 SALAM, A. Weak and electromagnetic interactions. *Conference of Proceedings C*, v. 680519, p. 367–377, 1968. DOI: 10.1142/9789812795915_0034.

11 WEINBERG, S. A Model of Leptons. *Physical Review Letters*, v. 19, p. 1264–1266, 1967.

12 ENGLERT, F.; BROUT, R. Broken symmetry and the mass of gauge vector mesons. *Physical Review Letters*, v. 13, n. 9, p. 321–323, 1964.

13 HIGGS, P. W. Broken symmetries and the masses of Gauge bosons. *Physical Review Letters*, v. 13, n. 16, p. 508–509, 1964.

14 AAD, G. *et al.* Observation of a new particle in the search for the Standard Model Higgs boson with the ATLAS detector at the LHC. *Physics Letters B*, v. 716, n. 1, p. 1–29, 2012.

15 HERZOG, F. *et al.* On Higgs decays to hadrons and the R-ratio at N^4LO. *Journal of High Energy Physics*, v. 08, p. 113, 2017. DOI: 10.1007/JHEP08(2017)113.

16 AAD, G. *et al.* Measurements of the Higgs boson production and decay rates and constraints on its couplings from a combined ATLAS and CMS analysis of the LHC pp collision data at $\sqrt{s} = 7$ and 8 TeV. *Journal of High Energy Physics*, v. 08, p. 045, 2016.

17 BOITO, D.; NEVES, G.; PICLUM, J. $H \to \gamma\gamma$ to all orders in α_s in the large-β_0 limit of QCD. *Physical Review D*, v. 106, n. 9, p. 094026, 2022.

18 BAKER, G. A.; GRAVES-MORRIS, P. *Padé approximants: encyclopedia of mathematics and it's applications*. 2nd. ed. Cambridge: Cambridge University Press, 1996.

19 BOITO, D.; LONDON, C. Y.; MASJUAN, P. Higher-order QCD corrections to $H \to b\bar{b}$ from rational approximants. *Journal of High Energy Physics*, v. 01, p. 054, 2022. DOI: 10.1007/JHEP01(2022)054.

20 BOITO, D.; MASJUAN, P.; OLIANI, F. Higher-order QCD corrections to hadronic τ decays from Padé approximants. *Journal of High Energy Physics*, v. 08, p. 075, 2018. DOI: 10.1007/JHEP08(2018)075.

21 ELLIS, J. R.; KARLINER, M.; SAMUEL, M. A. A prediction for the four loop beta function in QCD. *Physics Letters B*, v. 400, p. 176–181, 1997.

22 BENEKE, M. Renormalons. *Physics Reports*, v. 317, p. 1–142, 1999.

23 BOITO, D.; JAMIN, M.; MIRAVITLLAS, R. Scheme variations of the QCD coupling. *EPJ Web of Conferences*, v. 137, n. 5, p. 05007, 2017.

24 CAPRINI, I.; FISCHER, J. Expansion functions in perturbative QCD and the determination of $\alpha_s(M_\tau^2)$. *Physical Review D*, v. 84, n. 5, p. 054019, 2011.

25 PICH, A. *Quantum chromodynamics*. 1995. Available at: https://arxiv.org/pdf/hep-ph/9505231.pdf. Accessible at: 23 Jan. 2023.

26 FERREIRA, L. A. *Lecture notes on Lie algebras and Lie groups*. 2000. Available at: https://edisciplinas.usp.br/pluginfile.php/6960037/mod_resource/content/1/notesfinal.pdf. Accessible at: 23 Jan. 2023.

27 CARTAN, É. *Sur la structure des groupes de transformations finis et continus*. Paris: Librairie Nony, 1894.

28 MANDL, F.; SHAW, G. *Quantum field theory*. Chichester: John Wiley, 1985.

29 HOOFT, G. 't; VELTMAN, M. J. G. Regularization and renormalization of Gauge fields. *Nuclear Physics B*, v. 44, p. 189–213, 1972. DOI: 10.1016/0550-3213(72)90279-9.

30 DJOUADI, A. *The anatomy of electro-weak symmetry breaking*: tome I: the Higgs boson in the standard model. 2003. Available at: https://arxiv.org/pdf/hep-ph/0503172.pdf. Accessible at: 20 Dec. 2023.

31 ADLER, S. L. Axial vector vertex in spinor electrodynamics. *Physical Review*, v. 177, n.5, p. 2426–2438, 1969.

32 DJOUADI, A. The Anatomy of electro-weak symmetry breaking: tome I: the Higgs boson in the standard model. *Physics Reports*, v. 457, n. 1-4, p. 1–216, 2008.

33 FERREIRA, F. *A extensão ub- l(1) do modelo padrão*. Universidade Federal da Paraíba, 2013. Available at: https://repositorio.ufpb.br/jspui/bitstream/tede/9549/2/arquivototal.pdf. Accessible at: 20 Dec. 2023.

34 ILISIE, V. *Concepts in quantum field theory*. Berlin: Springer, 2016. (UNITEXT for physics). ISBN 978- 3-319-22965-2.

35 YUKAWA, H. On the Interaction of elementary particles I. *Proceedings of the Physico-Mathematical Society of Japan*, v. 17, p. 48–57, 1935.

36 SAKAI, N. Perturbative QCD corrections to the hadronic decay width of the Higgs boson. *Physical Review D*, v. 22, p. 2220, 1980. DOI: 10.1103/PhysRevD.22.2220.

37 DREES, M.; HIKASA, K.-i. Heavy quark thresholds in Higgs physics. *Physical Review D*, v. 41, n.5, p. 1547, 1990.

38 PASCUAL, P.; TARRACH, R. *QCD*: renormalization for the practitioner. Berlin: Springer-Verlag, 1984. (Lecture notes in physics, v. 194).

39 JAMIN, M. QCD and renormalisation group methods. Lecture presented at Herbstschule für Hochenergiephysik, Maria Laach. 2006. Available at: https://www.maria-laach.tp.nt.uni-siegen.de/downloads/files/2006/Jamin-2006.pdf. Accessible at: 21 Dec. 2023.

40 BREIDENBACH, E. C. G. S.; PETERMANN, A. Normalization of constants in the quanta theory. *Helvetica Physica Acta*, v. 26, p. 499–520, 1953. DOI: 10.5169/seals-112426.

41 CALLAN JR., C. G. Broken scale invariance in scalar field theory. *Physical Review D*, v. 2, p. 1541–1547, 1970. DOI: 10.1103/PhysRevD.2.1541.

42 SYMANZIK, K. Small distance behavior in field theory and power counting. *Communications in Mathematical Physics,*, v. 18, p. 227–246, 1970.

43 BAIKOV, P. A.; CHETYRKIN, K. G.; KüHN, J. H. Five-Loop running of the QCD coupling constant. *Physical Review Letters*, v. 118, n. 8, p. 082002, 2017.

44 GROSS, D. J.; WILCZEK, F. Ultraviolet behavior of nonabelian gauge theories. *Physical Review Letters*, v. 30, n.26, p. 1343–1346, 1973.

45 GROSS, D. J.; WILCZEK, F. Asymptotically free Gauge theories - I. *Physical Review D*, v. 8, n.10, p. 3633–3652, 1973.

46 ZYLA, P. A. *et al*. Review of Particle Physics. *Progress of Theoretical and Experimental Physics*, v. 2020, n. 8, p. 083C01, 2020.

47 BOITO, D.; JAMIN, M.; MIRAVITLLAS, R. Scheme variations of the QCD coupling and hadronic τ decays. *Physical Review Letters*, v. 117, n. 15, p. 152001, 2016.

48 CELMASTER, W.; GONSALVES, R. J. QCD perturbation expansions in a coupling constant renormalized by momentum space subtraction. *Physical Review Letters*, v. 42, n. 22, p. 1435, 1979.

49 HEINEMEYER, S.; JADACH, S.; REUTER, J. Theory requirements for SM Higgs and EW precision physics at the FCC-ee. 2021. Available at: https://arxiv.org/pdf/2106.11802.pdf. Accessible at: 21 Dec. 2023.

50 ILISIE, V. SM higgs decay and production channels. Available at: http://ific.uv.es/lhcpheno/PhDthesis/master_vilisie.pdf. Accessible at: 21 Dec. 2023.

51 VERMASEREN, J. A. M. New features of FORM. 2000. Available at: https://arxiv.org/pdf/math- ph/0010025.pdf. Accessible at: 21 Dec. 2023.

52 VERMASEREN, J. A. M. FORM facts. *Nuclear Physics B*, v. 205-206, p. 104–109, 2010. DOI: 10.1016/j.nuclphysbps.2010.08.027.

53 HERZOG, F. *et al*. FORM, diagrams and topologies. *Proceedings of Science*, p. 073, 2016. DOI: 10.48550/arXiv.1608.01834.

54 UEDA, T. *et al*. Further developments of FORM. *Journal of Physics: conference series*, v. 1525, n.1, p. 012013, 2020.

55 PESKIN, M. E.; SCHROEDER, D. V. *An Introduction to quantum field theory*. Reading: Addison-Wesley, 1995. ISBN 978-0-201-50397-5.

56 PASSARINO, G.; VELTMAN, M. J. G. One loop corrections for e^+e^- annihilation into $\mu^+\mu^-$ in the Weinberg model. *Nuclear Physics B*, v. 160, p. 151–207, 1979. DOI: 10.1016/0550-3213(79)90234-7.

57 CHETYRKIN, K. G.; KNIEHL, B. A.; STEINHAUSER, M. Decoupling relations to $\mathcal{O}\left(\alpha_s^3\right)$ and their connection to low-energy theorems. *Nuclear Physics B*, v. 510, p. 61–87, 1998.

58 SHIFMAN, M. A. *et al*. Low-Energy theorems for Higgs boson couplings to photons. *Soviet Journal of Nuclear Physics*, v. 30, n. 6, p. 711–716, 1979.

59 SHIFMAN, M. A.; VAINSHTEIN, A. I.; ZAKHAROV, V. I. QCD and resonance physics. sum rules. *Nuclear Physics B*, v. 147, p. 385–447, 1979.

60 ELLIS, J. R.; GAILLARD, M. K.; NANOPOULOS, D. V. A phenomenological profile of the Higgs boson. *Nuclear Physics B*, v. 106, p. 292, 1976.

61 NOGUEIRA, P. Automatic Feynman graph generation. *Journal of Computational Physics*, v. 105, n. 2, p. 279–289, 1993.

62 RITBERGEN, T. van; VERMASEREN, J. A. M.; LARIN, S. A. The four-loop beta function in quantum chromodynamics. *Physics Letters B*, v. 400, p. 379–384, 1997. DOI: 10.1016/S0370-2693(97)00370-5.

63 CHETYRKIN, K. G.; KUHN, J. H.; STEINHAUSER, M. RunDec: a Mathematica package for running and decoupling of the strong coupling and quark masses. *Computer Physics Communications*, v. 133, n. 1, p. 43–65, 2000.

64 HERREN, F.; STEINHAUSER, M. Version 3 of RunDec and CRunDec. *Computer Physics Communications*, v. 224, p. 333–345, 2018.

65 BONVINI, M. Probabilistic definition of the perturbative theoretical uncertainty from missing higher orders. *European Physical Journal C*, v. 80, n. 10, p. 989, 2020. DOI: 10.1140/epjc/s10052-020-08545-z.

66 CAPRINI, I. *et al*. *Perturbative expansions in QCD improved by bonformal mappings of the Borel plane*. 2017. Available at: https://arxiv.org/pdf/1711.04445.pdf. Accessible at: 21 Dec. 2023.

67 DYSON, F. J. Divergence of perturbation theory in quantum electrodynamics. *Physical Review*, v. 85, n. 4, p. 631–632, 1952.

68 MANOHAR, A. V.; WISE, M. B. *Heavy quark physics*. Cambridge: Cambridge University Press, 2000. (Cambridge monographs on particle physics, nuclear physics and cosmology, v. 10) ISBN 978-0-521- 03757-0.

69 NARISON, S. Di-gluonium sum rules, I=0 scalar mesons and conformal anomaly. *Nuclear Physics A*, v. 1017, p. 122337, 2022. DOI: 10.1016/j.nuclphysa.2021.122337.

70 AHMED, T.; CHEN, L.; CZAKON, M. A note on quark and gluon energy-momentum tensors. *Journal of High Energy Physics*, v. 01, p. 077, 2023. DOI: 10.1007/JHEP01(2023)077.

71 JAMIN, M. The Scalar gluonium correlator: Large-β_0 and beyond. *Journal of High Energy Physics*, v. 04, p. 099, 2012. DOI: 10.1007/JHEP04(2012)099.

72 HOANG, A. H. *et al*. Inclusive tau hadronic decay rate in a renormalon-free gluon condensate scheme. *Proceedings of Science*, v. 416, p. 016, 2022. DOI: 10.22323/1.416.0016.

73 BENITEZ-RATHGEB, M. A. *et al*. Reconciling the contour-improved and fixed-order approaches for τ hadronic spectral moments. part II. renormalon norm and application in α_s determinations. *Journal of High Energy Physics*, v. 09, p. 223, 2022. DOI: 10.1007/JHEP09(2022)223.

74 BENITEZ-RATHGEB, M. A. *et al*. Reconciling the contour-improved and fixed-order approaches for τ hadronic spectral moments. part I. renormalon-free gluon condensate scheme. *Journal of High Energy Physics*, v. 07, p. 016, 2022. DOI: 10.1007/JHEP07(2022)016.

75 NEUBERT, M. Scale setting in QCD and the momentum flow in Feynman diagrams. *Physical Review D*, v. 51, p. 5924–5941, 1995.

76 GROZIN, A. *Lectures on QED and QCD. In*: DUBNA INTERNATIONAL ADVANCED SCHOOL OF THEORETICAL PHYSICS, 3., 2005, Dubna. *Proceedings*[...] Dubna: DIAS - TH, 2005.

77 BENEKE, M.; SMIRNOV, V. A. Ultraviolet renormalons in Abelian gauge theories. *Nuclear Physics B*, v. 472, p. 529–590, 1996.

78 CAPRINI, I. Renormalization-scheme variation of a QCD perturbation expansion with tamed large-order behavior. *behavior. Physical Review D*, D98, n. 5, p. 056016, 2018.

79 POMMERENKE, C. Padé approximants and convergence in capacity. *Journal of Mathematical Analysis and Applications*, v. 41, n. 3, p. 775–780, 1973.

80 CACCIARI, M.; HOUDEAU, N. Meaningful characterisation of perturbative theoretical uncertainties. *Journal of High Energy Physics*, v. 09, p. 039, 2011. DOI:10.1007/JHEP09(2011)039.

81 Brodsky, Stanley J. *et al*. Comment on P.M. Stevenson, " 'Maximal conformality' does not work", Physics Letters B 847 (2023) 138288. 11 2023. Available at: https://arxiv.org/pdf/2311.17360.pdf. Accessible at: 21 Dec. 2023.

82 BRODSKY, S. J.; LEPAGE, G. P.; MACKENZIE, P. B. On the elimination of scale ambiguities in perturbative quantum chromodynamics. *Physical Review D*, v. 28, n.1, p. 228, 1983.

83 STEVENSON, P. M. 'Maximal conformality' does not work. *Physics Letters B*, v. 847, p. 138288, 2023. DOI: 10.1016/j.physletb.2023.138288.

84 BOITO, D. Consequences of the renormalization group for perturbative quantum chromodynamics. *Nature Physics*, v. 19, n. 11, p. 1533–1535, 2023.

85 BOITO, D.; MATEU, V. Precise α_s determination from charmonium sum rules. *Physics Letters B*, v. 806, p. 135482, 2020. DOI: 10.1016/j.physletb.2020.135482.

86 ABBAS, G. *et al*. Renormalization-group improved Higgs to two gluons decay rate. 2022. Available at: https://arxiv.org/pdf/2205.06061.pdf. Accessible at: 21 Dec. 2023.

Appendix A

To understand how the representation decompositions are carried out, the Young tableaux method can be employed. This method provide a straightforward approach to determining the dimensions of algebraic decompositions. To put this into practice, it is necessary to follow the next steps:

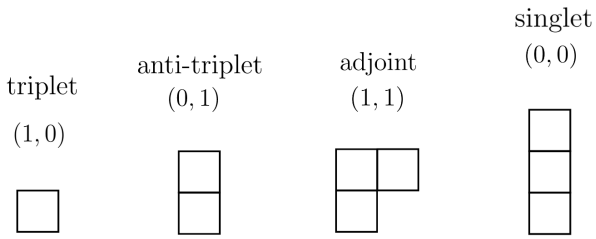

Figure A. 1 – This figure represents the Young tableaux of different dimensions in terms of (m_1, m_2) for the SU(3) group.

Source: By the author.

1. Each representation will be denoted by a number of rows and each row will contain a number of boxes. The representation dimension will be determined by the value of fundamental weights (m_1, m_2), with $m_{1/2}$ beeing non-negative integers, where the weight is written as $\lambda = m_1\lambda_1 + m_2\lambda_2$. Here the λ_1 and λ_2 are the fundamental weights. For the SU(3) group, the fundamental representation is shown by the Figure A. 1.

2. There are rules for the tensorial products between the representations. Considering that the main goal is the decomposition of the products which correspond to a reducible representation in others irreducible. The other are obtained via: combining the boxes by always placing more squares above the rows, i.e., it is prohibited to have a back row with a greater number of squares as is shown in the Figure A. 2. The main objective was to combine the two columns on the left-hand side of the equation and then create a product with the last one, primarily resulting in a singlet state and proving that this state is possible.

3. Evaluate the dimension of representations $\dim D^{\lambda}$ obtained in the final of this method. To do this, simply employ the formula for the dimensionality of the SU(3) group, which is given in terms of m_1 and m_2. In the context of Young diagrams, m_1 represents how many more boxes the first row had than the second one, and m_2 follows the same rule between the second and third row.

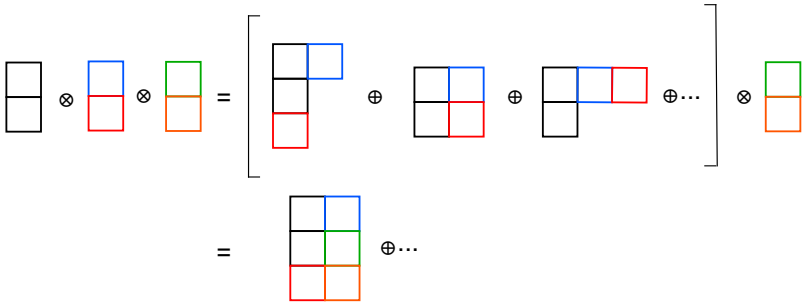

Figure A. 2 – This figure represents the Young Tableaux of a decomposition of three anti-triplet products.

Source: By the author.

The underlying principle of this method lies in evaluating the dimensions of all possible combinations. The approuch used here is employing the Weyl dimension formula (26)

$$\dim D^{\lambda} = \frac{\prod_{\alpha_i>0}[(m_1+1)\lambda_1 + (m_2+1)\lambda_2]\cdot\alpha_i}{\prod_{\alpha>0}\delta\cdot\alpha_i}, \tag{4}$$

where δ is the dominant weights of the su(3) algebra, while α_i, with $i = 1,2,3$ represents the simple roots, which after making the product is structured as follows

$$\dim D^{\lambda} = \frac{1}{2}(m_1+1)(m_2+1)(m_1+m_2+2).$$

One interesting example is evaluate the possibility of the existence of a anti-baryon that is a state made of three anti-quarks $\bar{B} \propto |\bar{q}\bar{q}\bar{q}\rangle$ the Young table method. To verify if the bound state of three anti-quarks, that is we can combine three anti-triplet representations and scrutinize whether there is the presence of a singlet state in the final result. As it is possible to see in Figure A. 2, the boxes are combined according to the rules established earlier: first, two columns are combined, and later the other one. It is not necessary to make all of these combinations to see that it will be possible to obtain an anti-baryon state, as shown in the singlet diagram presented in the final result. It is sufficient to note that in this last result, the difference between the number of boxes in each row is zero ($m_1 = m_2 = 0$), indicating a singlet state.

Appendix B

Last Known Wilson Coefficient C_1

$$
\begin{aligned}
c_4^{(\mathrm{SI})} = &-\frac{854201072999}{2041200} + \frac{28121193841}{75600}\zeta_3 + \frac{4674213853}{28350}\zeta_2^2 + \frac{913471669}{3780}\zeta_5 \\
&- \frac{577744954}{4725}\ln 2\zeta_2^2 + \frac{93970579}{567}\ln^2 2\zeta_2 - \frac{84531544}{2835}\ln^3 2\zeta_2 \\
&- \frac{93970579}{3402}\ln^4 2 + \frac{42265772}{14175}\ln^5 2 - \frac{375882316}{567}a_4 - \frac{338126176}{945}a_5 \\
&- \frac{47987641}{216}L_t + \frac{9364157}{48}L_t\zeta_3 + \frac{29494}{3}L_t^2 + 2299L_t^3 \\
&+ n_f\left(\frac{76094378783}{2041200} - \frac{12171659669}{151200}\zeta_3 + \frac{608462731}{113400}\zeta_2^2 - \frac{22104149}{1890}\zeta_5\right. \\
&+ \frac{37273868}{4725}\ln 2\zeta_2^2 - \frac{11679301}{1134}\ln^2 2\zeta_2 + \frac{5453648}{2835}\ln^3 2\zeta_2 \\
&+ \frac{11679301}{6804}\ln^4 2 - \frac{2726824}{14175}\ln^5 2 + \frac{23358602}{567}a_4 + \frac{21814592}{945}a_5 \\
&\left.+ \frac{5343385}{162}L_t - \frac{258056}{9}L_t\zeta_3 + \frac{12547}{9}L_t^2 + \frac{1100}{3}L_t^3\right) \\
&+ n_f^2\left(-\frac{48073}{108} + \frac{4091305}{1296}\zeta_3 - \frac{576757}{540}\zeta_2^2 - \frac{230}{3}\zeta_5\right. \\
&- \frac{685}{27}\ln^2 2\zeta_2 + \frac{685}{162}\ln^4 2 + \frac{2740}{27}a_4 - \frac{42302}{27}L_t + \frac{28297}{36}L_t\zeta_3 \\
&\left.- \frac{5107}{54}L_t^2 - \frac{628}{9}L_t^3\right) \\
&+ n_f^3\left(-\frac{270407}{5832} + \frac{844}{27}\zeta_3 + \frac{1924}{81}L_t - \frac{77}{27}L_t^2 + \frac{64}{27}L_t^3\right). \qquad (5)
\end{aligned}
$$

Last Known Coefficient of Imaginary Part of Π_{G^2}

$$
\begin{aligned}
g_4 = &+C_A^4\left(\frac{5974862279}{8748} - \frac{58922654}{243}\zeta_2 - \frac{25166402}{81}\zeta_3 + \frac{292556}{45}\zeta_2^2 + \frac{266200}{9}\zeta_2\zeta_3\right. \\
&\left.+\frac{1817200}{27}\zeta_5 + \frac{121000}{9}\zeta_3^2 - \frac{96250}{9}\zeta_7\right) \\
&+ \frac{d_A^{abcd}d_A^{abcd}}{N_A}\left(-\frac{6416}{27} + \frac{54160}{9}\zeta_3 + \frac{1408}{5}\zeta_2^2 - \frac{13760}{3}\zeta_5 + \frac{19360}{3}\zeta_3^2 - \frac{6160}{3}\zeta_7\right) \\
&+ C_A^3 n_f\left(-\frac{1025827736}{2187} + \frac{41587004}{243}\zeta_2 + \frac{8812352}{81}\zeta_3 - \frac{211736}{45}\zeta_2^2 - \frac{9680}{9}\zeta_2\zeta_3\right. \\
&\left.- \frac{109220}{9}\zeta_5 + \frac{8800}{9}\zeta_3^2 - \frac{3500}{9}\zeta_7\right) \\
&+ C_A^2 C_F n_f\left(-\frac{348948545}{2916} + \frac{22340}{\zeta_2} + \frac{1869710}{27}\zeta_3 - \frac{656}{15}\zeta_2^2 - \frac{19360}{3}\zeta_2\zeta_3 + \frac{35540}{3}\zeta_5\right. \\
&\left.-\frac{17600}{3}\zeta_3^2 + \frac{7000}{3}\zeta_7\right)
\end{aligned}
$$

$$
\begin{aligned}
&+ C_A C_F^2 n_f \left(\frac{609521}{162} - \frac{484}{3}\zeta_2 + \frac{450374}{27}\zeta_3 + \frac{352}{15}\zeta_2^2 - \frac{63040}{3}\zeta_5 - 5600\zeta_7\right) \\
&+ C_F^3 n_f \left(\frac{1034}{3} - \frac{388}{\zeta_3} - 4560\zeta_5 + 5600\zeta_7\right) \\
&+ \frac{d_F^{abcd} d_A^{abcd}}{N_A} n_f \left(\frac{44864}{27} - \frac{140128}{9}\zeta_3 - \frac{3328}{5}\zeta_2^2 + \frac{20800}{3}\zeta_5 - \frac{14080}{3}\zeta_3^2 + \frac{2240}{3}\zeta_7\right) \\
&+ C_A^2 n_f^2 \left(\frac{26855351}{243} - \frac{3479386}{81}\zeta_2 - \frac{83536}{9}\zeta_3 + \frac{19472}{15}\zeta_2^2 + \frac{1760}{3}\zeta_2\zeta_3 - \frac{1240}{9}\zeta_5 + \frac{160}{9}\zeta_3^2\right) \\
&+ C_F C_A n_f^2 \left(\frac{29816212}{729} - \frac{71888}{9}\zeta_2 - \frac{563948}{27}\zeta_3 + \frac{224}{15}\zeta_2^2 + \frac{7040}{3}\zeta_2\zeta_3 - \frac{7000}{3}\zeta_5 - \frac{640}{3}\zeta_3^2\right) \\
&+ C_F^2 n_f^2 \left(\frac{90491}{81} - \frac{200}{3}\zeta_2 - \frac{138968}{27}\zeta_3 - \frac{352}{15}\zeta_2^2 + 4400\zeta_5 + 640\zeta_3^2\right) \\
&+ \frac{d_R^{abcd} d_R^{abcd}}{N_A} n_f^2 \left(-\frac{68096}{27} + \frac{39424}{9}\zeta_3 + \frac{1024}{5}\zeta_2^2 - \frac{1280}{3}\zeta_5 + \frac{2560}{3}\zeta_3^2\right) \\
&+ C_A n_f^3 \left(-\frac{46491973}{4374} + \frac{1099028}{243}\zeta_2 + \frac{23720}{81}\zeta_3 - \frac{1408}{9}\zeta_2^2 + \frac{320}{9}\zeta_2\zeta_3 + \frac{800}{27}\zeta_5\right) \\
&+ C_F n_f^3 \left(-\frac{2282351}{729} + \frac{6224}{9}\zeta_2 + \frac{5200}{3}\zeta_3 - \frac{640}{3}\zeta_2\zeta_3\right) \\
&+ n_f^4 \left(\frac{773024}{2187} - \frac{40640}{243}\zeta_2 - \frac{2240}{81}\zeta_3 + \frac{64}{9}\zeta_2^2\right).
\end{aligned}
$$

Appendix C

Form is a computational system designed to optimize calculations using machine resources more fundamentally and compactly than other algebraic computing systems. It will be employed for computing the numerator of $h \to gg$ process. After variables are declared, the numerator can be obtained using the function Trace4,1, which makes all contractions of γ^{μ}'s matrix and gives the final result as shown above by N.

```
FORM 4.2 (Sep 14 2017) 64-bits             Run: Wed Oct 26 09:17:01 2022
Vectors k,p2,p3;
Symbols mt,i,gs,z,x;
Indices mu, nu, rho, teta, alfa,beta,gamma;
Local N = (g_(1,rho)*k(rho)- g_(1,beta)*p2(beta) + mt)*g_(1,mu)*(g_(1,teta)*
k(teta) + mt)*g_(1,nu)*(g_(1,alfa)*k(alfa)+ g_(1,gamma)*p3(gamma) + mt);
Trace4,1;
Print +s;
.End;

Time = 0.00 sec    Generated terms = 21
N Terms in output =  8
Bytes used  = 404

N =
+ 16*k(mu)*k(nu)*mt
+ 8*k(mu)*p3(nu)*mt
- 8*k(nu)*p2(mu)*mt
- 4*p2(mu)*p3(nu)*mt
+ 4*p2(nu)*p3(mu)*mt
+ 4*d_(mu,nu)*mt^3
- 4*d_(mu,nu)*k.k*mt
- 4*d_(mu,nu)*p2.p3*mt
 ;
```

Appendix D

Wick Rotation

We need to work with Euclidean quantities, and therefore, we will perform a Wick rotation (55). Essentially, what is realized is a shift $k^0 \to ik^0$, and thus

$$\begin{aligned} k^2 &= -(k_E^0)^2 - \mathbf{k}_E^2 \equiv -k_E^2, \\ dk^0 &= i dk_E^0, \\ d^D k &= i d^D k_E. \end{aligned}$$

Here, k_E is the Euclidean momentum. Then, consequently, the integral (8) can be rewritten as

$$G(D,\alpha,\beta,a^2) = i(-1)^{\alpha-\beta} \int \frac{d^D k_E}{(2\pi)^D} \frac{(k_E^2)^\alpha}{(k_E^2+a^2)^\beta}. \tag{6}$$

The angular integral can be simply written as (34)

$$\int d\Omega_d = \frac{2\pi^{D/2}}{\Gamma(D/2)}. \tag{7}$$

With this last relationship (7), it is possible to rewrite Eq. (6) considering only a radial integral in the momentum variable from zero to infinity

$$G(D,\alpha,\beta,a^2) = \frac{2i(-1)^{\alpha-\beta}}{(4\pi)^{D/2}\Gamma(D/2)} \int_0^\infty dk_E \, \frac{k_E^{2\alpha+D-1}}{(k_E^2+a^2)^\beta}. \tag{8}$$

For practical reasons, we want to express the integral in terms of a variable that ranges from 0 to 1. Thus, the chosen variable is

$$z \equiv \frac{a^2}{(k_E^2+a^2)} \to dz = -\frac{2a^2 k_E}{(k_E^2+a^2)^2} dk_E, \tag{9}$$

where, in order to rewrite k_E and dk_E in terms of z, it is necessary to isolate these terms in the previous equation, resulting in

$$k_E = \left[\frac{a^2}{z}(1-z)\right]^{1/2}, \quad dk_E = -\frac{1}{2} dz (1-z)^{-1/2} (a^{-a}) \left(\frac{a^2}{z}\right)^{3/2}. \tag{10}$$

Then, it is sufficient to extend this structure to the integral (8) to arrive at

$$G(D,\alpha,\beta,a^2) = \frac{i(-1)^{\alpha-\beta}}{(4\pi)^{D/2}\Gamma(D/2)} \int_0^1 dz (a^2)^{\alpha-\beta+D/2} z^{\beta-\alpha-D/2-1} (1-z)^{\alpha+D/2-1}. \tag{11}$$

This enables us to write (34)

$$G(D,\alpha,\beta,a^2) = \frac{i(-1)^{\alpha-\beta}(a^2)^{\alpha-\beta+D/2}}{(4\pi)^{D/2}\Gamma(D/2)} \mathcal{B}(\beta-\alpha-D/2, \alpha+D/2), \tag{12}$$

where $\mathcal{B}(m,n)$ is the beta function

$$\mathcal{B}(m,n) = \int_0^1 dz z^{m-1}(1-z)^{n-1} = \frac{\Gamma(m)\Gamma(n)}{\Gamma(n+m)}. \tag{13}$$

$\alpha-$Parametrization

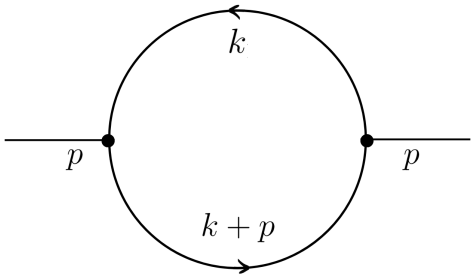

Figure D. 3 – Topology of the one-loop massless propagator diagram.

Source: By the author.

With the objective of solving the loop integral in Figure D. 3, we arrive at(76)

$$\int \frac{d^dk}{D_1^{n_1}D_2^{n_2}} = i\pi^{d/2}(-p^2)^{d/2-n_1-n_2}G(n_1,n_2), \qquad D_1 = -(k+p)^2, D_2 = -k^2. \tag{14}$$

Before developing $G(n_1, n_2)$, it is necessary to introduce the so-called α-parametrization . With this parametrization, we can rewrite the denominator of an integral as:

$$\frac{1}{a^n} = \frac{1}{\Gamma(n)}\int_0^\infty e^{-a\alpha}\alpha^{n-1}d\alpha. \tag{15}$$

After employing Wick rotation in conjunction with the parametrization α for the integral, one arrives at

$$G(n_1,n_2) = \frac{\pi^{-d/2}}{\Gamma(n_1)\Gamma(n_2)}\int e^{-\alpha_1(\boldsymbol{k}+\boldsymbol{p})-\alpha_2\boldsymbol{k}^2}\alpha_1^{n_1-1}\alpha_2^{n_2-1}d\alpha_1 d\alpha_2 d^d\boldsymbol{k}, \tag{16}$$

that one can still simplify the exponent through a change of variables in momentum

$$\boldsymbol{k}' = \boldsymbol{k} + \frac{\alpha_1}{\alpha_1+\alpha_2}\boldsymbol{p}, \tag{17}$$

after making this change, the following result is obtained

$$G(n_1,n_2) = \frac{\pi^{-d/2}}{\Gamma(n_1)\Gamma(n_2)}\int \exp\left[\frac{-\alpha_1\alpha_2}{\alpha_1+\alpha_2}\right](\alpha_1+\alpha_2)^{-d/2}\alpha_1^{n_1-1}\alpha_2^{n_2-1}d\alpha_1 d\alpha_2. \tag{18}$$

Then, performing the variable changes $\alpha_1 = \eta x$ and $\alpha_2 = \eta(1-x)$, we arrive at

$$\begin{aligned} G(n_1,n_2) &= \frac{1}{\Gamma(n_1)\Gamma(n_2)}\int_0^1 x^{n_1-1}(1-x)^{n_2-1}dx\int_0^\infty e^{-\eta x(1-x)}\eta^{-d/2+n_1+n_2-1}d\eta \\ &= \frac{\Gamma(-d/2+n_1+n_2)}{\Gamma(n_1)\Gamma(n_2)}\int_0^1 x^{d/2-n_2-1}(1-x)^{d/2-n_1-1}dx. \end{aligned} \tag{19}$$

In which it is possible to use the Euler beta function discussed earlier, finally arriving at

$$G(n_1,n_2) = \frac{\Gamma(-d/2+n_1+n_2)\Gamma(d/2-n_1)\Gamma(d/2-n_2)}{\Gamma(n_1)\Gamma(n_2)\Gamma(d-n_1-n_2)}. \tag{20}$$